Automotive Electromagnetic Compatibility

Prediction and Analysis of Parasitic Components in Conductor Layouts

Sabine Alexandersson

LUND UNIVERSITY

Doctoral Dissertation in Industrial Electrical Engineering
Department of Industrial Electrical Engineering and Automation

2008

Department of Industrial Electrical Engineering and Automation
Faculty of Engineering
Lund University
Box 118
221 00 LUND
SWEDEN

http://www.iea.lth.se

ISBN 978-91-88934-48-2
CODEN:LUTEDX/(TEIE-1056)/1-221/(2008)

Printed in Sweden by Media-Tryck, Lund University
Lund 2008

Adaequatio intellectûs nostri cum re

[Conformity of our minds to the fact]

Abstract

The electronics in the automotive industry is facing a new era where safety critical functions are electrified, as for example drive-by-wire technology. At the same time as the number of electrical loads in the vehicles is increasing, the time to market is decreasing. Full scale prototypes of a vehicle are often only available at a late stage in the development process where changes are rather costly. This implies that prediction and simulation of a system are of importance and are useful already at an early stage of the development process. There are economic benefits that can be gained by prediction and simulation of the system such as: reduction of time to market, virtual tests, virtual prototypes and optimization of electronic circuits with respect to safety margins of filters.

The high number of electrical loads in the vehicle leads to different cable harnesses routed along the body and chassis of the vehicle. These cable harnesses will contain both power conductors and communication conductors, routed close together. When conductors are routed close to each other, a signal on one conductor can interfere with the signal on another conductor. This phenomenon is called crosstalk.

Crosstalk can increase the noise levels, create unplanned spikes or destroy data on nearby conductors. Hence it should always be a prime suspect in an electromagnetic interference investigation or a candidate for prediction. Crosstalk between two conductors is coupled by the mutual inductance and capacitance. When these parameters are known, the crosstalk can be estimated by using a circuit simulation.

The mutual inductance and capacitance between the conductors as well as the self inductance and capacitance of each conductor depend on the surrounding environment. This implies that the conductor layout is an important factor when it comes to designing a system that is robust against crosstalk.

This thesis focuses on estimation of the parasitic components in a system with two conductors and a ground structure. Since the parasitic components are affected by the conductor layout, five different layouts are investigated. The parameters are estimated by using analytical calculations, electromagnetic simulations with the software CableMod and measurements. An approximate method for fast analytical calculations is proposed and evaluated.

The parameter values estimated with the different methods are compared in the thesis. The values yielded from the accurate analytical calculation and the simulations agree well. Some of the measured values deviate from the theoretical values, and it is shown that the differences emanate from the fact that the theoretical models do not exactly describe the measurement setup.

The different parameter setups from the different estimation methods and the investigated conductor layouts are employed in circuit simulations in the software LTSpice/ Switchercad III. The circuit simulations show that the proposed approximate analytical calculation method is sufficient to use for prediction of crosstalk and comparison between different conductor layouts.

Acknowledgements

During the work with this thesis, I have had the privilege to get to know people that have become very important to me. Their support and encouragement has meant a lot and I would hereby like to express my gratitude.

Anders Lundgren and Dr Hans Bängtsson are two people who are always there to support me and make sure that everything is progressing. Many of the more complex measurements in this thesis are carried out with the help from both Anders and Hans.

Professor Mats Alaküla has been my main supervisor during this work and always works as support and source of inspiration. Professor Gerhard Kristensson has also been my supervisor and his enthusiasm over my work is gratefully acknowledged.

I am very grateful to Dr Richard Lundin at the Electromagnetic Theory Group. Richard has been very patient with me although the investigated problems have been far from ideal or theoretically attractive. My experiments would not have been the same without the help from Kjell Attback, Håkan Berg and Thomas Törnvall at Volvo Cars who presented information from their experiments to me and invited me to an inspiring atmosphere for discussions. Johan Wedlin at Volvo 3P provided me not only with the part of the frame rail that has been used in the measurements, but also with confidence and valuable comments during the last part of the project. Johan Nilsson at the department of Electrical Measurements has always been willing to lend me their measurement equipment and also shown interest in the measurements. Also Bengt Simonsson and Getachew Darge at the department have been valuable resources during the measurements. I am also thankful to Ronald Brander at Ronshield AB and the people at SimLab Software GmbH for introducing me to the software CableMod and all the technical support.

Dr Per Karlsson at Emotron AB has contributed to this thesis through his productive discussions along the way and by helping me with the circuit model.
The reference group, including my two supervisors, Björn Bergqvist, Hans Bängtsson, Sture Eriksson, Lars Hoffmann, Göran Johansson, Joachim Lindström, Frans Lindwall and Tryggve Tuveson have given me a lot of valuable inputs and support during the years which is gratefully acknowledged.

I also want to thank the people at the department for providing an inspiring working environment. Specially thanks to Carina Lindström who always takes very good care of me and to my current and former room mates; Tomas Bergh, Dan Hagstedt, Raissa Kruse and Yury Loayza-Vargas.

After my Licentiate degree, I started working part time at Haldex Brake Products AB in Landskrona. The time at Haldex has enriched my work to a large extent and given me valuable inputs and experiences. The support I have received from all the people working in the Laboratory and the Test Center is gratefully acknowledged. I would specially like to thank Ola Ahlqvist, Andreas Holmgren, Anders Lindqvist, Fredrik Lundby, Anders Nilsson, Peter Nilsson, Ola Nockhammar, Lisette Pedersen, Anders Persson Ingemar Pålsson and Jacob Svendenius for their support.

I would also like to thank all the people who have provided me with information during my work, and Jerker Delsing, Jonas Ekman, Mathias Enohnyaket, Kalevi Hyyppä, Tore Lindgren and Åke Wisten at Luleå University of Technology for giving me valuable comments.

I am very thankful for all the support I have received during the years from my family and friends. To my two dear supporters at home: I am most grateful for the love and patience you both have shown me during this time. Tomas, thank you for believing in me and for all the support you have given me during all these years. Your love has completely changed my life. My dear little Benjamin, your hard hugs and wet kisses have enriched my life to an extent I never thought was possible.

This work is part of the research program Gröna Bilen/Fuel Cell Hybrid Electric Vehicle, which is been financially supported by the Swedish government, Saab Automobile AB, Scania AB, AB Volvo and Volvo Cars Corporation. Their support is gratefully acknowledged.

Löddeköpinge, May 2008
Sabine Alexandersson

Contents

Chapter 1

Introduction

This chapter serves as an introduction to the thesis. The motives behind the thesis are presented and also a brief description of some of the previous work done in the research area. Finally the author's publications are listed.

1.1 Motivation

Customer demands and added functionalities increase the number of electrically driven loads within the vehicles. Some of the new electrical loads in the vehicle replace loads that were formerly mechanically driven, but many new electrical loads are also introduced. One advantage with electrical loads is the increased control over the load. The increased control facilitates not only a better efficiency of the vehicle but also possibilities to easily implement new functionalities. This has led to a new era within automotive electronics where also safety critical loads are electrically implemented.

X-by-wire

One of the new technologies implemented in future vehicles is the X-by-wire technique. X-by-wire or drive-by-wire is a name for technology where traditional mechanic and hydraulic driven and controlled loads are replaced by electrically driven and electronically controlled loads. One example is a brake-by-wire system for heavy duty vehicles. The brake system for a heavy-duty vehicle today normally utilizes pneumatically controlled brake actuators where a central electronic control box controls the air pressure for each brake actuator. In a brake-by-wire system the pneumatically control relay valve is replaced by an electrical motor that will push the pad to the disc. The electromechanical brake will provide a much faster and more accurate control of the braking. This is for example useful in hybrid vehicles where the

regenerative braking then can be utilized to a large extent, and thereby increase the efficiency of the vehicle.

Electromagnetic compatibility

The increased number of electrical loads leads to an increased amount of cables in the vehicle. The cables are routed tightly together, and the chassis is often used as a ground return path. Although there are not very many alternatives for cable routing due to spacing and cost, the alternatives that are present should be taken into account when designing an electrical system. Solutions to electromagnetic interference problems tend to get more expensive the closer the vehicle is to the market and it is therefore important to try to predict all possible coupling paths for the disturbances.

At the same time as the number of electrically driven loads is increasing is the time to market in the automotive industry constantly being shortened. This puts pressure on the automotive engineers who must be able to predict the vehicles electromagnetic environment without having any full scale prototypes at hand.

Crosstalk

A common type of electromagnetic interference problem is crosstalk. Cables routed close to each other without any shielding will have a capacitive and inductive coupling to each other. If these couplings and their roots of causes are known, the possibility to adapt the design in order to get an electromagnetically "cleaner" system increases. Estimation of electromagnetic interferences in and nearby a cable harness can be performed in different ways. "Rules of thumb" represent one possibility. These rules could for example state that the capacitance between two cables is 100-150 pF/m if the cables are routed less than 5 cm apart and that the self inductance is around 1 μH/m. In many cases, these "rules" provide an apprehension of the system behavior. However, for electromagnetic compatibility (EMC) modeling, these rules are not always accurate enough.

Another way to predict the electromagnetic behavior of the system is to estimate the parasitic components affecting the crosstalk between different cables [21], [46] and [62] and turn them into a lumped circuit model of a transmission line. When these parameters are known, they can easily be used in standard circuit simulation software programs, such as SPICE. The benefits of investigating the circuit in a SPICE software are that it allows the user to comprehend what is going on, and it is also possible to modify and

implement different terminations and compare them from an EMC perspective. A circuit model in SPICE will also facilitate system investigations in both time and frequency domains.

Advantages with prediction

This thesis deals with prediction of the parasitic components in a conductor layout that may cause interferences. Predictions of this type are valuable early in the design stage of a vehicle, when the geometry is not finally decided. The predictions can serve as a base for EMC simulations, which is a good tool to predict disturbances and avoid late and expensive changes.

Some of the advantages with prediction and simulation of the system are

- Better understanding of the phenomena among the designers
- Reduction of time to market in the development of electronic systems since tasks can be performed in parallel and the exploration and examination of the alternatives are fast
- Preliminary tests can be performed virtually, and hence more tests can be carried out to a lower cost
- Virtual validation of system behavior, which implies that a significant cost reduction is achieved when it comes to prototype costs
- Electronic circuits might be optimized and many passive components (resistors, capacitors, and inductors) that today are introduced as a safety margin might be found unnecessary during the analyses and thereby save both complexity and costs

1.2 Objectives and restrictions

A dream that exists among most automotive electrical engineers is to have a set of guidelines and rules of thumb that will assure that they never will have any electromagnetic compatibility issues within the vehicle. If these guidelines would have existed, publishers would have fought about getting the rights to print them. But there are no such general guidelines and so the major objective of this thesis is to create an understanding of the physical phenomena that are present when two conductors are routed next to each other in the vicinity of a ground structure. There are different ways to

estimate the parasitic components of a transmission line and the aim is to compare these and to propose a method that hopefully will facilitate the understanding of what will happen if a conductor is moved in any direction in relation to another conductor.

Unfortunately the time is often limited in a project of this type, and some areas have to be left to be discovered by some one else. In this thesis, the following restrictions are made

- the length of the conductors that are used is 1 m, longer conductors can be modelled by cascading the transmission line models that are developed

- only two conductors are used, whilst in a real world application there will most likely be more than two conductors; however also an analysis of only one source of disturbances and the presumed victim can be useful to reach an understanding of the proposed concept

- no shielded conductors are used since the automotive industry to a large extent avoids them due to cost and reliability of the grounding of the shield

- no twisted pair conductors are investigated

- Only frequencies up to 30 MHz are taken into account

1.3 Contributions

The contributions of this thesis are presented in Chapter 6-9 and concluded in Chapter 10. A brief summary of the results are given in this section.

This thesis focuses on the parasitic components that are present in a setup with two conductors and a ground structure.

- the values for the parasitic components from five different conductor layouts are gained from analytical calculations, simulations and measurements

- an approximate method for analytical calculation of the parameter values is suggested and compared to more detailed calculations,

simulations and measurements

- Divergences between measured and calculated or simulated parameter values are analyzed and explained

- Circuit simulation models are built to compare the levels of crosstalk for the different parameter setups

- The circuit simulation models are used for comparison of different conductor layouts regarding crosstalk

- Two Matlab scripts are given, one for an accurate analytical calculation of the parameters, and one for an approximate.

1.4 Previous work

Transmission lines and their characteristics is a research area that has been under investigation for more than half a century [50]. Many of the key references in the area are written by Clayton R. Paul. His work has been in both the field of analytical calculations [52] [55] [56] [57] [58] as well as building up SPICE models for the transmission lines [51]. Clayton R. Paul et al. have also performed investigations of crosstalk modeling for automotive harnesses [68].

Since the electrical loads are increasing and the lead times are getting shorter, the interest for electromagnetic modeling is increasing in the automotive industry. A number of different cooperative EU-projects have been carried out.

One EU-project is the AutoEMC [10], which deals with numerical simulation for early EMC design of cars. In this project, different simulation software programs are tested against an experimental setup in order to estimate whether the simulation tools could give a good enough prediction of the real world. Both radiated and conducted emissions are studied.

Where AutoEMC ended, the next European project, COSIME (Continuous simulation of electromagnetic compatibility in automotive application) [18] continued. The COSIME project has focused on the corporation between automotive manufacturers and manufacturers of Integrated Circuits (IC) in order to create useful simulation models from an EMC perspective. The

project has also proposed a continuous EMC simulation process during the development.

Another European project that is carried out is the GEMCAR project (Guidelines for Electromagnetic Compatibility Modeling for Automotive Requirements) [23]. In this project, guidelines for how electromagnetic modeling should be performed in order to give the automotive engineers any valuable information about the electromagnetic compatibility of the vehicle are given. The project uses the Feature Selective Validation method (FSV) to decide whether a simulation result is valid or not.

1.5 Outline of the thesis

This chapter contains a brief introduction to the thesis and the work that is presented. In Chapter 2 the electromagnetic environment within a vehicle is described. Since the investigations presented in the author's licentiate thesis [41] served as inspiration for this thesis, some of the major results from these experiments are presented in this chapter. The chapter also describes an attempt to measure the capacitance from the vehicle to earth.

Chapter 3 gives a brief theoretical background to transmission lines and crosstalk. Different coupling paths for disturbances are described. Phrases like knee frequency and weak coupling are also explained in this chapter.

Since an electromagnetic simulation software is employed in the investigations of this thesis, different methods for electromagnetic simulations are described in Chapter 4. There is no single method that will solve all problems and hence a number of methods are briefly described. Also some thoughts regarding electromagnetic compatibility and functional safety are presented here.

In Chapter 5 the investigated problem in the thesis is formulated and described. The background is described, and the five different conductor layouts examined in the thesis are described in detail.

One way to examine the parasitic components of a conductor layout is to analytically calculate the parameters. In Chapter 6 a brief background to electromagnetic calculations is given and the parameters are calculated by using well known formulas and an approximate method proposed by the author.

The same model that is used for the analytical calculations is also implemented in an electromagnetic simulation software called CableMod from SimLab. The simulation software and the model are described in Chapter 7. Parameter values for the different conductor layouts are extracted from two dimensional transmission line simulation models.

Chapter 8 describes the experimental setup and the measurements that are performed in order to estimate the parameters.

The different parameter setups that are gained from the analytical calculations, the simulations and the measurements are all collected and compared in Chapter 9. Deviations between the different values are analyzed and explained. The different parameter setups are employed in a circuit simulation in order to compare both the different conductor layouts, and also the levels of crosstalk when the different methods for parameter estimation are employed. A short summary of the results and some reflections are finally presented in Chapter 10.

1.6 Publications

The results regarding estimation of the parasitic components of transmission lines presented in Chapter 6-8 in this thesis are also presented in the following publications:

S. Alexandersson, M. Alaküla, H. Bängtsson, "Prediction of Parasitic Components in an Automotive Environment", 2008 IEEE International EMC Symposium, Aug. 18-22, 2008, accepted.

S. Alexandersson, H. Bängtsson, "Analytic prediction of electromagnetic behaviour", SPEEDAM 2008 International Symposium on Power Electronics, Electrical Drives, June 11-13, 2008, accepted.

At Haldex Brake Products AB, the author got in contact with the issues of functional safety in an IVSS project named AutoVal. Thoughts from this project are presented in Chapter 4.1 and in:

S. Alexandersson, "Functional Safety and EMC for the Automotive Industry", 2008 IEEE International EMC Symposium, Aug. 18-22, 2008, accepted.

S. Alexandersson, "EMC and Functional Safety for the Automotive Industry",

NORPIE 2006 Nordic Workshop on Power and Industrial Electronics, Lund, Sweden, June 12-14, 2006, CD-ROM pages 6.

The previous work done in the research area regarding electromagnetic compatibility and pulse width modulated loads within vehicles serve as a basis for this thesis, and is presented in the Licentiate's thesis:

S. Marksell, "EMC Aspects of PWM Controlled Loads in Vehicles", Licentiate Thesis, Department of Industrial Electrical Engineering and Automation, Lund Institute of Technology, Media Tryck Lund University, Sweden, 2004.

The following publications also present some of the previous work done:

S. Alexandersson, M. Alaküla, "Automotive power electronic future - from an EMC perspective", SPEEDAM 2006 International Symposium on Power Electronics, Electrical Drives, Automation and Motion, Taormina, Italy, May 23-26, 2006, CD-ROM, pages 5.

S. Marksell, M. Alaküla, "Electromagnetic Compatibility Problems in Automotive Applications", NORPIE 2004, Nordic Workshop on Power and Industrial Electronics, Trondheim, Norway, June 14-16, 2004, CD-ROM pages 7.

S. Marksell, M. Alaküla, G. Lindstedt, "EMC Test System for Low Power Drives", The 20th International Battery, Hybrid and Fuel Cell Electric Vehicle Symposium, Nov. 15-19, 2003, CD-ROM, pages 11.

Chapter 2

Automotive electromagnetic compatibility

The number of electrically driven loads in a vehicle is increasing, which means that many different systems should be squeezed into an already dense space. Since the space is dense, there are often long distances between the loads and the ECUs (electrical control units). One example is a system that involves a pulse width modulated power converter to a load. For many pulse width modulated loads, there will be a long conductor between the load and the power electronic converter. In the best electromagnetic interference case, these long conductors work as antennas and transmit noise to the AM band of the radio, but the interferences could also be far more severe and seriously degrade the functionality of the vehicle.

In this chapter, some automotive electromagnetic compatibility issues will be presented. Some of the results presented in this chapter were also presented in the licentiate's thesis of the author [41].

2.1 Common problems

Many electrical loads benefits from being controlled on demand, thereby saving energy and in the end also fuel. A common and energy efficient way to control an electrical load is to use pulse width modulation (PWM) where the battery voltage is supplied to the load in pulses of selected pulse width to pulse period in order to create the desired average output voltage (see Appendix B). Pulse width modulation enables control of the torque, the output current or the output voltage irrespective if it is AC or DC.

When the method with pulse width modulation is employed, the voltage pulses of the output voltage are distributed on the cables between the power

electronic converter and the load. The edges of these voltage pulses are steep with high derivatives and these pulses could be coupled into other systems in the vehicle, thereby disturbing them. Also the fundamental of the output voltage, which is equal to the switching frequency, could disturb other systems in the vehicle. One example of a system which is often affected by pulse width modulation is the AM-band of the radio. The disturbances are then noticed as a noise in the radio.

Electromagnetic fields and vehicle electronics

There are two ways for the electromagnetic fields to be coupled into the vehicle electronics. The first way is coupling into the electronic system via printed circuit board tracks or internal wiring. Both act as antennas and convert the field into a conducted voltage or current. The second way of coupling is when the vehicle wiring harness acts as an antenna and conducts the interference into the electronic system.

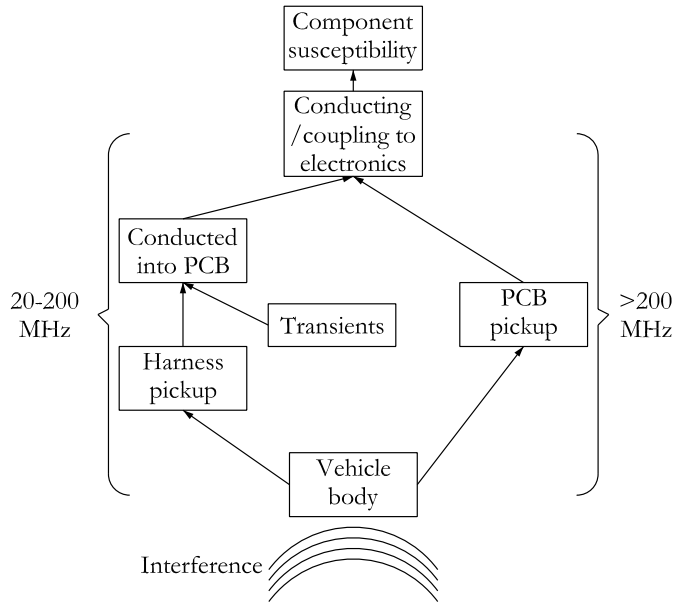

Figure 2.1. Coupling of interference into vehicle electronics. (PCB = printed circuit board)

Since the coupling process is strongly dependent on the frequency of the

interference, the wiring harness or the electronic system will not work as efficient antennas for frequencies at or below 20 MHz. This is due to their length, which is relatively short compared to the wavelength of the interference (a good antenna has a length equal to a quarter of a wavelength). The wiring harness works as a reasonably efficient antenna between 20 and 200 MHz. Currents in the magnitude of 1 mA could then be caused to flow for each volt per meter of interference field.

The vehicle harness attenuates high frequencies above 200 MHz and is therefore no longer a good antenna. But the lengths of the printed circuit board tracks are becoming comparable to the quarter wavelength value and the interference could then be coupled directly into the electronic system. The electronic circuit themselves are fortunately prone to losses at such high frequencies, so no problems generally occur.

2.2 Common mode and differential mode

Electromagnetic disturbances appear in the form of common mode (CM) or differential mode (DM) disturbances. The differential mode voltage component of a circuit is a voltage that can be measured between phase conductors and the differential mode current component flows in the supply wires, including the neutral wire. The common mode current component on the other hand flows from the phase and neutral conductor toward earth. The circuit for the common mode current is closed by stray capacitances between the earthed parts and the circuit.

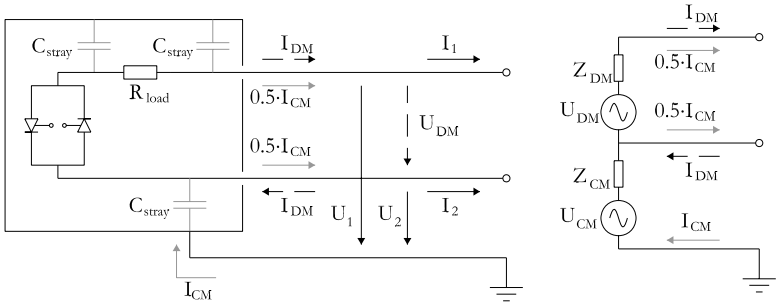

Figure 2.2. Differential mode (DM) and common mode (CM) electromagnetic interference voltage and current components. A typical electromagnetic interference source to the left, and the high frequency substitution circuit of the electromagnetic interference source to the right [73].

Definitions for the DM and CM components can be seen in Figure 2.2 and equation 2.1.

$$U_{DM} = U_1 - U_2 \quad (2.1a)$$

$$I_{DM} = \frac{I_1 - I_2}{2} \quad (2.1b)$$

$$U_{CM} = \frac{U_1 + U_2}{2} \quad (2.1c)$$

$$I_{CM} = I_1 + I_2 \quad (2.1d)$$

The radiation from an electronic circuit could occur as either common mode or differential mode radiation.

Differential mode radiation

Differential mode radiation is caused by a current that flows in a loop formed by the conductors of the circuit. These small current loops will then act as antennas, radiating a magnetic field. The most effective antennas are loop antennas where the circumference is smaller than one quarter of a wavelength. The current in such a current loop is in phase everywhere, which adds to rather than subtracts from the overall emission of the circuit, which may happen when the loop area is larger. The radiation from a loop antenna is proportional to the current in the loop, the loop area and the square of the frequency. If the magnitude and the frequency or the harmonic content of the current is reduced, also the radiation will decrease. Minimizing the area enclosed by the current flow will also decrease the radiation, and this could easily be done by placing signal leads and their associated return leads close together.

Common mode radiation

The common mode radiation has a large influence on the emission performance of a product, and is harder to control than the differential mode radiation. When the differential mode radiation is controlled by a proper circuit layout, the control of common mode radiation demands that the common mode currents in all cables are minimized.

Common mode radiation originates from the cables in the system. The frequencies that are radiated differ from the differential mode signal frequencies in the cable and are instead determined by the common mode

potential (usually the ground voltage). The common mode radiation is proportional to the frequency, the length of the antenna (the cable) and the magnitude of the common mode current on the antenna. For lower frequencies of a symmetrical square wave, the common mode emission spectrum is flat. The spectrum is flat up to a frequency, proportional to the rise time of the signal ($1/(\pi \cdot t_{rise})$), where the spectrum starts to decrease. This implies that the common mode emissions are mostly a problem in the lower frequency areas, which is not all true since the capacitive coupling is increased for the higher frequency areas. If the magnitude of the common mode current that is needed to produce a certain radiated field is compared to the magnitude of the differential mode current needed to produce the same radiated field (in a case where the loop area, cable length and frequency is constant), there ratio between these two currents is large. This means that a common mode current of a few microamperes can cause the same amount of radiated emissions as a few milliamperes of differential mode current.

When the common mode radiation should be controlled, it is desirable to limit both the rise time and the frequency of the circuit just as in the case with differential mode radiation. Since the common mode radiation emanates from the cables of the system, it is important to keep these short. This is often not possible, but on the other hand, the emissions cease to increase for cables longer than one quarter of a wavelength due to the presence of out of phase currents.

The common mode current is often the only controllable parameter and is therefore an important control parameter for the radiated emissions. The common mode current is not required for system operation, but it is important to ensure that although the components used for common mode suppression not affects the functional differential mode currents. One of the first things to be done in order to control the common mode currents is to minimize the source voltage driving the antenna. This is usually the ground potential, and one solution to this problem can be to use for example a ground plane in order to reduce the voltage drop in the ground system. One positive side effect of introducing a ground plane is that it also decreases the differential mode radiation, due to the induced mirror current (see Chapter 6.1). Another way of controlling the common mode current is to put a large common mode impedance (for example a common mode choke) in series with the cable. A common mode choke is the only technique that does not require a ground to function and also the only technique that does not affect the differential mode current. Decoupling the cables (shunting the current to

ground) or shielding are methods that also affects the common mode current. The problem with these methods is that they require a "quiet" or "clean" ground in order to work properly.

2.3 Investigation of radiated magnetic field

In the thesis "EMC Aspects of PWM Controlled Loads in Vehicles" [41] is a setup with a pulse width modulated load investigated. It consists of a car battery, two line impedance stabilization networks (LISNs), a drive circuit for MOSFETs, a PWM converter, and an inductive load, see Figure 2.3.

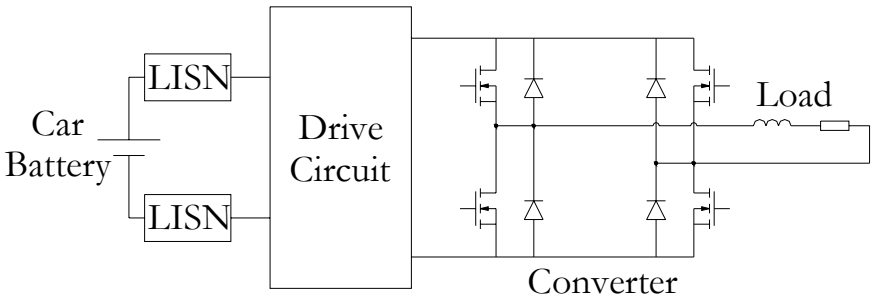

Figure 2.3. The laboratory test setup

According to the standard CISPR 25 [12], [31], two LISNs are required in setups where the equipment under test is remotely grounded, i.e. has a power return line longer than 200 mm. Since this is the case in the test setup, one LISN is used for the power supply line and one for the power return line. The LISNs used in the setup are designed according to the CISPR 25 standard. This standard prescribes that the inductor in the LISN should be 5 μH in order to simulate a 5 m long cable between the battery and equipment under test.

The LISNs are built as Figure 2.4 shows.

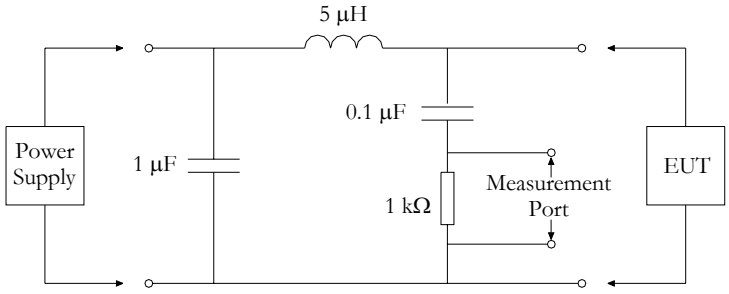

Figure 2.4. The circuit diagram for the LISNs used in the tests, which are designed according to the CISPR25 standard.

A 0.5 m wide and 1.98 m long ground plane is located underneath the setup. This plane is far from being a perfect ground, since it in a vehicle often is spot-welded or bolted together. In order to reconstruct this grounding situation, the plane is made of two 0.7 mm thick steel plates each 0.5 m wide and 1 m long. These two plates are spot-welded together in their short ends with the spots at distances of about 1.5 cm apart.

The car battery used in the setup is an Exide Maxxima 900 with orbital wounded cells. It has a nominal voltage of 12 V, a capacity of 50 Ah, and a maximal starting current of 900 A.

The load in the setup is a model of a small permanent magnet DC motor. It is designed for intermittent operation as a motor for an electrically operated window in a car. The armature inductance of the motor is about 0.3 mH and the current when the motor is operating at nominal load with 9 V is about 2 A. To get a realistic model of this motor when it is operating at nominal speed and load, a 0.3 mH inductor and a resistor of 3 Ω in series are used instead of the motor.

During the tests, two 1.8 m long unshielded 2.5 mm^2 cables are used between the power electronic converter and the load.

Measurement setup

Measurements of the radiated magnetic field (H-field) are carried out in a semi-anechoic chamber at Delta Development Technology AB in Västerås, Sweden. The investigated frequency spectrum is 9 kHz to 30 MHz.

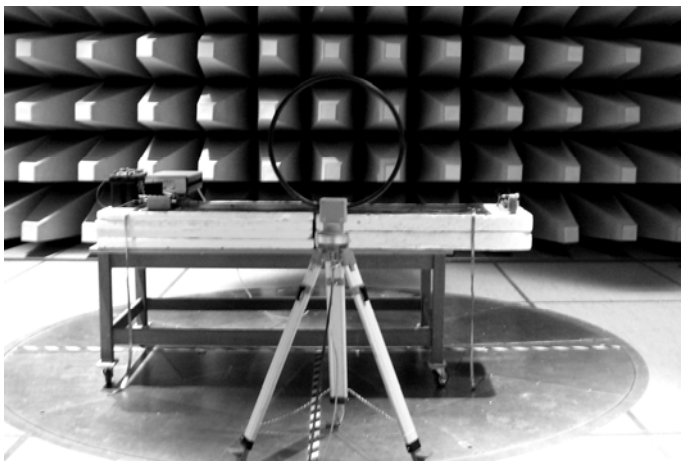

Figure 2.5. Setup in the semi-anechoic chamber at Delta Development Technology AB.

The ground plane, the power electronics and the load are placed 1 m above the floor ground plane in the chamber. Two copper braids are mounted to the ground plane and also attached to the floor ground plane of the chamber. The supply for the power electronics are provided by a 12 V car battery, located in the chamber and a 24 V DC supply which is placed outside the chamber. The car battery is placed at one end of the ground plane together with the power electronics. On the other side of the ground plane the load is located. The setup looks like Figure 2.5.

The antenna used in the measurements is a loop antenna from Rohde & Schwarz (HFH2-Z2) for magnetic field measurements. The diameter of the antenna is 50 cm and it is placed 1 meter from the ground plane, parallel to the cables between the power electronics and the load (Figure 2.6).

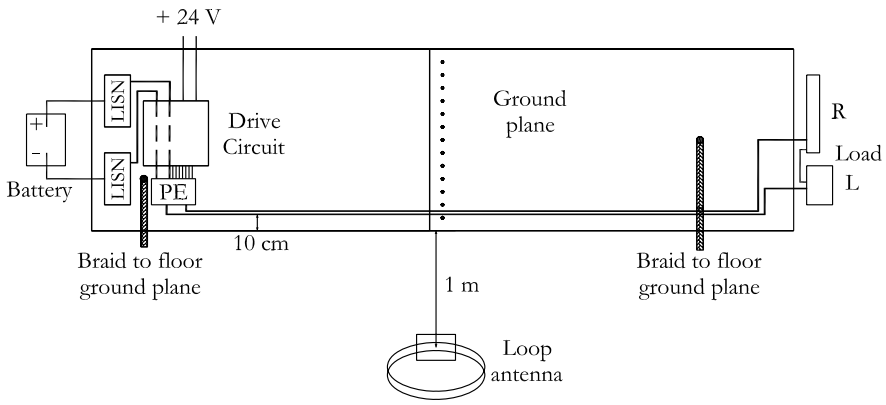

Figure 2.6 A sketch of the reference setup. The battery, the LISNs, the drive circuit for the MOSFETs and the power electronic (PE) converter are located to the left. Between the load and the power electronics there are two 1.8 m long unshielded cables routed next to each other on the ground plane.

The power electronic converter has a switching frequency of 20 kHz and a rise and fall time for the voltage pulses of 545 ns (rise) and 38 ns (fall).

Since no real vehicle is used in the measurements, the results presented here should only be seen as relative measurements wherefore no exact values are of interest. The relative measurements will give a good apprehension of which setups that are most likely to cause any electromagnetic interference.

In the measurements, no distinction between common mode and differential mode disturbances are made. For more information about common mode and differential mode, see Chapter 2.2.

Measurements with a conductor for current return

In the first measurements a separate conductor is used for current return. Although this is not a very common situation in the automotive industry, these investigations are performed in order to see if it is possible to gain anything from having a conductor for current return.

Reference measurement

During the measurements different conductor layouts are tested. In the

reference setup, both the lead in and current return are routed next to each other on the ground plane, 10 cm from the edge. The measurement receiver is set to measure the peak values.

The measurement of the radiated magnetic emissions from the reference setup is shown in Figure 2.7.

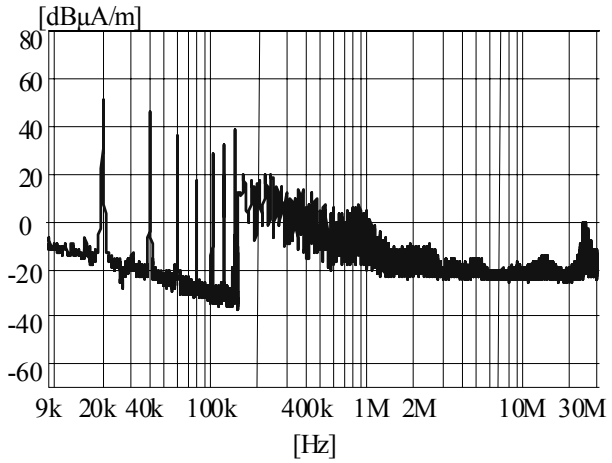

Figure 2.7. Results from the measurement of the radiated magnetic field of the reference setup.

The switching frequency and its harmonics are easily visible in the diagram. At 150 kHz, there is a step in the measurements due to the change of bandwidth for the instrument from 200 Hz to 9 kHz. There is also a peak at about 24 MHz. This peak could be due to oscillations between the input capacitance of the MOSFETs in the power electronic converter and the inductance in the wire to the gate. The input capacitance for the IPU20N03L MOSFET is typically 530 pF, which gives a value of the inductance as in

$$\omega_{osc} = 2 \cdot \pi \cdot f_{osc} = \frac{1}{\sqrt{L \cdot C_{input}}} \tag{2.2a}$$

$$L = \frac{1}{C_{input} \cdot \left(2 \cdot \pi \cdot f_{osc}\right)^2} = \frac{1}{530 \cdot 10^{-12} \cdot \left(2 \cdot \pi \cdot 24 \cdot 10^6\right)^2} = 83\ nH \tag{2.2b}$$

If the rule of thumb that a wire length of one meter corresponds to 1 μH is employed, it implies that the length of the wire should be about 8 cm according to equation 2.2. This matches the length of the actual wire needed, since the power electronic converter is not built into the box used for the drive circuit and the modulator card.

Both conductors 11 cm above ground plane

In one of the test setups, both conductors are raised 11 cm above the ground plane by using a long piece of cellular plastic.

The conducted emissions measurement for this setup is shown in Figure 2.8

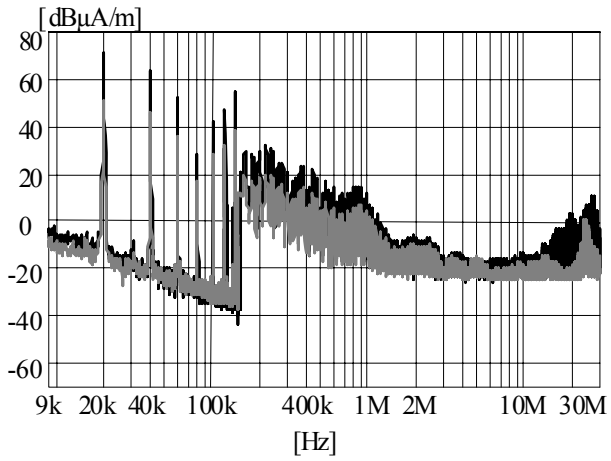

Figure 2.8. The results from the measurement of the radiated magnetic emissions when the cables between the power electronic converter and the load are placed 11 cm above the ground plane (black) compared to the reference setup (grey).

This setup should provide a larger loop area for the common-mode current, which is returning through the ground plane since the cables are raised. This increase in distance between the cables and the ground plane decreases the size of the parasitic capacitance between the ground plane and the cables, thereby decreasing the common-mode current. As can be seen in Figure 2.8 the radiated magnetic field increases in the higher frequency range when the cables are raised. This is due to the increase of the loop area for the antenna formed by the common mode current in the cables and the parasitic

capacitance to ground.

Both conductors 11 cm above ground plane, 10 cm apart

In the next setup, the conductors are still raised 11 cm above the ground plane and are now also separated 10 cm.

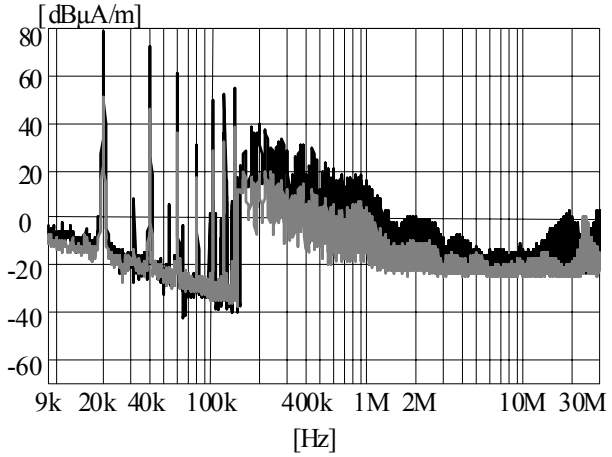

Figure 2.9. The results from the measurement of the radiated magnetic emissions when the cables between the power electronic converter and the load are placed 11 cm above the ground plane and separated by 10 cm (black) and the reference setup (gray).

In the measurements of radiated emissions for this setup, the effect from the differential mode radiation is apparent already in the low frequency range where the magnitude of the fundamental and the first harmonics have increased. The ground plane together with the two cables now works as a distributed antenna, for both common mode and differential mode radiation.

Current return through the ground plane

As mentioned before it is common to use the chassis of the vehicle for current return. In the following two setups, the conductor for current return is removed and the ground plane is used instead.

Lead in conductor close to ground plane, return through ground plane

In the first setup where the current return goes through the ground plane, the lead in conductor is located on the ground plane, 10 cm from the edge.

The radiated emissions from this setup are compared to the reference setup where the current return goes through a conductor in Figure 2.10.

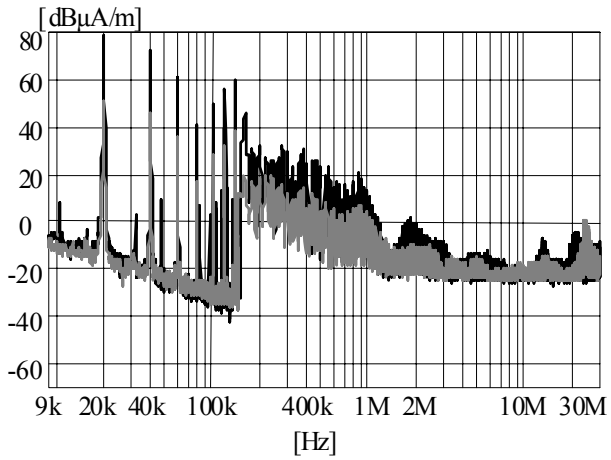

Figure 2.10. The results from the measurement of the radiated magnetic emissions when the current return is through the ground plane and the lead-in conductor is placed on the ground plane (black) and the reference setup (gray).

Since the ground plane is used as current return path, it is possible for the return current to spread out over the ground plane. This makes the setup an efficient antenna for differential mode radiation, which can be seen in Figure 2.10. The frequency peak at 24 MHz is attenuated, and this could be due to interference phenomenon since the peak is still present if looking at the load voltage frequency spectrum [41].

Lead in conductor 11 cm above ground plane, return via ground plane

In the last setup, the lead in conductor is raised 11 cm above the ground plane by using a piece of cellular plastic. The results from the measurements are shown in Figure 2.11.

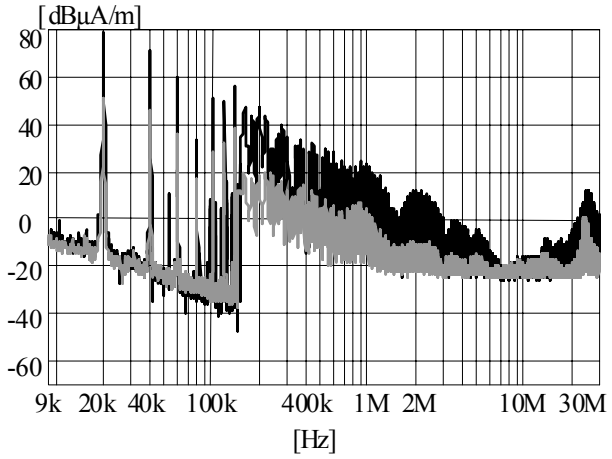

Figure 2.11. The results from the measurement of the radiated magnetic emissions when the current return is through the ground plane and the lead-in conductor is placed 11 cm above the ground plane (black) and reference setup (gray).

Raising the lead-in cable above the ground plane when the ground plane is used as a current return path creates a loop antenna with a large area. This antenna radiates mainly differential mode disturbances, see Figure 2.11.

As can be seen in the measurements above, the layout where the ground plane is used as a current return is the worst case when it comes to radiated emissions. It is also obvious what a great impact the conductor layout has on the electromagnetic environment within the vehicle. The results from these measurements in the licentiate thesis work have served as a ground for the ideas behind this thesis.

2.4 Vehicle investigation

During the work of this thesis, some measurements on a vehicle are performed. The vehicle used in the measurements is a 4x2 tractor of type FH12 from Volvo. 4x2 means that it has four wheels (or actually six, but the wheels at the rear are twin tires) of which two are driven. A tractor is used for towing semitrailers and does not have any cargo space. The length of the vehicle is 5.8 m and the width is 2.3 m. The test vehicle is equipped with air suspension.

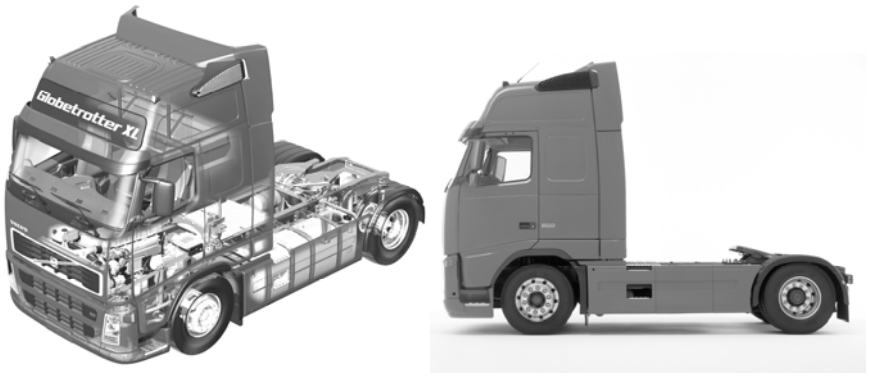

Figure 2.12. 4x2 tractor from Volvo Trucks [76].

Grounding

Conductors referred to as ground often perform more than one task in an electrical system [38]. Sometimes the systems are intentionally constructed that way, or it is an unintentional effect. In a vehicle, the term ground is even more diverse.

Although the trend within the automotive industry is towards composite or plastic body panels in the vehicles, the majority of the vehicle bodies still have a large content of metal. Since the body sheet metal is present almost everywhere where there are any electrical loads in the vehicle, it is convenient to use this for current return, potential reference, shielding, and noise reduction [38].

The large surface area and shape of the body sheet metal provide a large self-partial capacitance. It is found that these attributes of the body sheet metal will make it an effective sink for high-frequency noise currents. Although it seems convenient to use the body sheet metal for noise suppression, it will most likely also introduce noise. The currents must pass through body panel joint which might cause common impedance couplings and if the body sheet metal is used indiscriminate as a current return path, it will finally create a significant source of radiated emissions.

The body sheet metal also works as the primary conductor through which the vehicle is shielded against lightning and human generated electrostatic discharges. A reliable electrical integrity of this shield is however not ensured by common methods of vehicle body construction, since they employ spot

welding (cars) or bolting together parts with nonconductive paint (trucks). In an ideally constructed body sheet metal, the sheet metal panels are bonded and the hood and doors are connected with auxiliary ground straps.

Also the investigated Volvo FH12 uses the chassis as a current return path for power lines. When measuring the galvanic contact between different points on the FH12, it turns out that the cab is connected to the frame members, the internal combustion engine, the gear box and the front axle. Between the gear box and the drive shaft there is a rubber bushing that disconnects the rear driving axle electrically from the rest of the vehicle. The rear axle is attached to the frame via rubber bushings as well, which keeps it electrically isolated from the rest of the vehicle. These rubber bushings keep the rear wheel galvanically isolated from the rest of the vehicle as well.

In some vehicles the rear axle is electrically connected to the rest of the vehicle, in order to avoid induced currents when it passes under overhead power lines.

The fuel tank of the tractor is also electrically separated from the rest of the vehicle in order to prevent electro static discharges when the vehicle is refuelled.

When it comes to lower current and/or digital signals, all ECUs have common grounding points inside the cab or in the battery box. All sensors are grounded in the ECU to which they are attached [8].

In some trucks, only one of the side rails is used as ground. This is due to packaging reasons, when the air hoses are separated from the electrical wiring.

The fact that the chassis is used as current return is investigated further in section 2.3 of this chapter.

Impedance between vehicle and earth

Although a vehicle is not mounted to the earth on which it stands, there is still an electrostatic and a highly resistive connection between the vehicle and earth [4], [66]. The electrostatic connection is constituted by a parasitic capacitance in parallel with a resistance. The impedance between the vehicle and earth can be of great importance when the vehicle for example is refueled (this will be even more important in the future with the new fuels) or located in the vicinity of an over head transmission line. In both cases mentioned, the

problem of electrostatic discharges (ESD) is the main concern, although this impedance is of importance if a full vehicle circuit model is to be built.

In the case when the vehicle is refueled, the impedance between vehicle and earth will be smaller than the impedance between the person and earth and therefore provide a ground connection for the charges that might be accumulated on a person. This means that when a person with accumulated charges on the skin comes near the vehicle, a discharge will occur from the person through the vehicle to ground. The spark that will arise during the discharge might in worst case ignite vaporized fuel and cause a fire. In the case where the vehicle is parked nearby over head transmission lines, charges might accumulate on the vehicle due to the high electric field strength between the transmission lines and the vehicle (this is mainly a concern for trucks and buses since their roofs are situated closer to the transmission lines than the roof of a passenger car). Although the impedance for a person to earth normally is higher than the impedance between the vehicle and earth, these charges might discharge through the person as well depending on the circumstances.

In this work, attempts have been made to measure the capacitance between the reference vehicle and earth. Since a heavy duty vehicle is a complex structure, it is difficult to estimate the value of this capacitance. The vehicle has a width of about 2.3 m and a length of 5.8 m when no trailer is attached. The belly clearance of the vehicle is about 30 cm at the lowest parts. If the wheels of the vehicle are neglected and the vehicle is approximated to be a plate capacitor, the capacitance will be given as

$$C = \frac{\varepsilon_0 \cdot A}{d} = \frac{\varepsilon_0 \cdot 2.3 \cdot 5.8}{0.3} \approx 0.4\ nF \qquad (2.3)$$

Where A is the area of the vehicle in square meters and d is the belly clearance in meters.

Measurements of the total capacitance

In order to measure the capacitance, a conducting ground plane is used under the tractor. This ground plane represents a situation when the tractor is driven on wet asphalt. The ground plane is made up from three lengths of galvanized chicken net, which are lashed and soldered together to form an 18 m^2 big plane. The plane is placed on a dry lawn and the tractor is placed on the plane. In order to get a galvanic contact to earth, a small area of the

lawn is watered with salt water and a brass bar is run down into the earth. The brass bar is connected to the net (Figure 2.13).

Figure 2.13. The chicken net and the brass bar are electrically connected, and the conductor that can be seen comes from the measurement equipment.

The measurements of the capacitance are performed by using an LCR-meter of type Agilent 4284A. The used cables are 1 m long, and the instrument is calibrated for the cables. The instrument is connected to the frame of the vehicle at a point on the left frame rail, behind the battery box (Figure 2.14).

In order to get a galvanic contact with the vehicle, the coating around a hole in the frame rail is removed. A fork connector is placed between a screw and the frame and crimped on to a conductor (Figure 2.14).

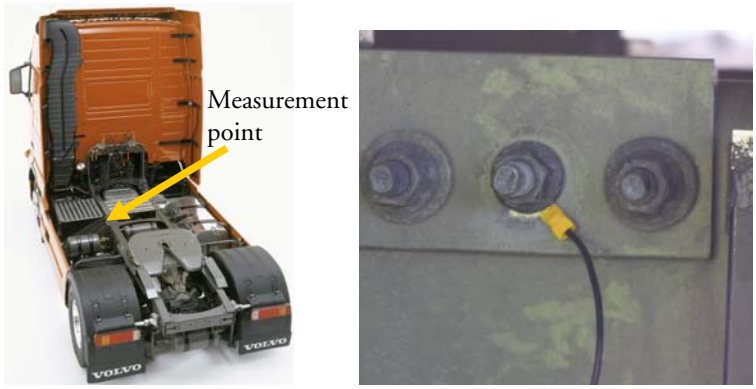

Figure 2.14. Measurement point for the capacitance between the vehicle and earth (left), and the measurement point on the frame rail in detail (right).

The capacitance is measured at 500 kHz and 1 MHz, with and without the ground plane connected to the brass bar. The results are shown in Table 2.1.

Table 2.1. Results from capacitance measurements.

Frequency	Capacitance (nF), brass bar attached	Capacitance (nF) brass bar unattached
500 kHz	4.2	4.1
1 MHz	4.4	4.3

The results in Table 2.1 shows that the brass bar only has a minor influence on the results and that the capacitance between the tractor and earth has a value of around 4 nF. These measurements are to be taken as approximate since it is very difficult to measure this capacitance. Also the situation with a conductive surface under the vehicle is an approximation. Normally, the conductance of the surface under the vehicle will vary depending on the material, where for example dry asphalt has the lowest conductivity compared to concrete and soil [4].

Capacitance for each wheel

Different metal structures in the tractor are located at different heights above the ground plane, which makes it hard to predict the average distance between the vehicle and earth for an approximation of the capacitance. The value of a capacitor is determined by the area of the plates and the distance

between the two plates, and therefore, the capacitive contribution from the tires is investigated.

Impact of the tire construction

A tire for a truck is mainly built up by rubber and metal, as can be seen in Figure 2.15.

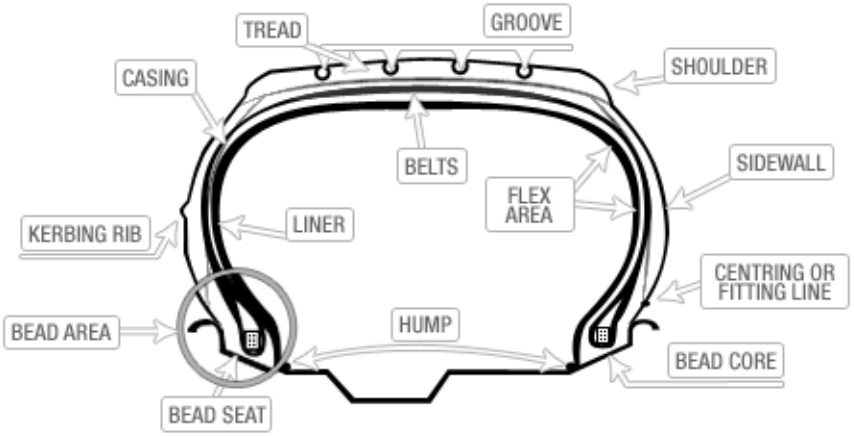

Figure 2.15. Tyre construction [60]

There are different types of rubbers in truck tyres depending on the wanted characteristics of the tyre. The types of rubber depends both on the wanted electrical characteristics of the tyre as well as the physical (handling and wear) features. A couple of years ago, the passenger cars changed the rubber mixture in the tyres from carbon black to silica. By doing this, they managed to decrease the rolling resistance with about 30%, but at the same time, the tyre stopped being conductive. There where some incidents with electrostatic discharges in the car factories before they started to ground the vehicles during the manufacturing. When it comes to tyres for trucks, the amount of silica in the tread is not as high since the trucks carries a heavier load and the owners want them to wear slowly [80]. When the truck tires are designed, the aim is to have a resistance between the tyre and ground of maximum 10 MΩ.

When looking at a cross-section of the truck tyre (Figure 2.16) it is possible to see that the tyre contains metal parts in the bead core, the belt and also the sidewalls.

Figure 2.16. Cross-section of a small part of a tyre.

The thick metal threads in the bead are not in any electrical contact with the rest of the thin metal threads in the tyre. These thin threads are also not in contact with each other in order to prevent wear. Since the threads do not have any galvanic contact, small capacitances will be present between them. The threads as well as the bead cores will have a capacitive connection to the rim. Since the threads are the metal parts of the truck that are closest to earth, they will have a large impact on the total capacitance between the vehicle and earth.

Measurement of the wheel capacitance

A truck wheel with the dimensions 225 65 R22.5 was placed on a ground plane in order to measure the capacitance (Figure 2.17). Both the ground plane and the rim of the wheel were connected to a LCR meter of type HP 4191A.

Figure 2.17. Measurement setup for determining the capacitance between one wheel and ground.

At 1 MHz, the capacitance between the wheel and ground plane is measured to be about 400 pF. Since there are six wheels (two on the front axle and four on the rear), the total capacitance between the wheels and ground will be about 2.4 nF. This implies that the capacitance between the wheels and earth constitutes almost 60% of the total capacitance between the vehicle and earth, which is reasonable due to the small distance between the belts in the tire and earth.

These values for the capacitances are highly dependent on the type of ground on which the tractor stands and also the types and ages of the tires. The capacitance values are also depending on the load on the truck since a heavy load will decrease the clearance between the vehicle and earth and also deform the tires.

Chapter 3

Crosstalk

As described in Chapter 2.1, disturbances in an automotive circuit are often coupled into the system via the conductors in the harnesses. This coupling effect is called crosstalk and will be described in this chapter.

3.1 Transmission lines

A transmission line is the medium on which energy is transmitted. In this thesis, a transmission line is typically a conductor in a vehicle transmitting energy and/or signals. Transmission lines and electromagnetic compatibility has been studied for more than half a century [50] from different point of views. In the 1950s and 60s, the main focus was on power transmission lines and how these could generate electromagnetic interferences in the frequency domain. In the 1970s, nuclear electromagnetic pulses was the great concern, and in the 1980s and forward, the high frequency content of the digital signals has been of main interest.

The transmission line model employed in this thesis contains two conductors and looks like Figure 3.1.

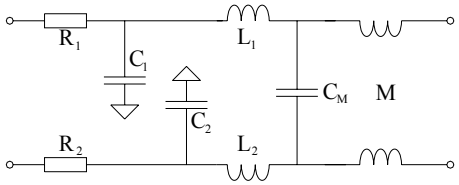

Figure 3.1. Circuit model for two conductors and their parasitic components.

where L_1 and L_2 are the self inductances of the lines, and M is the mutual

inductance between the lines. The self-partial capacitances are C_1 and C_2, and C_M is the mutual capacitance. All terms are depending on the surrounding environment and the distances between the conductors. The capacitance is also depending on the insulator material of the conductors. The resistance of the conductor, R, is depending on the conductor material, the frequency, and the cross-sectional area of the conductor. G is the conductance of the conductor, which is the term describing the conduction current flowing between two conductors due to the conductivity and permittivity of the surrounding media of the line [72]. This term is often very small (≈0) for insulated conductors.

In a model of a transmission line, the mutual inductance term, M, is modeled by using the coupling coefficient, k, which defines how much of the magnetic flux that is shared between the wires in a transmission line model. The coupling coefficient is defined as

$$k = \frac{M}{\sqrt{L_1 \cdot L_2}} \tag{3.1}$$

In the case where the transmission lines consist of two lossless transmission lines in a homogeneous medium, there is a relation between the per unit length inductance and capacitance as

$$L' \cdot C' = \mu \cdot \varepsilon = \frac{1}{\nu^2} \tag{3.2}$$

where μ is the magnetic permeability surrounding the conductors, ε is the material permittivity, and ν is the resulting velocity of the wave propagation. It is however important to remember that this relation is only valid under the circumstances described above, i.e. it will not work for most real transmission lines.

Lumped and distributed parameters

Transmission line models could either be lumped or distributed. A lumped model is suitable for an "electrical short" circuit where the length of the line is much shorter than the wavelength and the propagation velocity does not effect the behaviour of the circuit. If the frequency is high and the propagation effects are not negligible, the parameters must be distributed along the line instead of lumped together at discrete points. In this thesis, the

investigated frequency spectrum contains only so low frequencies that a lumped transmission line model is utilized. This implies that only one resistance, one capacitance and one inductance for a whole line segment is calculated and used in the circuit theory to describe the line.

General transmission line equations

A general transmission line model looks like Figure 3.2

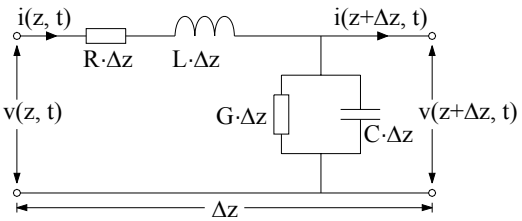

Figure 3.2. Circuit model for a two-conductor transmission line, where R is the resistance, L the inductance, G the conductance and C the capacitance. All parameter values are per-unit-length.

Applying Kirchoff's voltage and current laws to the circuit in Figure 3.2, will yield the following expression

$$u(z,t) = r\Delta z \cdot i(x+\Delta z,t) + l\Delta z \frac{\partial i(z+\Delta z,t)}{\partial t} + u(z+\Delta z,t) \tag{3.3a}$$

$$i(z,t) = g\Delta z \cdot u(z,t) + c\Delta z \frac{\partial u(z,t)}{\partial t} + i(z+\Delta z,t) \tag{3.3b}$$

Rearranging the equations will give

$$\frac{u(z,t) - u(z+\Delta z,t)}{\Delta z} = r \cdot i(x+\Delta z,t) + l \frac{\partial i(z+\Delta z,t)}{\partial t} \tag{3.4a}$$

$$\frac{i(z,t) - i(z+\Delta z,t)}{\Delta z} = g \cdot u(z,t) + c \frac{\partial u(z,t)}{\partial t} \tag{3.4b}$$

Letting $\Delta z \rightarrow 0$ will yield two differential equations as

$$\frac{\delta u}{\partial z} = -r \cdot i - l\frac{\partial i}{\partial t} \qquad (3.5a)$$

$$\frac{\delta i}{\partial z} = -g \cdot u - c\frac{\partial u}{\partial t} \qquad (3.5b)$$

These equations are often referred to as the general transmission line equations or the telegrapher's equation.

3.2 Crosstalk

Automotive harnesses are used to transmit a wide variety of signals as for example low level control signals, high current signals for electrical motors, and high frequent signals for multimedia applications. All conductors are collected to thick bundles that are routed through the vehicle. A potential problem with these harnesses is the presence of crosstalk [68].

Crosstalk is a phenomenon where a signal present on one conductor will create an undesired signal on another conductor. This unwanted signal may decrease the performance of the system by for example

- Increase the noise levels
- Create unplanned spikes
- Create jitter on data edges

Crosstalk should always be a prime suspect in an EMI investigation, or a candidate for investigation in a prediction, if high transient currents or fast rise-time voltages are present on conductors in close proximity to signal carrying conductors [79].

There are mainly three sources for crosstalk, and those are; capacitive coupling, inductive coupling, and common impedance coupling. These three coupling paths do not exist by themselves, so the system is often described by a combination.

Common impedance coupling occurs when currents from two different circuits flow through a common impedance [48], [54]. In automotive applications, this is a common problem since the chassis is often used as ground return. Since the chassis is not a solid metal part, but is built up from

many smaller parts that are spot welded or bolted together, the return path for the current in the automotive applications will contain significant impedances. The return current of different loads goes through the same ground impedances and hence will the ground potential of each load be modulated by the currents from the surrounding loads. The currents from the nearby circuits will therefore have an impact on a load. In order to manage these effects, it is important to decrease the magnitude of the common line impedance. This can be done by either attaching a separate conductor for current return or by ensuring that the different metal parts in a vehicle have good electrical contact by for example using additional ground straps.

Although common impedance coupling could cause EMC problems, this thesis will concentrate on the capacitive and inductive coupling of crosstalk. Both of these types of crosstalk are highly influenced by the conductor layout and will be described in more detail here below.

3.3 Capacitive coupling

Capacitive coupling, also known as electric coupling, is a result from the interaction of electric fields between circuits. If two conductors are placed close to each other, there will be a stray capacitance between them.

Figure 3.3 shows an example of this phenomenon and an equivalent circuit diagram.

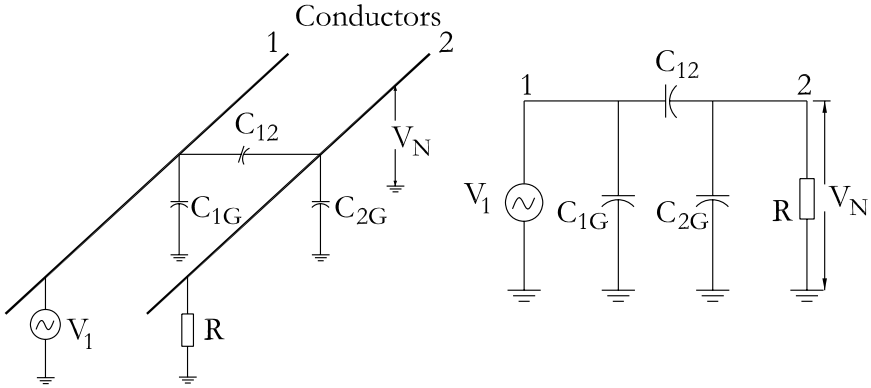

Figure 3.3. Capacitive coupling between two conductors.

Capacitance C_{12} in Figure 3.3 is the stray capacitance between the two conductors. Capacitor C_{1G} and C_{2G} are the total capacitance between each conductor and ground. The resistance, R, is the resistance of conductor 2 and ground, and is the result of the circuitry connected to this conductor. In the figure the voltage V_1 is the source of interference, and circuit 2 the receptor. The noise voltage, V_N, picked up by conductor 2 can be expressed as

$$V_N = \frac{j\omega\left[\frac{C_{12}}{C_{12}+C_{2G}}\right]}{j\omega + \frac{1}{R(C_{12}+C_{2G})}} \cdot V_1 \qquad (3.6)$$

In most practical cases the resistance R represents a much lower impedance than the impedance for the stray capacitance C_{12}+C_{2G}. Equation 3.6 could therefore be reduced to the following

$$V_N = j\omega RC_{12}V_1 = j2\pi fRC_{12}V_1 \qquad (3.7)$$

These equations show clearly how the noise voltage on conductor 2 depends on the various parameters. It can be seen in equation 3.7 that the noise voltage is directly proportional to the frequency of the noise source, the resistance R of the affected circuit to ground, the stray capacitance between the circuits and the magnitude of the source voltage. In many cases it is not possible to change the voltage or the frequency of the noise source, which leaves only two parameters to reduce the capacitive coupling. In order to decrease the resistance, R, it is necessary for the receiving circuit to work at a lower resistance level. It is in many cases easier to decrease the value of the stray capacitance since this is affected by the orientation of the conductors and shielding. If the conductors are moved farther apart, the stray capacitance will decrease. The other way to affect the stray capacitance is to use electric field shielding of the conductor. When the conductor is shielded, the length of the conductor that extends beyond the shield determines the stray capacitance, and it is therefore important to keep this length short. Also a good ground connection of the shield is necessary in order to provide a good electric field shield.

3.4 Inductive coupling

Inductive coupling, also known as magnetic coupling, is a result from the

interaction between the magnetic fields of two circuits. A magnetic flux is created when a current flows in a closed circuit. The flux is given by the current in the circuit times the inductance of the circuit. The value of the inductance is depending on the geometry of the circuit and the magnetic properties of the medium that contains the field. A current flow in one circuit may produce a magnetic field in another circuit, and the connection between these two circuits is called the mutual inductance, M.

Due to a magnetic field with the flux density $\overline{B}$, the noise voltage, V_N, induced in a loop of area $\overline{A}$ can be derived from Faraday's law as in equation 3.8

$$V_N = -\frac{d}{dt}\int_A \overline{B} \cdot d\overline{A} \qquad (3.8)$$

where $\overline{B}$ and $\overline{A}$ are vectors. For a stationary closed loop with a sinusoidally varying flux density that is constant over the loop area the expression for the noise voltage reduces to

$$V_N = j\omega BA\cos\theta \qquad (3.9)$$

where θ is the angle between the area and the magnetic flux density. Since BAcosθ represents the total flux coupled to the receptor circuit, this means that equation 3.9 can be rewritten as

$$V_N = j\omega MI_1 = M\frac{di_1}{dt} \qquad (3.10)$$

where I_1 is the current in the source circuit and M the mutual inductance between the receptor and the source circuit. Corresponding physical representation and equivalent circuit for the magnetic coupling between two circuits are shown in Figure 3.4.

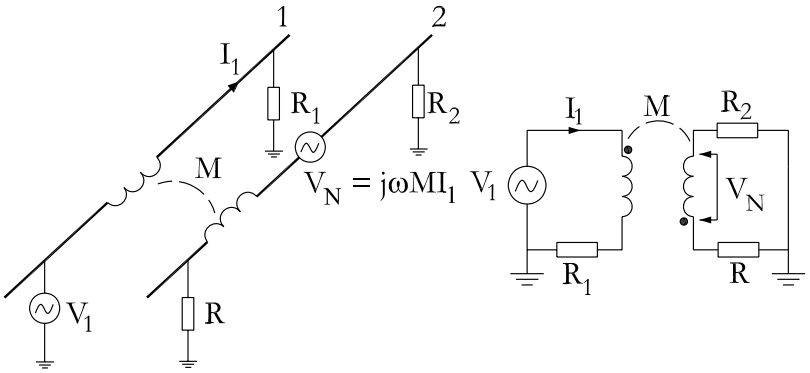

Figure 3.4. Inductive coupling between two conductors.

As can be seen in equation 3.9 and equation 3.10 the coupling between the two circuits is directly proportional to the frequency via $\omega = 2\pi f$. The three parameters which are left for reduction of the noise are the magnetic flux density, B, the loop area, A, and the angle between A and B. The magnetic flux density can be reduced by physically separating the circuits or by twisting the source wires. Twisting the wires causes a cancellation of the magnetic fields from the wires, but can also be used to decrease the area of the receiver circuit. If the return current of the receiving circuit instead is led through a ground plane, placing the conductor close to the ground plane can decrease the area. A proper orientation of the source and receiver circuits reduces the $\cos\theta$ term.

A nonmagnetic shield placed around a conductor and grounded at one end has no effect on the magnetically induced voltage in that conductor since the shield does not have any effect on the geometry or magnetic properties between the two circuits. A conductor with a nonmagnetic shield which is grounded in both ends will have a current on the shield. This shield current will decrease the H-field from the conductor.

3.5 Circuit model

Since both capacitive and inductive crosstalk are present in most circuits, a circuit model of two parallel conductors will look like Figure 3.5.

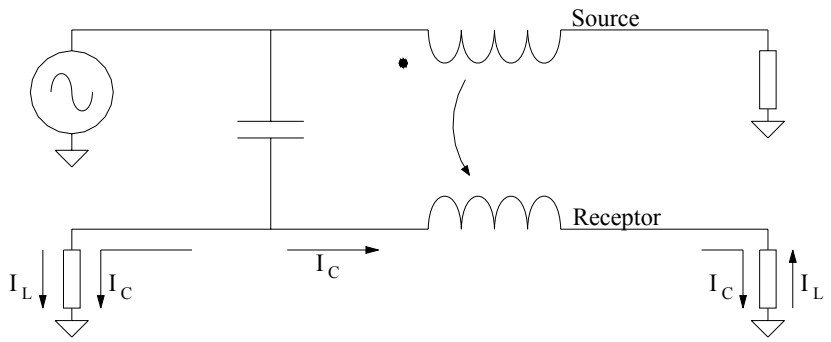

Figure 3.5. Electric field (capacitive) and magnetic field (inductive) crosstalk.

Although the mutual capacitance in Figure 3.5 is represented by only one capacitance, this is not really true. The mutual capacitance exists along both conductors and the current created in the receptor circuit by the mutual capacitance will flow in both directions with the same sign, as seen in Figure 3.5. The amplitude of the capacitively coupled voltage is defined by the value of the mutual capacitance. The mutual inductance of the circuit is to be seen as a transformer where the source conductor is the primary of the transformer and the receptor conductor is the secondary. The current induced by the mutual inductance will also flow in both directions but with opposite signs in the receptor circuit due to the induced magnetic field. This implies that the capacitive and inductively induced currents in the far end (the end that does not contain any generator) of the receptor circuit might cancel each other for a well designed circuit [28].

Building a circuit model for the transmission lines in order to investigate the crosstalk is an efficient way to examine the setup [68][51][66]. When the values for the self and mutual inductances and capacitances are determined, the model can be built according to Figure 3.1.

The model is easy to implement in circuit simulation software like SPICE, where the behaviour can be investigated. There are many advantages with a circuit model, like for example

- It is straight forward for also inexperienced persons to simulate and analyze the behaviour of the circuit

- A SPICE model does not require any expensive softwares to be

analyzed, there are for example free softwares on the Internet that can be utilized for these investigations [40]

- It is possible to investigate the circuit in both time and frequency domain

- Additional losses in the system such as pigtails on shielded conductors or resistance in connector pins are also easily incorporated in the model

When investigating the model it could be of interest to look at the different noise voltages and frequency response. The model could also provide useful information about resonance frequencies.

3.6 Dominant coupling

In most circuits, it is either the inductive coupling or the capacitive coupling between the two conductors that dominates over the other [59]. As can be seen in Figure 3.6, the dominant effect is often so much larger than the other one, that this is the most important to take care of in order to reduce crosstalk. It is therefore necessary to know which effect that is dominating.

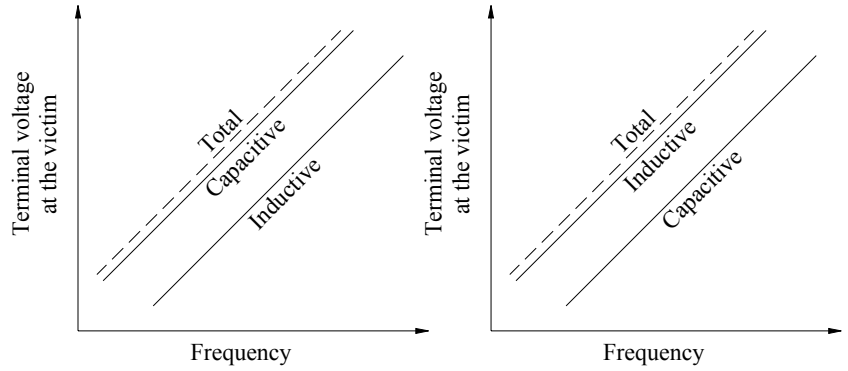

Figure 3.6. Illustration of the separation of crosstalk into inductive and capacitive components of which one is dominant [59].

A way to find out if the crosstalk is mainly capacitively or inductively coupled is to determine the characteristic impedance, Z_0, of the transmission lines. This is defined as [15][48][57]

$$Z_0 = \sqrt{\frac{L}{C}} \qquad (3.11)$$

where L is the self inductance and C the self-partial capacitance for each circuit.

If the characteristic impedance is less than the termination impedance of the circuit, the crosstalk is mainly capacitively coupled. And if the termination impedance is less than the characteristic impedance, the inductive coupling will dominate the capacitive. In other words, if the circuit contains low impedance loads, the inductive coupling must be reduced, as seen in Figure 3.6. The same holds for capacitive coupling in the case of high impedance loads.

3.7 Weak coupling

Crosstalk is an unwanted effect where two transmission lines in the vicinity of each other couple unwanted signals from one line to the other. This connection between the two lines can be more or less strong. In order to simplify calculations, it is beneficial if the coupling between two conductors is to be considered as weak [53][72], since it is then only the mutual inductance and capacitance that effects the crosstalk. When a disturbance is transmitted from one conductor to the other, it will create a signal in the receptor circuit. If the coupling is weak, this signal will not be transmitted back to the generator circuit. That is, the back interaction is negligible.

It is possible to determine if the circuits have a weak coupling by looking at the coupling coefficient

$$k = \frac{M}{\sqrt{L_1 \cdot L_2}} \qquad (3.12)$$

If the coupling coefficient in equation 3.12 is reasonably small so that

$$\sqrt{1-k^2} \cong 1 \qquad (3.13)$$

the coupling can be assumed to be weak.

Knee frequency

When a system should be designed to avoid crosstalk, it is important to analyse what frequencies that are present in the system. For systems with high frequencies using a lumped circuit model will not be enough since time delays for the signals are present in such a system. A high frequency system must be modelled by a number of cascaded models instead of one lumped model. By calculating the knee frequency for the system, it is possible to determine which frequencies that will have an effect on the crosstalk [48]. The knee frequency is given by

$$f_{knee} = \frac{0.5}{t_{rise}} \qquad (3.14)$$

Frequencies below the knee frequency are the frequencies that have high enough power to affect the operation of the circuit. The other frequencies are attenuated to such an extent that they will not influence the circuit.

Chapter 4

EMC prediction and precautions

There are different ways to deal with electromagnetic interferences and electromagnetic compatibility. One is to take care of problems when they arrive. This is the most expensive solution since it is often done late in the development phase of a product and hence not many things can be altered which implies that components, like filters, must be added. Another way that is gaining in popularity is to predict the emissions and disturbances by employing electromagnetic simulations. There are numerous ways to simulate an electromagnetic system, that all have their pros and cons. Some of the methods used will be briefly described in this chapter.

Although a product fulfills the legal demands regarding emission and immunity, it might not work in the real world and can cause functional safety failures. It is therefore a good idea to include electromagnetic compatibility in the safety life cycle of a product.

4.1 EMC modeling

For many years, electromagnetic compatibility has all been about practical rule of thumb protection, and no modeling or mathematical estimations were performed. It was primarily the development of electronics for military applications that drove the development of EMC modeling activities. Since it is such a young discipline, it is still growing due to the increasing demand for software programs for design and development of electrical devices [72].

The performance of the electromagnetic modeling tools is constantly increasing due to the growth in computer capacity and improvements of the algorithms.

When employing an electromagnetic simulation tool for analyzing the

electromagnetic interference aspects of a system, it is important to choose the right method for the problem. This is one of the largest concerns with electromagnetic modeling: no single modeling technique will be the most effective and accurate for every possible problem. Which the best method to use for a given problem is depends on the type of the solution region, initial conditions (for the time variable), and boundary conditions (for the space variable) [36].

All of the different numerical techniques have their certain types of problems where they are well suited and optimal. But on the other hand, it is possible to force in most problems into any technique. Only because it is possible to force the problem into the technique, does not say that it is appropriate. Utilization of the wrong technique will lead to extra work to create the model and the result will most likely take longer time to compute and be less accurate than if a better suited method was chosen. One example of what can happen if the wrong simulation method is employed will be shown in Chapter 4.3.

4.2 Electromagnetic simulation methods

Computational electromagnetics employs various numerical techniques. As mentioned above, the algorithms are constantly being developed wherefore new and hybrid techniques will arise. One of the first techniques that were developed was the Method of Moments that were described by Roger Harrington in 1968 [26]. After that the Finite Element Method and the Finite Different Time Domain followed [25]. In general, the available techniques can be divided into two categories, namely Differential Equation model (DE) and Integral Equation models (IE). The two classes of computation techniques can be utilized in both time and frequency domain [36]. To solve the problem, the differential equation methods uses Maxwell's curl equations or their integral counterparts whereas the integral equation methods uses Green's function for infinite medium or special boundaries [43].

In this section, some of the most common techniques and their pros and cons will be shortly described.

Method of Moments (MoM)

The method of moments, MoM, is an integral equation method based on the Green's functions. MoM solves these integrals by reducing them to a system

of linear equations. A metal object will be made up of small segments on which the current distribution is of interest. All segments will be represented in the matrix formulation and the current distribution will be found by inverting the matrix. The current distributions will be used for calculations of the impedances and near and far field [36].

MoM is a very good method for analyzing unbounded radiation problems and is suited for modeling electrically long resonant wires or other threadlike objects. It is therefore widely used in antenna and electromagnetic scattering analysis. It is also good for analysis of small metal objects.

MoM is not very well good at analyzing complex inhomogenous geometries or dielectric materials. As the number of segments increase in a model, the memory and computation time requirements will drastically increase since the matrix built up by the method is very large and dense.

Boundary Element Method (BEM)

The boundary element method, BEM, is a type of MoM where the technique is applied to solve surface equations. The difference from MoM is that its basis and weighting functions are only defined on a boundary surface. The dense matrix and the other pros and cons are the same as for the MoM.

Finite Element Method (FEM)

The Finite Element Method, FEM, is a widely used method within many different disciplines in science. One of the main reasons for the techniques popularity is its ability to deal with complex geometries, since FEM uses unstructured grids for meshing a geometry [7].

FEM requires that the entire volume of the configuration is meshed opposed to surface integral techniques where only the surfaces have to be meshed. Each element in the FEM mesh may have completely different material properties from the surrounding elements [36].

The FEM starts an analysis by subdividing the solution domain into finite elements. After that, field equations in and on each surface of each element in terms of unknown coefficients are obtained. When the equations are acquired, all elements are assembled into a matrix of equations. Finally the system of equations is solved.

The matrix created by the FEM is a sparse matrix and material boundaries are

handled efficiently. It is a good technique for modeling complex inhomogenous structures, and it provides a possibility to define the field properties of each mesh element. FEM is useful for accurately calculating scattered or radiated fields from complex 3D objects in which the geometry varies on the scale of a fraction of a wavelength. It is also suitable for parameter studies.

However, FEM is not well suited for modeling thin electrically long or resonant wires. It cannot model unbounded radiation problems as effectively as MoM since it requires that the entire volume shall be meshed. It is actually not very well suited for solving most electromagnetic interference problems.

Finite Different Time Domain (FDTD)

The Finite Different Time Domain method, FDTD, is one of the most popular time domain methods. It was originally proposed by Kane Yee in 1966, and has gained in popularity since it is simple to program, highly efficient and easily adapted to various applications [7].

The method is based on the discretization of Maxwell's two curl equations directly in time and spatial domains. It will divide the region of interest into rectangular boxes, with a size defined by the smallest detail of the configuration. Each box edge is an electric field location and the material for each edge can be specified independently of other edges [36].

The FDTD method works by taking time steps. The input to the technique are time-sampled analogue signals. At each time step, the magnetic and electric fields are calculated alternately. By doing so, the fields are propagated throughout the mesh.

FDTD is well suited for transient analysis and is good at modeling complex inhomogeneous geometries. It is also good at modeling electrically short conductors and thin metal surfaces.

The method is not well suited for modeling thin, electrically long wires or unbounded geometries. It is also not good for investigating the properties of large objects with regions that contains small complex geometries since these cases will require a large dense grid.

Partial Element Equivalent Circuit (PEEC)

The Partial Element Equivalent Circuit, PEEC, is a method that can use

either time or frequency domain and was first described in [64]. The essence of the method is to interpret all elements of a full matrix in the MoM as corresponding circuit elements [81].

The development of a PEEC model starts by discretizing the structure by placing the initial nodes [20][65]. The current and charge densities are then taken to have the same value over each cell in the mesh. This is described mathematically by defining pulse-basis functions for the conductors and dielectric materials. Finally, a mixed potential integral equation will be interpreted as Kirchoff's voltage law over each PEEC cell. The resulting terms can be described by a circuit model.

The PEEC method is well suited for investigations of printed circuit boards and the investigation of transmission lines. One of its greatest advantages is that it will produce a circuit model that can be investigated in both time and frequency domain. It does not take the air around the object into account and requires only a small amount of memory when used.

Although the integral equation approach of PEEC is often faster than a differential equation approach, it leads to fewer degrees of freedom. It is not well suited for applications where the current inside a conductor has to be resolved in detail or if there are large dielectric regions, since the degrees of freedom will increase and make the method unnecessary slow.

Hybrid methods

Since no electromagnetic modeling technique is a universal solution to all problems, a number of hybrid methods have arised. Most hybrid methods combine two techniques into one code that will be able to model problems that one technique alone would not be able to. Each technique is then applied to the region of the problem where it is best suited.

Usually surface integrals methods such as MoM or BEM will be combined with a finite method such as FEM or FDTD [36]. Combining FEM with MoM will for example give a method capable of modeling radiation conditions. Although both FEM and FDTD are finite methods, a combination of them will provide a method suitable when small details are present in a problem where the wave propagation shall be investigated.

4.3 EMC simulations in the automotive industry

One of the major challenges when it comes to EMC simulations in vehicle applications is to be able to deal with very different relevant geometric scales [10]. In Figure 4.1, a model of a quarter of a tractor is shown. It is the rear axle with the frame rail in which a conductor is placed. Efforts where done to try to simulate this model with a Finite Element Method solver. It was not possible to mesh or analyze the model until the cross-sectional area of the conductor was enlarged ten times and the current carrying part in the conductor was approximated by a square.

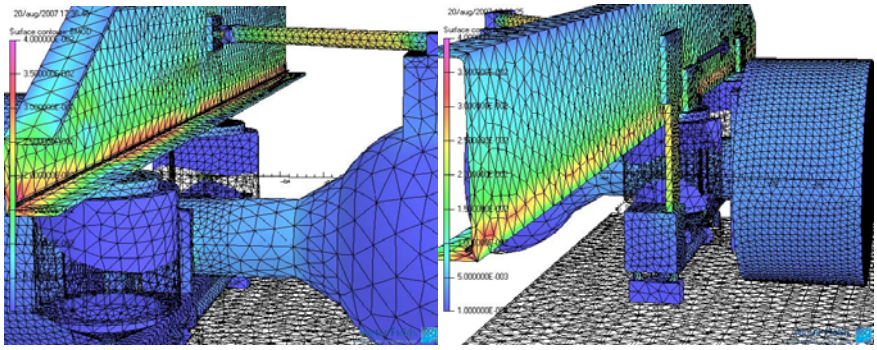

Figure 4.1. Magnetostatic FEM model of the rear axle of a heavy duty vehicle. A current carrying conductor is located in the frame rail.

This is one example of how inadequate the simulation results might be if an inappropriate simulation tool is used.

Numerical predictions of EMC in vehicles are often divided into two separate parts; device level and vehicle level simulations [14]. At the device level, the simulations calculate the total or equivalent interference currents produced by one of the electronic devices in the vehicle, and at the vehicle level, the simulations handles the interference currents transmission to the vehicle body and surrounding devices via crosstalk on the harness. When the investigations are divided like this it is possible to overcome some of the difficulties regarding the different sizes of the objects since it might be a good enough solution to overlook some of the smaller parts at vehicle level simulation.

The model building for EMC simulations in the automotive industry may not take more than a couple of minutes. Since a vehicle body is a rather

complex structure, it is important to maximize the synergy effects between different CAD/CAE groups [21]. Most electromagnetic simulation softwares start the analysis of a model by building up a mesh. Meshes are also used for mechanical analysis of for example the vehicle body, and the idea is that this mesh could serve as a base for electromagnetic simulations. The mechanical analyses are often carried out in some kind of FEM analysis tool and since FEM contains sparse equation systems, the calculation models of a vehicle can contain as much as 400'000 mesh elements. As seen above, FEM is not the best choice for electromagnetic simulations on vehicle level, where MoM or a hybrid version of MoM is more suitable. Since MoM contains a much more dense equation system, the number of unknowns has to be smaller, and in the order of 10'000-50'000 triangular elements. Reducing the number of triangular elements without loosing any important information can be rather time consuming. There are available software programs, as for example EMC studios [10][21], that could be employed in order to facilitate this. When the number of triangular elements is decreased, the model is still not ready for electromagnetic simulations, and the next step is to remove all redundant surfaces and make sure that parts that for example are welded together are represented by a solid piece. When this is done, the model is ready to use for EMC simulations. It could be good to generate a number of models for different frequency areas. Low frequency models, for example, require fewer triangular elements (with larger size), and are therefore faster to use than a high frequency model.

When the model of the vehicle is created, it is important to remember that the accuracy of the simulation results does not only depend on the model of the vehicle body, but also the model of the cable harnesses, and the models for ICs and electronics at equipment level [46][18]. To model these accurately is not a problem that is specific for the automotive industry, but something that most industries are working with. It is therefore easier to find an available commercial software programs. In the project COSIME [18], the responsibility for developing satisfactory models of the integrated circuits was taken by the manufacturers of the circuits.

There are three problems of major interest in automotive EMC that often are simulated, and that is

- Crosstalk that is simulated by using a transmission line model and a network simulator

- Emissions from the harnesses to the surrounding environment including antennas that are investigated by using transmission line models, a network simulator and a field solver in that order

- Immunity of the equipment that is simulated by using the same tools as in the emission case, but in the opposite direction, that is, first a field solver, then a transmission line solver and finally a network simulator

4.4 Crosstalk prediction

A straight forward and efficient analysis of crosstalk in a circuit is to make a circuit model with the conductors of interest. This can be done when the parameters (self and mutual inductances and capacitances) of the conductors are determined.

The parameters can be determined by using electromagnetic modeling as mentioned above. Suitable techniques are for example the MoM or the PEEC method where the latter is actually solved in the circuit domain [69]. When the parameters are determined, a circuit model is built in a circuit simulator software as for example SPICE or Saber.

Some benefits of performing the crosstalk investigation in a circuit model is that it is intuitive for most electrical engineers and that it is possible to investigate the circuit in both time and frequency domain, as mentioned in Chapter 3.5.

4.5 Safety Analysis

Up until here, this thesis has focused on common EMC problems in the automotive industry and how to predict these in order to handle them. All of this work is essential and the predictions are a good way to decrease both the time to market and the development costs. But even though a vehicle is very thoroughly simulated and investigated before going into production, there are still no guarantees that the vehicle will work properly when out on the road.

Since a vehicle is inherently mobile, it is impossible to fully predict the disturbances to which it might be exposed. Although the importance of keeping the vehicle in a safe state when an electromagnetic interference occurs, many of the vehicle manufacturers do not give the highest priority to

mandatory requirements, but instead product reliability and quality, which then becomes the driving force behind safety issues of the vehicle [34]. Some of the reasons behind this prioritising are mentioned in the following list:

- Around 45 000 deaths are caused on EU roads each year and not one of these has ever been claimed to be descended from an EMC problem. Most accidents are caused by driver arrogance, incompetence and error.

- Currently, the most likely cause of an accident when using a car telephone while driving is lack of concentration and not EMC, but the scenario may change as the vehicle complexity increases.

- On-board radio reception quality is often the driving force behind emissions reduction.

In the next few years, the importance of the electromagnetic environment within a vehicle will increase since fully electronically controlled and powered braking, steering and anti-collision systems are likely to be introduced. These new electronic safety systems will provide enhanced primary and secondary safety (safety systems that are active before and during/after an accident) to the passengers, but at the same time introduce safety critical electronic systems. Many of these future systems are often more or less depending on each other. It has turned out that safety of the systems is one of the key issues of future automobile development, which implies the importance for the vehicle manufacturer to be able to prove that the systems are safe in a way that they neither will put the driver nor the vehicle in any dangerous states due to implementation or operational errors.

It is important to try to take into account all possible and foreseeable use and misuse cases when testing a product since all electronic technologies are inherently prone to suffering from inaccuracy, malfunction or even permanent damaging when exposed to electromagnetic disturbances. The safety directives from the European Union regarding CE marking are “total safety” directives, which means that they cover all functional safety problems caused by electromagnetic interference but they do not say how this should be accomplished [4]. The EMC directive and its standards do not cover safety issues and the IEC 61508 (which is a basic IEC standard for functional safety in electrical/electronic/programmable electronic systems) requires EMC to be taken into account but does not say how it should be done. This leaves a

great gap in the control of an increasingly important safety issue [34].

Functional safety

In safety analysis, there is a term named functional safety. For a vehicle, this term can be defined as:

"Safety that the vehicle function does not cause any intolerable endangering states"

which implies that the vehicle has to be fail-safe.

Up until now, the IEC (International Electrotechnical Commission) meta-standard 61508 has been the only available standard for proving functional safety in the automotive industry. In IEC 61508, the term functional safety is defined as [32]:

"part of the overall safety relating to the equipment under consideration (EUC) and the EUC control system which depends on the correct functioning of the electrical/electronic/programmable electronic safety-related systems, other technology safety-related systems and external risk reduction facilities"

IEC 61508 is a well known industry standard implemented in the automation and process industry, which addresses functional safety of electrical/electronic/programmable electronic (E/E/PE) safety-related systems. This is a meta-standard, which means that it is intended to provide a basis for different sector specific standards or, in those cases where no sector specific standard exists, a direct use. Since there is no sector specific standard regarding functional safety for the automotive industry, IEC 61508 has been employed. However, the use of IEC 61508 for automotive applications is not totally problem-free. Some of the drawbacks when employing IEC 61508 in the automotive industry are mentioned in [2].

ISO 26262

The IEC only handles standards for E/E/PE systems. Since most safety-related systems in a vehicle rely on different technologies (e.g. mechanical, pneumatic, E/E/PE), a safety strategy for a vehicle must consider not only all the elements within an individual system but also all the safety-related systems making up the total functionality.

In order to adapt the IEC 61508 to the automotive industry, ISO has put together a new working group in the road vehicle technical committee that is

preparing a new standard (ISO 26262). ISO 26262 exists today as a committee draft and is available for the public. It will become a standard in 2010-2011 and the first vehicles that will be developed following the ISO 26262 will probably be available 2015-2020.

EMC and functional safety

The existing automotive EMC directive does not treat functional safety satisfactorily. This means that the directive is inadequate from a safety point of view in that:

- It does not fully cover the fitting of after-market equipment including mobile transmitters
- Its tests are limited rather than thorough
- Radiated immunity tests are only carried out at steady state speed, and does not test for dynamic situations (such as changing gear or unlocking the vehicle)
- It does not include transient requirements and does not adequately cover after-market products and their potential to interfere with OEM systems

When testing the immunity to electromagnetic disturbances for a vehicle the result will actually not prove that an acceptable level of EMC-related functional safety performance has been achieved. This is since the traditional approach taken by the EMC testing community is quite different from the approach taken by the safety community. There are a number of reasons why traditional EMC testing is inadequate to ensure functional safety [4] of which some are presented here;

- Immunity testing only covers one electromagnetic disturbance at a time
- Immunity tests do not simulate real-life exposure
- Effects of the physical environment on electromagnetic performance is not investigated
- An EMC “risk analysis” is not done

- Foreseeable faults/misuse are not addressed by immunity testing

When the vehicle is produced and put on the road, it will encounter by far worse situation then the environment within the controlled chamber in which the vehicle has been tested and approved. In the real outdoor environment, the vehicle is exposed to more than one electromagnetic disturbance at a time. There could for example be a radar unit near the road where the vehicle travels and at the same time that another vehicle, driven by a radio amateur, on the road is transmitting a radio message. According to the EMC tests, the vehicle should be able to cope with these disturbance one at a time, but when they arise simultaneously one of the electromagnetic disturbances consumes most of the noise margin in the vehicle's system. Consequently, when more than one disturbance is present, also even very low level disturbances could cause malfunctions. The surrounding physical environment is also different on the road compared to a semi anechoic chamber. On the road there are different surfaces that more or less effectively reflect electromagnetic fields.

EMC testing

The standards used as a frame for the EMC testing only attempts to cover a typical electromagnetic environment and do not cover any low probability electromagnetic disturbances, which could affect the functional safety of the vehicle. It is therefore important to make an EMC risk analysis in order to find out what electromagnetic disturbances the vehicle could be exposed to. Furthermore, there are no demands on testing the immunity of the vehicle when any commonplace electric faults are present in the vehicle. These faults could for example be a short circuit in for example a filter, loose fixings in an enclosure or cable shielding assembly or a missing conductive gasket. Only one of these faults does not affect the performance of the vehicle, but it could seriously affect the behaviour against electromagnetic disturbances of the vehicle.

When it comes to cable harnesses that is one of the main topics of this thesis, the EMC standards specify specific standard lengths of the cables for test purposes. The standard CISPR 25 [12] suggests up to 2 m (1.5 m recommended) harness length for radiated emissions tests, and 0.2 m for conducted emissions tests. These lengths make comparisons easy between different products, but they do not reflect the reality. In a vehicle it is not uncommon to find automotive harnesses with lengths of up to 10 m.

CISPR 25 do prescribe two different lengths of the cable harnesses (1.5 m and 0.2 m respectively), but these differences does not give any input to a comparison of the effect from the harness length since the two lengths are for different tests (radiated and conducted). In practice, the harnesses will never be as short as the CISPR 25 suggests, and according to the results in [47] resonances at other harness lengths may appear. The test results for compliance testing to CISPR 25 are therefore to be considered as guidance only and untypical of what will be expected in a real vehicle.

Whether a test of the immunity of the vehicle should be included in an EMC standard or in a safety standard is dependent on the approval criterion. The test should be included in an EMC immunity standard if it is required that during or after the test the vehicle or the equipment mounted to the vehicle should continue to operate as intended. If it is required that no unsafe situations occur (but the performance may be degraded incidentally or permanently) during or after the test, the test should be included in a safety standard.

EMC and safety life cycle

The framework of a safety standard including all safety activities from the concept phase to decommissioning is the safety life cycle. In the safety life cycle, the safety analysis forms the basis for the specification of the safety requirements and the safety validation is performed before commissioning. In order to achieve functional safety, EMC aspects should be considered throughout the life cycle of the vehicle. A safety life cycle for a vehicle is shown in Figure 4.2 [31]

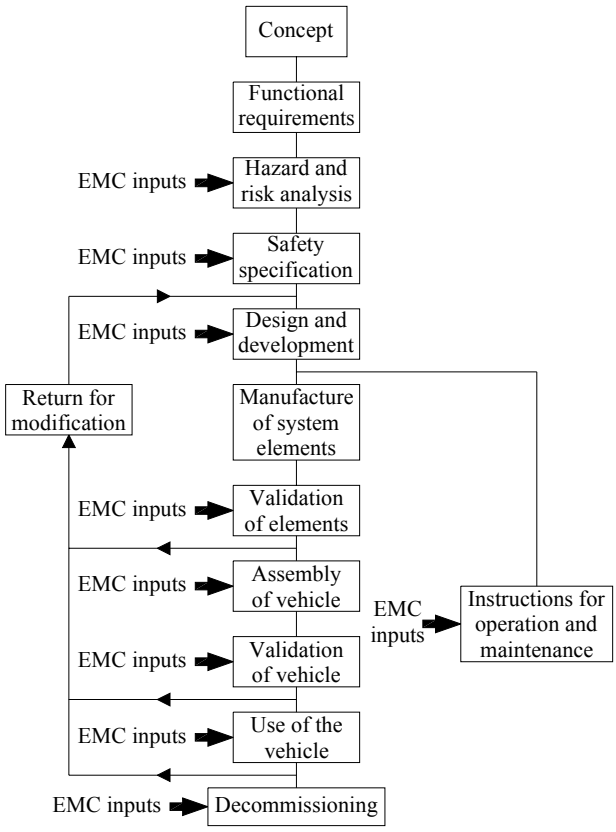

Figure 4.2. Safety life cycle with EMC inputs.

The specific actions that should be undertaken in the safety life cycle in order to achieve functional safety with regard to electromagnetic influences starts with a definition of the structure, design and the intended functions of the vehicle. It is then important to describe the relevant electromagnetic environment for the vehicle. There are some electromagnetic phenomena which occur infrequently and that are not mentioned in the standards but should still be considered in some cases. An example of such phenomena is the conducted or radiated disturbances in the frequency range below 150 kHz. When the electromagnetic environment is described, the safety requirements and failure criteria should be specified. This implies that some

aspects of performance of the vehicle in the presence of electromagnetic disturbances have to be considered. Firstly, the functional safety of the equipment in the vehicle or the vehicle it self shall not be unduly affected by the electromagnetic environment in the place where the equipment is used. Secondly, any electromagnetic disturbances generated in a system or vehicle shall not unduly affect the functional safety of other parts in the system or vehicle.

It is important to perform a dependability analysis in order to identify the hazards, which can cause safety risks due to electromagnetic disturbances. The hazards should be identified in terms of events and the corresponding parts of the vehicle. The methods for identifying the hazards are in general based on two principles; bottom-up or top-down methodologies. Some of these principles will be described more in detail below. When the different hazards are identified, it is time to perform EMC tests for safety. EMC tests for functional safety require special considerations regarding selection of types of immunity tests and testing levels. When the EMC tests are performed the design and installation measures may have to be modified in order to reduce the risks to acceptable values. The final design has to be validated in order to prove that the vehicle performs accordingly to the specified safety requirements.

It is also important to produce operation and maintenance instructions to ensure the specified functional safety in the products life cycle.

Analysis methods for EMC and functional safety

In order to correctly control EMC-related functional safety for the vehicle, hazard and risk assessments are needed. During this work, the following issues should be considered [34]:

- What electromagnetic disturbances, although infrequent, might the vehicle be exposed to?

- What are the reasonably foreseeable effects of such disturbances on the vehicle?

- How might the electromagnetic disturbances emitted by the vehicle affect the surrounding environment?

- What could be the reasonably foreseeable effects of the above

mentioned disturbances?

- What level of confidence or proof is required to show that the above mentioned issues have been fully considered and all necessary actions have been taken to achieve the desired level of safety?

Some of the methods used for proving functional safety could be very useful for determining possible weaknesses of the vehicle to electromagnetic disturbances [24]. Fault tree analysis is one example of a method that could be used in order to find out weak spots in the vehicle and give some input on how to test for EMC immunity of the vehicle. The fault tree analysis method will be described more in detail later. It is important that the method chosen for analysis is able to model the behaviour of the system or vehicle in presence of electromagnetic disturbances which are likely to be present in the intended environment. It is especially important that the analysis method is able to handle the fact that the electromagnetic disturbances often have different or over time varying characteristics.

As mentioned above, most methods for reliability studies are based on two principles; bottom-up or top-down.

Bottom-up methodology

The bottom-up, or inductive, methodology emanates from component level and will show the effect from different individual components in the system. One common method that uses the bottom-up methodology is fault modes and effects analysis [22].

Fault Modes and Effects Analysis (FMEA)

The FMEA is an analysis method that was originally aiming on predicting reliability in systems and the purpose of the method is to systematically eliminate identified failures within a component. The technique behind FMEA is quantitative since each identified failure mode is assigned a probability. The advantage with the method is that the analysis will be very detailed at a component level which could be used to identify single faults or the need for changes in the design as implementing redundancy or fail safe technology.

An FMEA could be performed using a hardware approach or a functional approach. The hardware approach considers the failure modes of identifiable

items of the hardware. The hardware approach focus on the effects from a failure of each component since it is normally not considered as an appropriate approach when analysing the effects from electromagnetic interferences. Effects from electromagnetic interferences are usually a result from disturbances in the operating conditions (currents and voltages) of components rather than failures of components, themselves.

The functional approach of an FMEA is on the other hand a more appropriate method for investigating the effects of electromagnetic disturbances. With the functional approach, the method asks the question "In what ways can this function deviate from the specified requirement?". This approach identifies the more critical functions and will therefore require a higher level of immunity.

When an FMEA is conducted, the work is emanated from a scheme showing how the component or function is connected to the rest of the system. Different failure modes are identified and an FMEA chart is filled in. In the FMEA chart, the causes and effects of each failure mode are analysed. An analysis of the critical behaviours is performed and the behaviour of the vehicle when the different faults are present is stipulated and actions are taken in order to compensate the various failure modes. This process is repeated after every change in the system.

However, a bottom-up methodology will overlook interacting contributions from different components. Since the bottom-up methodology considers all fault modes, including fault modes not relevant to electromagnetic disturbances, this will be an unnecessarily extensive and complicated method for complex systems, such as a vehicle.

Top-down methodology

The top-down, or deductive, methodology is an event-oriented method, which allows the user to identify the responsible system levels and components for each specified top event. The user starts with a top event at the highest level of interest and works down to the level where the undesirable system operation occurs. The most well known top-down method is the fault tree analysis, which offers some advantages with regard to EMC.

Fault Tree Analysis (FTA)

The fault tree analysis method was first used in 1962 by Bell Telephone Laboratories in connection with the safety analysis of the Minuteman missile launch control system. The method was later improved by Boeing Company and is today a well known method for analysis of a system.

An FTA emanates from an unwanted event (also called top-event) which is investigated in order to find possible causes. When the possible causes for the top-event are found, the causes for these causes are investigated. Finally a logical tree which starts on a system level and works its way down to the primary causes is constructed.

Interacting, independent causes in the fault tree will be expressed by "and"-gates and alternative causes will be expressed by "or"-gates, see Figure 4.3.

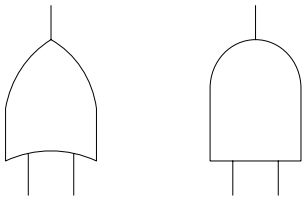

Figure 4.3. To the left, an or-gate and to the right an and-gate.

The or-gates are the most critical parts and has to be taken care of first since they correspond to added probabilities for the fault causes and thereby an increased risk. This is particularly important if there is a way through the tree that only consists of or-gates. In this case, a single fault will cause the top-event, and this is seldom tolerable. The strength of an FTA is that it is a structured search for causes to a specific event with the purpose to eliminate safety threats.

When an FTA should be performed with the intention to carry out an EMC analysis the work starts with a definition of the system that should be investigated and the electromagnetic environment to which the system is exposed. Before a fault tree can be built, all undesirable safety events have to be specified. Most of the events can be found as hazards from the hazard analysis that is carried out on the system. These events often involve no

operation, unwanted operations or wrong operations from the system. This will then serve as top-events in the fault tree analysis. On the next level beneath the top event are the first level events, which are events that together (and-gate) or separately (or-gate) could cause the top-event. Beneath the first level events are the second level events, which as in the case with the top-event and first level events are the events that could cause the first level event to happen. The analysis continues with several levels until the base events (leafs) are found (See Figure 4.4). In the case where the FTA method is used for analysing the circuit from an EMC point of view, electromagnetic disturbances are considered as base events.

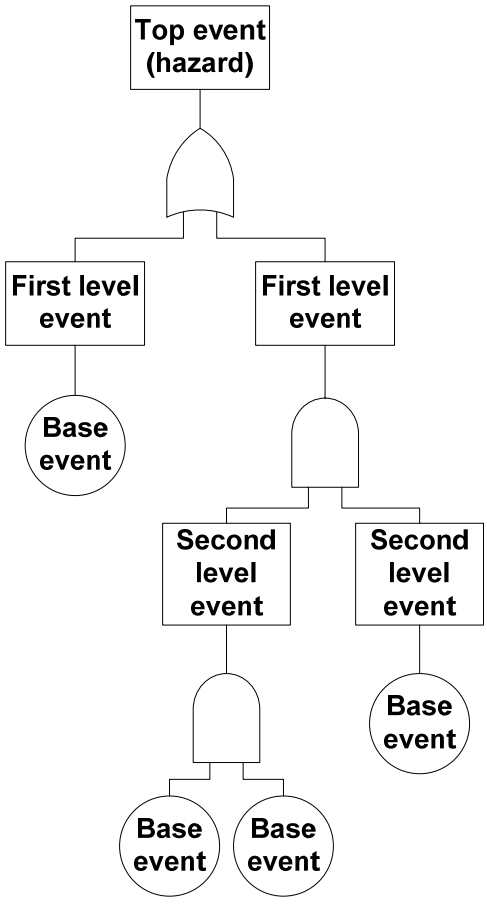

Figure 4.4. Example of a fault tree

For a large system such as a vehicle the fault trees are often many, large and complex. It is therefore important to limit the FTA to safety critical top-events. The results from the FTA could be used to find different cases that ought to be tested in order to provoke a wanted top-event.

There are some advantages when using fault tree analysis for evaluating EMC. The method can handle both common cause failures and time varying failure rates which is important when the behaviour during the presence of electromagnetic disturbances in a vehicle is analyzed. Another advantage is that the events in an FTA analysis are not limited only to faults, but could also involve degradation in performance. When a fault tree is constructed, it is possible to calculate probabilities using Boolean algebra.

The key advantage of FTA is that it only requires consideration of those parts of the equipment or system which can contribute to hazards. This advantage makes the method economical.

There are of course other top-down techniques with the same purposes as FTA; such as dependability diagrams and Markov analysis.

EMC testing from a functional safety point of view

As mentioned above, a normal EMC test is often not sufficient to prove functional safety for a vehicle. The test levels in the immunity tests often have to be increased in order to simulate the actual electromagnetic environment that the vehicle will be exposed to when it is out on the roads. This implies that the product committees or manufacturers have to specify the maximum levels likely to occur in the environments where it is expected that the vehicle will operate. It is also necessary to take the statistical distribution into account together with the possible consequences of failures in terms of degree of injury or harm to health.

It is important to perform the tests at the highest degree of integration as possible, which in the case of a vehicle means that the whole vehicle should be tested. Due to the complexity of a system or software malfunction in a vehicle it is recommended that the vehicle is in operation during the test and should also be put into different dynamic situations to as large extent as possible.

When preparing a test plan for a vehicle regarding functional safety the focus

should be on the undesirable events in both software and hardware that have been identified in the previous analyses. It may also be of importance to force the vehicle to malfunction during the tests. In this way it is possible to determine whether and how it creates safety hazards when subjected to extremes of the electromagnetic environment. Testing under fault conditions, i.e. testing with a fault deliberately introduced in the vehicle is not required in any EMC standards, but may be useful in a safety standard in order to check the behaviour of the vehicle after a possible degradation of its parts or components.

When the vehicle is tested, all malfunctions involving safety risks should be carefully evaluated and particularly the behaviour of safety-related elements and fail safe modes should be studied.

As described in this section, it is not possible to verify EMC-related aspects of functional safety by using normal EMC test methods. If it would be possible, it would cost more and take longer time than any manufacturer could possibly afford. This problem has already been dealt with using safety-related software. Since it is impractical to prove such software by testing it, software engineers all over the world have devised and validated design methods that will help them to achieve the required levels of safety integrity. The same thing has to be done for EMC testing.

Chapter 5

Problem Formulation

In this chapter, the investigated problem will be formulated. Some background information will be provided and the five cases that will be investigated through the rest of the thesis will be described in detail.

5.1 Background

There are many automotive electrical engineers all over the world that on a daily basis struggle towards an interference free environment within the vehicles. Many of these engineers wish that they would have some easy guidelines to follow when designing a new vehicle. These guidelines should not only be applicable to various kinds of setups but also guarantee that no electromagnetic interferences will arise.

If it were possible to write down such guidelines, they would have existed for decades. There are general non-automotive EMC guidelines that one could follow [3], but in most cases, the demands from the automotive industry will not make these guidelines applicable.

For example, when it comes to cable harnesses, a cable harness must be as flexible as possible, as light as possible, and as cheap as possible why generally single wires or twisted pairs are used rather than shielded or coaxial cables. In addition, many other compromises have to be done since the mechanical structures of the vehicles will put constraints on the cable routing [74].

Objectives

Since no general guidelines are available, the trend within the automotive industry has up until now been towards relying on the know-how from the EMC experts and/or attach a couple of decoupling capacitors or filter and/or

cross the fingers and hope that the solution will work from the very beginning without any late and expensive changes. There are many very skilled EMC experts in the automotive industry, but since the amount of electronics is increasing in the vehicle, they can not handle all problems that will arise. It is therefore important that all electronics engineers become aware of the EMC issues, and how to solve them.

A set of general guidelines might be a dream to many, but the belief of the author of this thesis is that knowledge is far more important. So, if an electronics design engineer chooses to mount a conductor close to the chassis, the aim is to make the engineer aware of why it should be done this way. The intention of this thesis could therefore be summarized by the following sentence:

Instead of knowing only WHAT to do,
the aim is also to know WHY to do it!

How to gain knowledge

There are different ways to learn why to design for example a cable layout in a specific way. One is to build a prototype and test. This is a rather time consuming experiment, that also could be costly due to the need for prototypes and measurement equipment.

Another way of learning is to simulate the setup. As mentioned in Chapter 4.2, there are numerous simulation methods and tools that could be utilized for this. The advantage with a simulation model is that once it is built, it is often rather easy to change the settings or layout and thereby investigate the behaviour. The problem with simulations is that many simulation tools can be rather costly, demands much computing power and are not always very user friendly [44]. If the aim is to simulate a complete vehicle, there is quite a lot work involved before acquiring a model that is appropriate and in a suitable format.

A third way is to understand the physics behind the phenomena. This can be done by evaluating the system analytically by calculations. The final equations describing the system will give a good hint about what will happen with the different parasitic components when the conductor layout is altered.

In this thesis, a common setup for heavy duty vehicles is investigated. Two

conductors are routed in a U-shaped channel, and the parasitic components are determined. It will be shown that it is possible to calculate the parameters analytically either quite accurate or more approximate. The approximate calculations will be shown to be good enough to get an apprehension about the crosstalk, and how it is possible to change the characteristics by altering the conductor layout. The calculated values are compared to simulated values in Chapter 7 and measured values in Chapter 8.

5.2 Investigated setup

Most heavy duty vehicles have two U-channels along the vehicle that together with cross members serves as frame rails (see Figure 5.1).

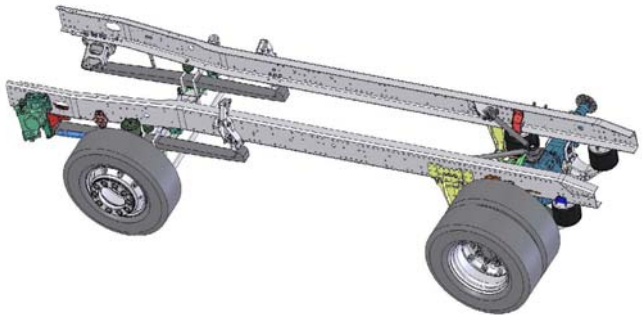

Figure 5.1. Frame rails on a heavy duty vehicle together with rear- and front axles and suspensions.

It is common to place all conductors and air hoses in these frame rails since they will be well protected from environmental and mechanical wear. A typical example of this is shown in Figure 5.2.

In this thesis, one of these frame rails from a truck is used for investigation. Two conductors are located inside the frame, one for communication and one for battery voltage. This setup is utilized to determine the parasitic components of the setup and investigate possible crosstalk.

Figure 5.2. Frame rail and conductor layout. Picture from [76].

Conductor types

Two types of conductors are utilized in the layouts. A thin conductor intended for communication, and a thicker conductor intended for voltage feed of electrical loads are employed.

The thin physical conductor is of type MKUX, and consists of a tinned annealed copper bunch with a PVC (polyvinyl chloride) insulation. The copper bunch has a cross-sectional area of 0.5 mm^2 and the PVC insulation is 0.7 mm thick [17]. In automotive setups, this type of conductor is used for CAN communication and is mostly twisted pairs.

The thicker conductor has a plain annealed copper bunch with a cross-sectional area of 6 mm^2 and a PVC insulation that has an average thickness of 0.76 mm [61].

The PVC insulation on both cables are assumed to be of wire grade, and the dielectric constant (permittivity) is therefore set to be 3.8 [42].

Ground Structure

In the investigated setups, a U-shaped frame rail is employed as ground structure. It is made of high strength hot rolled steel. A cross-section of the channel is shown in Figure 5.3.

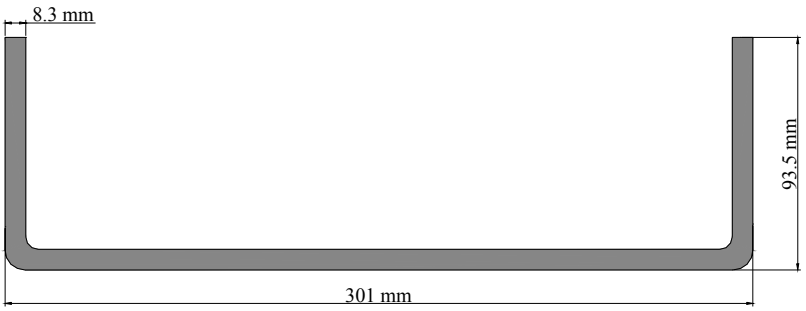

Figure 5.3. Cross-section of the U-channel used in the investigations.

5.3 Conductor layouts

In this thesis, five different conductor layouts are investigated. These layouts are employed in the analytical analysis, the simulation models and the measurements. The different conductor layouts are chosen with the intention to illustrate how the parasitic components are affected by the geometrical properties.

Case 1, Single conductor

In the first case, one single communication conductor is used. The conductor is placed 10 mm from both the vertical and the horizontal part of the ground structure, as shown in Figure 5.4.

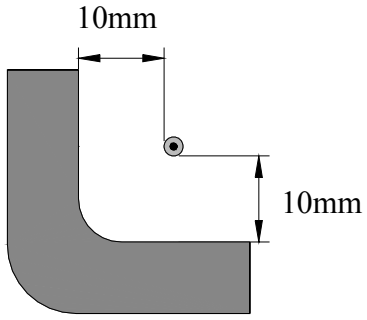

Figure 5.4. Conductor layout, Case 1.

This case is the simplest one of the investigated cases. It is constructed to serve as an easy basic layout with only one conductor.

Case 2, Two conductors together, close to ground

In the second case, both conductors are present. They are placed tight together and close to the ground structure as shown in Figure 5.5.

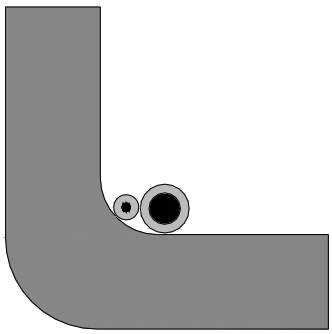

Figure 5.5. Conductor layout, Case 2.

Case 2 is intended to represent a case where both conductors are clamped to the frame. This is not likely to be a real case, but it is important since it will show what happens if the designer tries to keep all conductors as close to the frame as possible.

Case 3, Two conductors together, away from ground

In Case 3, the two conductors are situated 5 mm above the ground structure and 5 mm from the vertical part of the ground structure. The conductors are routed close to each other as shown in Figure 5.6.

Case 3 is the case that is closest to reality since the cable harnesses in the vehicle often are attached to the frame by plastic clips and there will be a distance between the conductor and the frame.

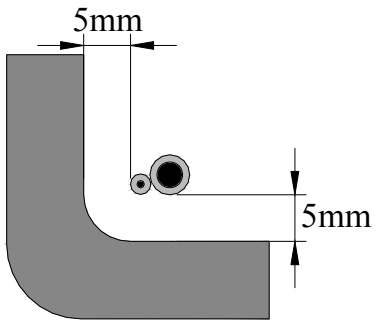

Figure 5.6. Conductor layout, Case 3.

Case 4, Two conductors apart, one close to ground

The layout of Case 4 looks like Figure 5.7. One conductor is placed close to the ground structure and the other conductor is placed 5 mm up and 5 mm out.

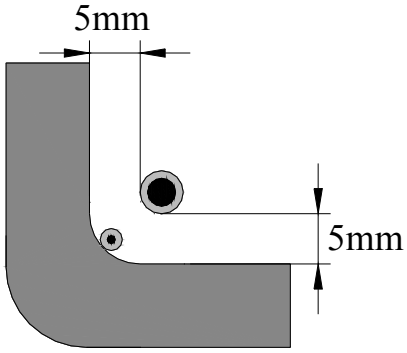

Figure 5.7. Conductor layout, Case 4.

Case 4 is a case that is constructed to show what happens if the conductors are separated and one conductor is close to the ground structure. The ground structure will partly serve as a shield.

Case 5, Two conductors apart, away from ground

In the last case, the two conductors are placed 6 mm apart and 5 mm above the ground structure. The innermost conductor is situated 5 mm from the

vertical part of the ground structure as shown in Figure 5.8.

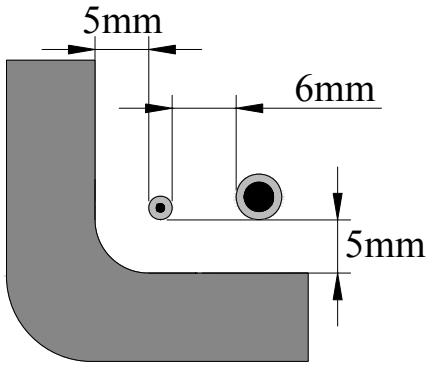

Figure 5.8. Conductor layout, Case 5.

In Case 5 are the conductors routed as if they were both parts of a real cable harness but located at a distance of 6 mm away from each other.

Chapter 6

Analytical Investigation

The behaviour of the crosstalk between the cables is depending on the parasitic components, which are influenced by physical characteristics. In this chapter, the different conductor layouts are investigated by using electromagnetic theory and a method for estimation of the parasitic components is proposed.

6.1 Theoretical Background

In order to determine the parasitic components for a conductor, electromagnetic theory is applied on the setup of interest. The goal is to build a circuit model of the conductors in order to simulate the behavior of the setup. These transmission line models are then used for investigating the severity and occurrence of crosstalk.

Model

In order to determine the parameters, a two dimensional electromagnetic model of the problem is set up. Since the conductors are shaped as long narrow cylinders, and the charge is spread over the length of these, line charges are used in the model to represent the conductors.

The ground structure is made of high-strength steel, and is assumed to have a conductivity of 10 MS/m. For the lowest frequency in the investigated frequency spectrum (10 kHz), the skin depth according to [15] is:

$$\delta = \frac{1}{\sqrt{\pi \cdot f \cdot \mu \cdot \sigma}} = \frac{1}{\sqrt{\pi \cdot 10 \cdot 10^{3} \cdot 4 \cdot \pi \cdot 10^{-7} \cdot 10 \cdot 10^{6}}} = 1.59\ mm \qquad (6.1)$$

Since the ground structure is expected to have a high conductivity, it is

approximated by a thin, perfectly conducting ground plane in the calculations.

Method of images

The method of images is a method for solving electrostatic problems by inserting image charges into a problem where a charge is located in the vicinity of a ground plane. By inserting these image charges, the boundary condition that the tangential component of the electric field vector must be zero is fulfilled [15]. The method is also applicable for line charges.

In the case where a single line charge is located at a distance, y, over a ground plane (see Figure 6.1), the image line charge will be located at the distance –y underneath the ground plane.

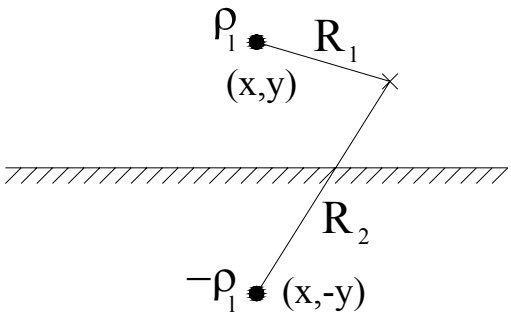

Figure 6.1. A line charge over a ground plane and the corresponding image charge.

The potential, V, at a point located at the distances R_1 and R_2 will then be:

$$V = \frac{\rho_l}{2 \cdot \pi \cdot \varepsilon_0} \cdot \ln \frac{1}{R_1} + \frac{-\rho_l}{2 \cdot \pi \cdot \varepsilon_0} \cdot \ln \frac{1}{R_2} \qquad (6.2)$$

At a location on the ground plane, where $R_1 = R_2$, the potential will be zero which is consistent with the assumption of a conducting ground plane.

Resistance

For low frequencies, the internal resistance of a conductor is a function of the cross-sectional area and the conductivity σ of the conductor according to

[15][72]

$$R' = \frac{l}{\pi \cdot r^2 \cdot \sigma} \Omega / m \tag{6.3}$$

where the prime symbol denotes that the value of the component is a per-unit-length value. In the case of high frequency signals, the resistance of the conductor will no longer be frequency independent, but a complex-valued frequency-dependent function. The resistance will increase proportional to $\sqrt{f}$ if the radius of the conductor is larger than the skin depth.

Since the frequencies of interest in the models are fairly low, the resistances in the following models are assumed to be the theoretical DC resistance presented in this chapter.

Inductance

Two types of inductances should be calculated for a transmission line system which contains more than one conductor; the self inductances and the mutual inductances between the conductors.

The self inductance of a conductor is defined as the magnetic flux per unit current [15]. Since the magnetic field around the conductor is affected by nearby current carrying objects, also the self inductance is depending on the surrounding environment.

The mutual inductance is the inductance between two cables that are routed parallel to each other. An alternating current in one conductor will induce a voltage in the other conductor (see Figure 3.4).

According to established theory in the case where two conductors are present, as in Figure 6.2, the following equations are valid [15]:

$$\begin{cases} \Phi_1^{'} = L_1^{'} I_1 + M^{'} I_2 \\ \Phi_2^{'} = M^{'} I_1 + L_2^{'} I_2 \end{cases} \tag{6.4}$$

L_1 and L_2 are the self inductances per-unit-length of the conductors and M is the mutual inductance per-unit-length between the two conductors. The magnetic flux, Φ, is determined by the line integral of the vector potential, A as;

$$\Phi = \oint \bar{A} \cdot d\bar{l} = [straight\ wire] = \frac{\mu_0 I}{2\pi} \ln\left(\frac{1}{r}\right) \qquad (6.5)$$

where r is the distance from the current to the point of interest (in this case the center of the conductor of consideration) and μ_0 is the permeability of free space ($4\pi \cdot 10^{-7}$ H/m).

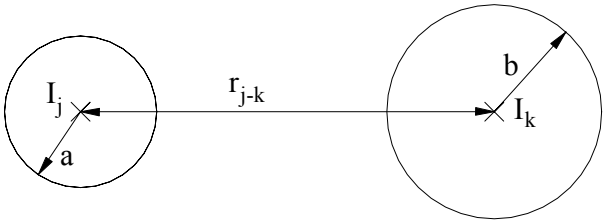

Figure 6.2. Two conductors carrying the currents I_j and I_k respectively.

Combining equations 6.4 and 6.5 gives a generally applicable expression for the self and mutual inductances as:

$$\begin{cases} \Phi_1' = \sum\limits_{\substack{k=current\ 1 \\ and\ its \\ image\ currents}} \frac{\mu_0 I_k}{2\pi} \ln\left(\frac{1}{r_k}\right) + \sum\limits_{\substack{j=current\ 2\ and \\ its \\ image\ currents}} \frac{\mu_0 I_j}{2\pi} \ln\left(\frac{1}{r_{j-k}}\right) \\ \Phi_2' = \sum\limits_{\substack{k=current\ 1\ and \\ its \\ image\ currents}} \frac{\mu_0 I_k}{2\pi} \ln\left(\frac{1}{r_{j-k}}\right) + \sum\limits_{\substack{j=current\ 2 \\ and\ its \\ image\ currents}} \frac{\mu_0 I_j}{2\pi} \ln\left(\frac{1}{r_j}\right) \end{cases} \qquad (6.6)$$

The terms in front of each current in equation 6.6 will give the self and mutual inductances per-unit-length values as

$$L_1' = \sum_{\substack{k=current\ 1 \\ and\ its \\ image\ currents}} \frac{\mu_0}{2\pi} \ln\left(\frac{1}{r_k}\right) \tag{6.7a}$$

$$L_2' = \sum_{\substack{j=current\ 2 \\ and\ its \\ image\ currents}} \frac{\mu_0}{2\pi} \ln\left(\frac{1}{r_j}\right) \tag{6.7b}$$

$$M'_{21} = \sum_{\substack{k=current\ 1\ and \\ its \\ image\ currents \\ j=current\ 2}} \frac{\mu_0}{2\pi} \ln\left(\frac{1}{r_{j-k}}\right) \tag{6.7c}$$

As can be seen in equation 6.7 the different inductances are highly depending on the distances to a ground plane and other conductors.

Capacitance

As in the case with the inductances, two types of capacitances should be calculated; self-partial capacitances and the mutual capacitance between conductors.

Capacitance is defined as the ratio between the charge of the conducting element Q and it's potential, V.

$$C = \frac{Q}{V} \tag{6.8}$$

The charge distribution on a conductor depends on both the insulation (if any) and the surroundings. Conductors are often insulated by a dielectric material. This material could for example be PVC (polyvinyl chloride), PE (polyethylene) or PTFE (polytetrafluoroethylene). A dielectric material has a dielectric constant, also called relative permittivity ε_r that describes how the material affects electric fields [42] (see Table 6.1).

Table 6.1 Relative permittivity for materials used as insulation

Material	Relative permittivity
PVC	3.8
PE	2.3
PTFE	2.1

The dielectric material around the conductor is polarized, i.e. there are bound dielectric charges in the material. This characteristic will change the charge density at the surface of the conductor (see Figure 6.3) [72].

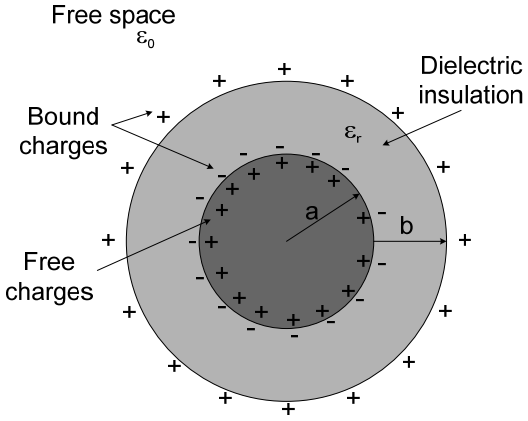

Figure 6.3. A conductor with radius a, and a dielectric insulation of thickness b. The bound charges in the dielectric material will affect the charge distribution.

The total amount of charges will not change, why the following equation shall be fulfilled:

$$\rho_l = \rho_{l,R=a} + \rho_{l,R=a+b} \qquad (6.9)$$

Since the total electric displacement field, D, of the conductor is independent of the insulation, it is convenient to set up an expression for this:

$$\overline{D} = \frac{\rho_l}{2 \cdot \pi \cdot R} \bar{e}_R \qquad a < R < \infty \qquad (6.10)$$

$$\overline{D} = \varepsilon_0 \cdot \varepsilon_r \cdot \overline{E} \tag{6.11}$$

Where ε_0 is the permittivity of free space ($\approx \frac{1}{36\pi} \cdot 10^{-9}$ F/m). The relationship between the electric displacement field D and the electric field E is given in equation 6.11 and this yield the following expressions for the electric fields:

$$\overline{E} = \frac{\rho_l}{2 \cdot \pi \cdot \varepsilon_0 \cdot \varepsilon_r \cdot R} \cdot \bar{e}_R \qquad a < R < (a+b) \tag{6.12a}$$

$$\overline{E} = \frac{\rho_l}{2 \cdot \pi \cdot \varepsilon_0 \cdot R} \cdot \bar{e}_R \qquad (a+b) < R \tag{6.12b}$$

which gives the following relationships for the line charges on the surface of the conducting material and the surface of the conductor:

$$\rho_{l,\,R=a} = \frac{\rho_l}{\varepsilon_r} \tag{6.13a}$$

$$\rho_{l,\,R=a+b} = \rho_l - \frac{\rho_l}{\varepsilon_r} = \rho_l \cdot \left(\frac{\varepsilon_r - 1}{\varepsilon_r} \right) \tag{6.13b}$$

It is not only the insulation of the conductor that influences the charge distribution, also the surrounding conductors have a big impact. If two conductors located close to each other are replaced by line charges, these line charges must be located at points so that the cylindrical surfaces of the conductors form equipotentials [15]. These line charges will not be placed in the centers of the conductors, but at locations where they keep the conductor surface at an equipotential although there are other line charges present. This effect will be more important the closer the cylinders or conductors are to each other. In a case where only one conductor is present over a ground plane, the image of the charge distribution and the charge distribution in Figure 6.4 shall be located in the following way in order to make the cylindrical surface at a radius equal to a an equipotential surface so that all boundary conditions are met.

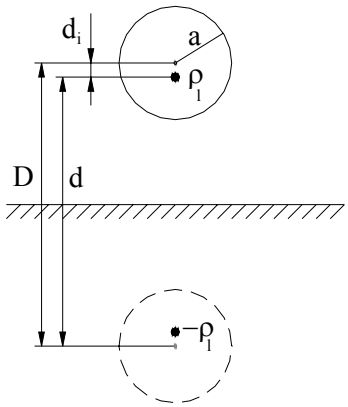

Figure 6.4. The location of the line charge is affected by the ground plane and the mirror charge. d_i is the displacement of the line charge from the middle of the conductor.

It has been shown [15], that in the case where the cylinders are of the same size, the distance d_i is given by

$$d_i = \frac{a^2}{d} = \frac{a^2}{D - d_i} \tag{6.14a}$$

$$d_i^2 - d_i \cdot D - a^2 = 0 \tag{6.14b}$$

$$d_i = \frac{D}{2} - \sqrt{\frac{D^2}{4} - a^2} \tag{6.14c}$$

The displacement of the line charges whit more than one conductor with different line charges is a complex problem that does not have an exact solution. A numerical iteration or simulation software is required to get an answer. This displacement is therefore not taken into account in this thesis, and the line charges are consequently assumed to be located at the center of each conductor.

When the charge distribution and distances between the two line charges are determined, it is possible to calculate the capacitances.

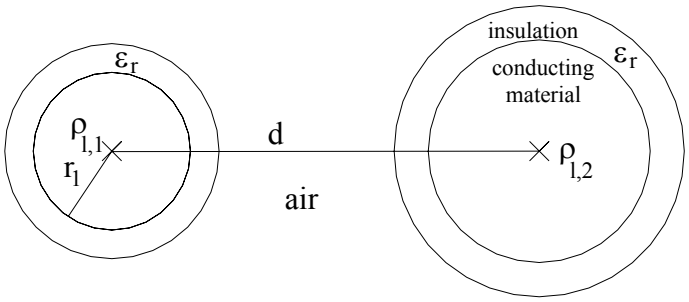

Figure 6.5. Two conductors separated by the distance d.

For the conductors in Figure 6.5, equation 6.8 will look like:

$$C = \frac{\rho_l}{V} \quad \Rightarrow \rho_l = C \cdot V \tag{6.15}$$

This will give the total line charges for the two conductors as shown in equation 6.15

$$\begin{bmatrix} \rho_{l,1} \\ \rho_{l,2} \end{bmatrix} = \begin{bmatrix} \sum_{j=1}^{2} c'_{1j} & -c'_{12} \\ -c'_{21} & \sum_{j=1}^{2} c'_{2j} \end{bmatrix} \begin{bmatrix} V_1 \\ V_2 \end{bmatrix} = \begin{bmatrix} C'_{11} & C'_{12} \\ C'_{21} & C'_{22} \end{bmatrix} \begin{bmatrix} V_1 \\ V_2 \end{bmatrix} \tag{6.16}$$

where $\rho_{l,i}$ are the per-unit-length line charges, c'_{ij} is the partial per-unit-length capacitances and C'_{ij} are the static capacitances per-length-unit. Static capacitances do not have a physical meaning, but can be used to calculate the physical capacitances between the conductors [72].

It is not possible to determine the static capacitances directly since the capacitances depend on the entire set of conductors. Instead, it is possible to calculate the static capacitances by defining a potential coefficient matrix, K' as

$$[V] = [K'][\rho'_l] \tag{6.17}$$

The electric potential from a line charge depends on the distance to the charge and is defined by

$$V(r) = k \cdot \rho_l = \frac{1}{2\pi\varepsilon_0} \ln\left(\frac{1}{r}\right) \cdot \rho_l \qquad (6.18)$$

When the method of images is applied, each line charge will be duplicated (but with different signs) one or more times depending on the surrounding geometry. This implies that each element in the potential coefficient matrix will be the sum of the contributions from each line charge and its image charges.

The static capacitance matrix, C, is the inverse of the coefficient matrix

$$\left[C^{'}\right] = \left[K^{'}\right]^{-1} \qquad (6.19)$$

The physical capacitances are then calculated by using the following formulas:

$$C_1 = C(1,1) + C(1,2) \qquad (6.20a)$$
$$C_2 = C(2,2) + C(1,2) \qquad (6.20b)$$
$$C_M = -C(1,2) \qquad (6.20c)$$

where C_1 and C_2 is the capacitance from each conductor to ground, and C_M is the capacitance between two conductors, as shown in Figure 6.6.

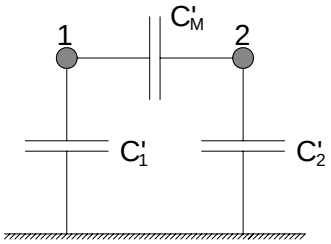

Figure 6.6. The self-partial capacitances and mutual capacitance of the conductors.

The mutual and self-partial capacitances of the conductors are depending on the charge distributions. Since the distribution of the charges depends on a number of different physical properties of the conductors like the insulation and the other charged objects in the vicinity of the conductor, theses

capacitances are difficult to estimate with a high accuracy. The error that is introduced due to the assumption that the line charge is located at the centre of the conductor in case of one single conductor above a ground plane can be estimated by comparing a case where the displacement of the line charge is not taken into account with a case where it is taken into account.

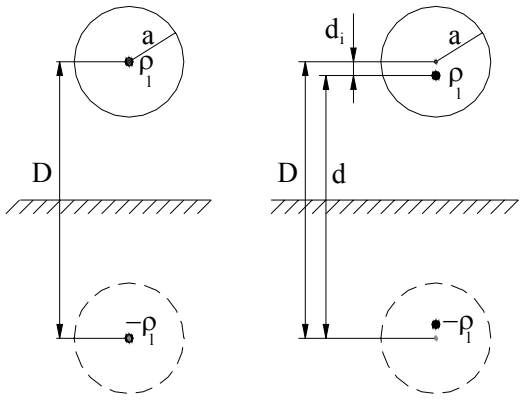

Figure 6.7. Left: The line charge is assumed to be located at the center of the conductor. Right: The line charge is displaced a distance d_i from the center of the conductor due to the ground plane and the image line charge.

The radius in Figure 6.7 is 1.38 mm and the distance D is 4.4 mm.

The capacitance in the leftmost case is:

$$C = \frac{1}{\frac{1}{2\cdot\pi\cdot\varepsilon_0}\left(\ln\left(\frac{1}{a}\right)-\ln\left(\frac{1}{D}\right)\right)} = \frac{1}{\frac{1}{2\cdot\pi\cdot\varepsilon_0}\left(\ln\left(\frac{1}{1.38}\right)-\ln\left(\frac{1}{4.4}\right)\right)} = 48\ pF \qquad (6.21)$$

For the rightmost case, the new distances d_i and d must be calculated:

$$d_i = \frac{D}{2} - \sqrt{\frac{D^2}{4} - a^2} = \frac{4.4}{2} - \sqrt{\frac{4.4^2}{4} - 1.38^2} = 0.49\ mm \qquad (6.22a)$$

$$d = D - d_i = 3.91\ mm \qquad (6.22b)$$

This will give the capacitance as:

$$C = \frac{1}{\frac{1}{2 \cdot \pi \cdot \varepsilon_0}\left(\ln\left(\frac{1}{a - d_i}\right) - \ln\left(\frac{1}{d - a}\right)\right)} = \\ = \frac{1}{\frac{1}{2 \cdot \pi \cdot \varepsilon_0}\left(\ln\left(\frac{1}{0.89}\right) - \ln\left(\frac{1}{2.53}\right)\right)} = 53\ pF \tag{6.23}$$

As can be seen will the capacitance be lower if the displacement of the line charge is not taken into account.

The parameter values for the conductors in the investigated cases are estimated by using two different procedures. These are described in the following sections.

6.2 Method 1, accurate

In the first method described in this thesis, the electromagnetic theory from Chapter 6.1 is utilized. This method is a rather accurate way of estimating the parasitic components for the conductors. A Matlab script for estimating the parameters is found in Appendix C.

Applying the method of images to a problem where the charge is located next to a ground structure spreading out in more than one direction demands a different approach. In the investigated cases, the ground shape has an L-profile in the vicinity of the charges. This implies that each charge should be mirrored in both the horizontal and vertical part of the ground structure. In Figure 6.8, charge A is situated at point (x_1,y_1). In order to make the potential of the vertical half-plane zero, a charge with the opposite polarity is placed at $(-x_1,y_1)$. This charge will however not make the potential zero on the horizontal half-plane. A second image charge, also with the opposite sign to charge A, is placed at $(x_1,-y_1)$ and will make the potential of the horizontal half-plane zero (but not the potential of the vertical half-plane). In order to make the potentials on the vertical and horizontal half-planes zero, a third image has to be placed in the third quadrant at point $(-x_1,-y_1)$. This charge should have the same polarity as charge A.

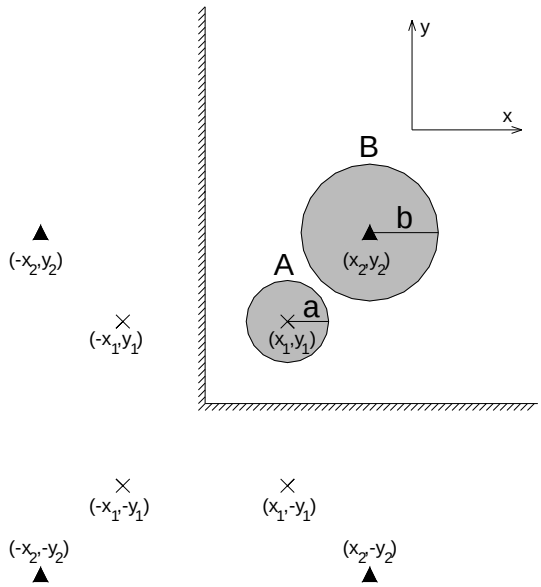

Figure 6.8. Two conductors and an L-shaped ground structure. The points where the image charges or currents are located for each conductor are indicated.

In the following calculations, the charges are represented by two conductors which are replaced by line charges or currents when capacitance and inductance calculations should be performed.

Inductance

In case of inductance calculations, the two charges in point A and B in Figure 6.8 are replaced by currents. When the locations of the currents and their image currents are known, it is possible to determine the self- and mutual inductances of the conductors according to the equations in Chapter 6.1.

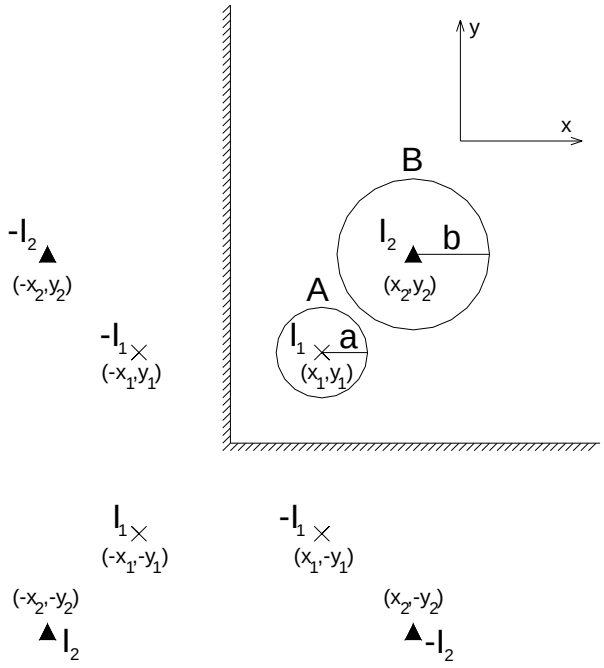

Figure 6.9. Two conductors and an L-shaped ground structure. The location of their currents and their image currents are indicated.

For the first current, I_1, placed in point A (see Figure 6.9) the flux Φ_1' will then be the sum of the contributions from both current I_1 and current I_2 and is determined by the following equation:

$$\Phi_1' = \frac{\mu_0}{2\pi}\ln\left(\frac{1}{a}\right)I_1 + \frac{\mu_0}{2\pi}\ln\left(\frac{1}{2x_1}\right)(-I_1) + \frac{\mu_0}{2\pi}\ln\left(\frac{1}{2\sqrt{x_1^2+y_1^2}}\right)I_1 + \frac{\mu_0}{2\pi}\ln\left(\frac{1}{2y_1}\right)(-I_1) +$$
$$+ \frac{\mu_0}{2\pi}\ln\left(\frac{1}{\sqrt{(x_1-x_2)^2+(y_1-y_2)^2}}\right)I_2 + \frac{\mu_0}{2\pi}\ln\left(\frac{1}{\sqrt{(x_1+x_2)^2+(y_1-y_2)^2}}\right)(-I_2) +$$
$$+ \frac{\mu_0}{2\pi}\ln\left(\frac{1}{\sqrt{(x_1+x_2)^2+(y_1+y_2)^2}}\right)I_2 + \frac{\mu_0}{2\pi}\ln\left(\frac{1}{\sqrt{(x_1-x_2)^2+(y_1+y_2)^2}}\right)(-I_2)$$

(6.24)

From equation 6.6 we see that the terms in front of current I_1 will give the self inductance of the conductor and that the terms in front of current I_2 will give the mutual inductance between the two conductors. This gives an expression for the self and mutual inductance for conductor 1 that will look like:

$$L_1 = \frac{\mu_0}{2\pi}\ln\left(\frac{4|x_1 y_1|}{a\sqrt{x_1^2 + y_1^2}}\right) \tag{6.25a}$$

$$M = \frac{\mu_0}{2\pi}\ln\left(\sqrt{\frac{\left((x_1 + x_2)^2 + (y_1 - y_2)^2\right)\left((x_1 - x_2)^2 + (y_1 + y_2)^2\right)}{\left((x_1 - x_2)^2 + (y_1 - y_2)^2\right)\left((x_1 + x_2)^2 + (y_1 + y_2)^2\right)}}\right) \tag{6.25b}$$

The inductance for the other conductor, conductor 2 in point B, will be determined the same way. First, a formula for the flux, Φ_2

$$\begin{aligned}\Phi_2^{'} = {} & \frac{\mu_0}{2\pi}\ln\left(\frac{1}{b}\right)I_2 + \frac{\mu_0}{2\pi}\ln\left(\frac{1}{2x_2}\right)(-I_2) + \frac{\mu_0}{2\pi}\ln\left(\frac{1}{2\sqrt{x_2^2 + y_2^2}}\right)I_2 + \frac{\mu_0}{2\pi}\ln\left(\frac{1}{2y_2}\right)(-I_2) + \\ & + \frac{\mu_0}{2\pi}\ln\left(\frac{1}{\sqrt{(x_1 - x_2)^2 + (y_1 - y_2)^2}}\right)I_1 + \frac{\mu_0}{2\pi}\ln\left(\frac{1}{\sqrt{(x_1 + x_2)^2 + (y_1 - y_2)^2}}\right)(-I_1) + \\ & + \frac{\mu_0}{2\pi}\ln\left(\frac{1}{\sqrt{(x_1 + x_2)^2 + (y_1 + y_2)^2}}\right)I_1 + \frac{\mu_0}{2\pi}\ln\left(\frac{1}{\sqrt{(x_1 - x_2)^2 + (y_1 + y_2)^2}}\right)(-I_1)\end{aligned} \tag{6.26}$$

As can be seen from equation 6.24 and 6.26, the terms for the mutual inductance are the same regardless of which conductor that serves as a reference due to reciprocity [15]. The expression for the self inductance of conductor 2 will be

$$L_2 = \frac{\mu_0}{2\pi}\ln\left(\frac{2|x_2 y_2|}{b\sqrt{x_2^2 + y_2^2}}\right) \tag{6.27}$$

Capacitance

The expressions used when calculating the capacitances are not so straight

forward as for the inductances. To begin with, the two charges A and B in Figure 6.8 will be replaced by two line charges, $\rho_{l,1}$ and $\rho_{l,2}$.

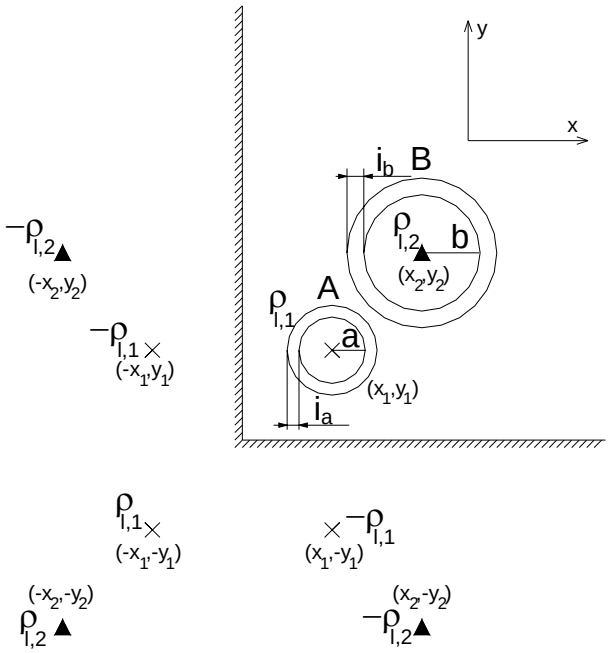

Figure 6.10. Two conductors and an L-shaped ground structure. The location of their line charges and their image charges are indicated.

When calculating the capacitances, the matrix elements in the potential coefficient matrix must be determined first. Since the conductors have insulation made of a dielectric material, the contribution from the conductor itself will be affected by the dielectric constant ε_r. The dielectric constant will affect the conductor since it introduces bound dielectric charges at the dielectric interference surfaces due to the polarization of the material (see Chapter 6.1). According to equation 6.13b the amount of free charges that will be located at the surface of the conductor will be

$$\rho_{l,conductor} = \rho_{l,total} \frac{\varepsilon_r - 1}{\varepsilon_r} = \rho_{l,total} \cdot \varepsilon_x \tag{6.28}$$

This will only affect the term describing the potential contribution from the

line charge at the point where the potential is investigated.

As mentioned in Chapter 6.1, equation 6.18 , the potential V_1 in point A becomes:

$$V_1 = \frac{\rho_{l,1}}{2\pi\varepsilon_0\varepsilon_r}\ln\left(\frac{1}{a}\right) + \frac{\rho_{l,1}\varepsilon_x}{2\pi\varepsilon_0}\ln\left(\frac{1}{a+i_a}\right) + \frac{-\rho_{l,1}}{2\pi\varepsilon_0}\ln\left(\frac{1}{2x_1}\right) + \frac{\rho_{l,1}}{2\pi\varepsilon_0}\ln\left(\frac{1}{2\sqrt{\left(x_1^2+y_1^2\right)}}\right) +$$
$$+\frac{-\rho_{l,1}}{2\pi\varepsilon_0}\ln\left(\frac{1}{2y_1}\right) + \frac{\rho_{l,2}}{2\pi\varepsilon_0}\ln\left(\frac{1}{\sqrt{(x_1-x_2)^2+(y_1-y_2)^2}}\right) +$$
$$+\frac{-\rho_{l,2}}{2\pi\varepsilon_0}\ln\left(\frac{1}{\sqrt{(x_1+x_2)^2+(y_1-y_2)^2}}\right) + \frac{\rho_{l,2}}{2\pi\varepsilon_0}\ln\left(\frac{1}{\sqrt{(x_1+x_2)^2+(y_1+y_2)^2}}\right) +$$
$$+\frac{-\rho_{l,2}}{2\pi\varepsilon_0}\ln\left(\frac{1}{\sqrt{(x_1-x_2)^2+(y_1+y_2)^2}}\right)$$

(6.29)

This will give the elements K_{11} and K_{12} in the coefficient matrix as

$$K_{11} = \frac{1}{2\pi\varepsilon_0}\left(\frac{1}{\varepsilon_r}\ln\left(\frac{1}{a}\right) + \varepsilon_x\cdot\ln\left(\frac{1}{a+i_a}\right) + \ln\left(\frac{4|x_1y_1|}{\sqrt{x_1^2+y_1^2}}\right)\right) \qquad (6.30a)$$

$$K_{12} = \frac{1}{2\pi\varepsilon_0}\ln\left(\sqrt{\frac{\left((x_1+x_2)^2+(y_1-y_2)^2\right)\left((x_1-x_2)^2+(y_1+y_2)^2\right)}{\left((x_1-x_2)^2+(y_1-y_2)^2\right)\left((x_1+x_2)^2+(y_1+y_2)^2\right)}}\right)$$

(6.30b)

The potential V_2 in point B will be described in a similar way

$$V_2 = \frac{\rho_{l,1}}{2\pi\varepsilon_0}\ln\left(\frac{1}{\sqrt{(x_1-x_2)^2+(y_1-y_2)^2}}\right)+\frac{-\rho_{l,1}}{2\pi\varepsilon_0}\ln\left(\frac{1}{\sqrt{(x_1+x_2)^2+(y_1-y_2)^2}}\right)+$$
$$+\frac{\rho_{l,1}}{2\pi\varepsilon_0}\ln\left(\frac{1}{\sqrt{(x_1+x_2)^2+(y_1+y_2)^2}}\right)+\frac{-\rho_{l,1}}{2\pi\varepsilon_0}\ln\left(\frac{1}{\sqrt{(x_1-x_2)^2+(y_1+y_2)^2}}\right)+$$
$$+\frac{\rho_{l,2}}{2\pi\varepsilon_0\varepsilon_r}\ln\left(\frac{1}{b}\right)+\frac{\rho_{l,2}\varepsilon_x}{2\pi\varepsilon_0}\ln\left(\frac{1}{b+i_b}\right)+\frac{-\rho_{l,2}}{2\pi\varepsilon_0}\ln\left(\frac{1}{2x_2}\right)+\frac{\rho_{l,2}}{2\pi\varepsilon_0}\ln\left(\frac{1}{2\sqrt{(x_2^2+y_2^2)}}\right)+$$
$$+\frac{-\rho_{l,2}}{2\pi\varepsilon_0}\ln\left(\frac{1}{2y_2}\right) \qquad (6.31)$$

As can be found above the expressions for describing the contribution to the potential on the reference conductor from the other conductor are equal in equations 6.29 and 6.31 due to reciprocity. This gives that the expression for the matrix element K_{21} will be the same as for K_{12} in equation 6.30b. The coefficient K_{22} will look like

$$K_{22} = \frac{1}{2\pi\varepsilon_0}\left(\frac{1}{\varepsilon_r}\ln\left(\frac{1}{b}\right)+\varepsilon_x\cdot\ln\left(\frac{1}{b+i_b}\right)+\ln\left(\frac{2|x_2y_2|}{\sqrt{x_2^2+y_2^2}}\right)\right) \qquad (6.32)$$

When the elements in the coefficient matrix, K, are known the matrix should be inversed in order to give the static capacitance matrix, C.

$$C = K^{-1} = \begin{pmatrix} C_{11} & C_{12} \\ C_{21} & C_{22} \end{pmatrix} \qquad (6.33)$$

The self and mutual capacitances will then be given by equation 6.20.

Results

The above described method for determining the components was applied on the different cases described in Chapter 5.3. A general picture of how the different symbols are defined can be seen in Figure 6.11.

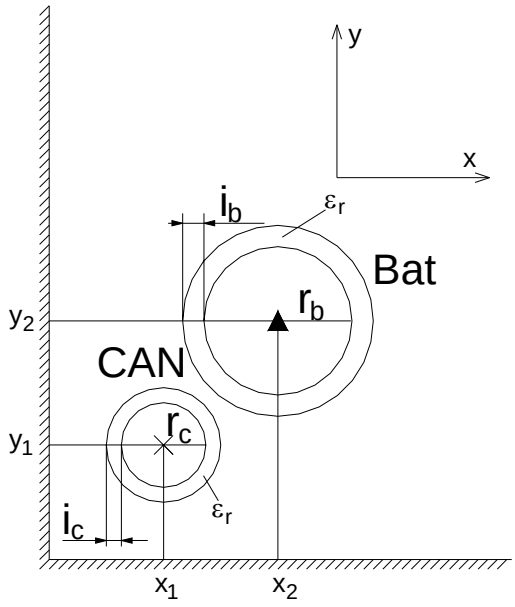

Figure 6.11. General picture of the investigated setup.

Common values for all five cases are the physical dimensions and characteristics of the conductors according to Table 6.2.

Table 6.2. Constants for the investigated setup

ε_r for the insulation	3.8
r_c	0.40 mm
r_b	1.4 mm
i_c	0.70 mm
i_b	0.76 mm

Case 1

In Case 1, only the communication conductor is present and located at a distance of about 10 mm up and out from the ground structure. The coordinates for the conductor are as follows

Table 6.3. Coordinates for Case 1

x_1	y_1
11.1 mm	11.1 mm

Inserting the above values into equation 6.2 will yield the following value on the inductance, L, per meter

$$L_1 = \frac{\mu_0}{2\pi}\ln\left(\frac{2|x_1 y_1|}{r_c\sqrt{x_1^2+y_1^2}}\right) = \frac{\mu_0}{2\pi}\ln\left(\frac{2|11.1\cdot 11.1|}{0.3989\cdot\sqrt{11.1^2+11.1^2}}\right) = 0.74\ \mu H \quad (6.34)$$

Since only one conductor is present in this case, the coefficient in equation 6.30a will be

$$K_{11} = \frac{1}{2\pi\varepsilon_0}\left(\frac{1}{\varepsilon_r}\ln\left(\frac{1}{r_c}\right)+\varepsilon_x\cdot\ln\left(\frac{1}{r_c+i_c}\right)+\ln\left(\frac{2|x_1 y_1|}{\sqrt{x_1^2+y_1^2}}\right)\right) =$$

$$= \frac{1}{2\pi\varepsilon_0}\left(\frac{1}{3.8}\ln\left(\frac{1}{0.3989}\right)+\frac{2.8}{3.8}\cdot\ln\left(\frac{1}{0.3989+0.7}\right)+\ln\left(\frac{2|11.1\cdot 11.1|}{\sqrt{11.1^2+11.1^2}}\right)\right) = 52.66\cdot 10^9$$

(6.35)

This will give capacitance per meter as the inverse of the coefficient K_{11}

$$C = K^{-1} = 19\ pF \quad (6.36)$$

Case 2

In Case 2, both conductors are present. They are located next to each other in the corner of the ground structure. The coordinates will be as follows

Table 6.4. Coordinates for Case 2

x_1	y_1	x_2	y_2
1.35 mm	1.35 mm	4.55 mm	2.35 mm

Inserting the coordinates into equation 6.7 will yield the following values for the inductances

$$L_1 = \frac{\mu_0}{2\pi}\ln\left(\frac{2|x_1 y_1|}{r_c\sqrt{x_1^2+y_1^2}}\right) = \frac{\mu_0}{2\pi}\ln\left(\frac{2|1.35\cdot 1.35|}{0.3989\sqrt{1.35^2+1.35^2}}\right) = 0.31\ \mu H/m \quad (6.37)$$

$$M = \frac{\mu_0}{2\pi}\ln\left(\sqrt{\frac{\left((x_1+x_2)^2+(y_1-y_2)^2\right)\left((x_1-x_2)^2+(y_1+y_2)^2\right)}{\left((x_1-x_2)^2+(y_1-y_2)^2\right)\left((x_1+x_2)^2+(y_1+y_2)^2\right)}}\right) =$$

$$= \frac{\mu_0}{2\pi}\ln\left(\sqrt{\frac{\left((1.35+4.55)^2+(1.35-2.35)^2\right)\left((1.35-4.55)^2+(1.35+2.35)^2\right)}{\left((1.35-4.55)^2+(1.35-2.35)^2\right)\left((1.35+4.55)^2+(1.35+2.35)^2\right)}}\right) = 0.045\ \mu H/m$$

(6.38)

$$L_2 = \frac{\mu_0}{2\pi}\ln\left(\frac{2|x_2 y_2|}{r_b\sqrt{x_2^2+y_2^2}}\right) = \frac{\mu_0}{2\pi}\ln\left(\frac{2|4.55\cdot 2.35|}{1.382\sqrt{4.55^2+2.35^2}}\right) = 0.22\ \mu H/m$$

(6.39)

The coefficients in the coefficient matrix in equations 6.30 and 6.32 will be

$$K_{11} = \frac{1}{2\pi\varepsilon_0}\left(\frac{1}{\varepsilon_r}\ln\left(\frac{1}{r_c}\right)+\varepsilon_x\cdot\ln\left(\frac{1}{r_c+i_c}\right)+\ln\left(\frac{2|x_1 y_1|}{\sqrt{x_1^2+y_1^2}}\right)\right) =$$

$$= \frac{1}{2\pi\varepsilon_0}\left(\frac{1}{3.8}\ln\left(\frac{1}{0.3989}\right)+\frac{2.8}{3.8}\cdot\ln\left(\frac{1}{0.3989+0.7}\right)+\ln\left(\frac{2|1.35\cdot 1.35|}{\sqrt{1.35^2+1.35^2}}\right)\right) = 14.7\cdot 10^9$$

(6.40)

$$K_{12} = \frac{1}{2\pi\varepsilon_0}\ln\left(\sqrt{\frac{\left((x_1+x_2)^2+(y_1-y_2)^2\right)\left((x_1-x_2)^2+(y_1+y_2)^2\right)}{\left((x_1-x_2)^2+(y_1-y_2)^2\right)\left((x_1+x_2)^2+(y_1+y_2)^2\right)}}\right) =$$

$$= \frac{1}{2\pi\varepsilon_0}\ln\left(\sqrt{\frac{\left((1.35+4.55)^2+(1.35-2.35)^2\right)\left((1.35-4.55)^2+(1.35+2.35)^2\right)}{\left((1.35-4.55)^2+(1.35-2.35)^2\right)\left((1.35+4.55)^2+(1.35+2.35)^2\right)}}\right) = 4.07\cdot 10^9$$

(6.41)

$$K_{22} = \frac{1}{2\pi\varepsilon_0}\left(\frac{1}{\varepsilon_r}\ln\left(\frac{1}{r_b}\right)+\varepsilon_x\cdot\ln\left(\frac{1}{r_b+i_b}\right)+\ln\left(\frac{2|x_2 y_2|}{\sqrt{x_2^2+y_2^2}}\right)\right)=$$

$$=\frac{1}{2\pi\varepsilon_0}\left(\frac{1}{3.8}\ln\left(\frac{1}{1.382}\right)+\frac{2.8}{3.8}\cdot\ln\left(\frac{1}{1.382+0.76}\right)+\ln\left(\frac{2|4.55\cdot 2.35|}{\sqrt{4.55^2+2.35^2}}\right)\right)=14.1\cdot 10^9$$

(6.42)

This will give the static capacitance matrix, C, as

$$C = K^{-1} = \begin{pmatrix} 14.7\cdot 10^9 & 4.07\cdot 10^9 \\ 4.07\cdot 10^9 & 14.1\cdot 10^9 \end{pmatrix}^{-1} = \begin{pmatrix} 0.737\cdot 10^{-10} & -0.213\cdot 10^{-10} \\ -0.213\cdot 10^{-10} & 0.771\cdot 10^{-10} \end{pmatrix}$$

(6.43)

The self and mutual capacitances per meter will be given from equation 6.20

$$C_1 = C(1,1)+C(1,2) = 52\ pF/m \quad (6.44a)$$

$$C_2 = C(2,2)+C(2,1) = 56\ pF/m \quad (6.44b)$$

$$C_M = -C(1,2) = 21\ pF/m \quad (6.44c)$$

Case 3

In Case 3, the conductors are located 5 mm above and 5 mm out from the ground structure according to Figure 5.6. The coordinates for the conductors will be

Table 6.5. Coordinates for Case 3

x_1	y_1	x_2	y_2
6.1 mm	6.1 mm	9.35 mm	7.14 mm

This together with equation 6.7 will yield values for the inductances as

$$L_1 = 0.62\ \mu H/m$$

$$L_2 = 0.22\ \mu H/m$$

$$M = 0.045\ \mu H/m$$

The capacitances will according to equations 6.16, 6.18, 6.19 and 6.20 be

$$C_1 = 52\ pF/m$$
$$C_2 = 56\ pF/m$$
$$C_M = 21\ pF/m$$

Case 4

In Case 4 will conductor 1, the thin conductor for communication, be located in the corner of the ground structure. Conductor 2 is located 5 mm up and 5 mm out from the ground structure.

Table 6.6. Coordinates for Case 4

x_1	y_1	x_2	y_2
1.35 mm	1.35 mm	7.14 mm	7.14 mm

When using the method described in this chapter, the following inductance and capacitance values per meter are gained

$$L_1 = 0.31\ \mu H/m$$
$$L_2 = 0.40\ \mu H/m$$
$$M = 0.014\ \mu H/m$$

$$C_1 = 65\ pF/m$$
$$C_2 = 31\ pF/m$$
$$C_M = 2.9\ pF/m$$

Case 5

In Case 5, the thin conductor is situated 5 mm up and 5 mm out from the ground structure according to Figure 5.8. The thicker conductor, conductor 2, is located 5 mm up and 6 mm away from conductor 1.

Table 6.7. Coordinates for Case 5

x_1	y_1	x_2	y_2
6.1 mm	6.1 mm	14.24 mm	7.14 mm

These coordinates yield the inductances and capacitances per meter as

$$L_1 = 0.45\ \mu H/m$$
$$L_2 = 0.62\ \mu H/m$$
$$M = 0.093\ \mu H/m$$

$$C_1 = 19\ pF/m$$
$$C_2 = 25\ pF/m$$
$$C_M = 6.1\ pF/m$$

6.3 Method 2, approximate

In many theoretical books [15][26][72], formulas for determining the parasitic components for a conductor over a ground plane are given. These formulas are useful as long as the ground plane is a flat conducting surface. This is however seldom the case in automotive applications where the chassis constitutes a ground structure. This implies that the ground structure will not only be under the conductor but also on the side of the conductor. In this thesis a rather "extreme" ground structure in the shape of a U-channel is utilized. It is extreme in the way that the angle between the vertical and horizontal plane is 90º and that it spreads out far away in both directions.

An approach to simplify this ground structure and the calculations will be made in this chapter. In order to do so, a number of simplifications and assumptions will be made. A short summary of them will be given here below:

- Line charges are assumed to be located in the middle of the conductors for electrostatic analysis
- The line charges of two conductors are assumed to have the same value but opposite signs
- The skin depth is assumed to be so small that the ground structure can be replaced by an infinitely thin structure
- The insulation of the conductors are not taken into account in the electrostatic analysis

A simple Matlab script for determining parameters of a system like this is provided in Appendix C.

Instead of using the whole ground structure when the self inductances and capacitances should be determined, an equivalent plane for each conductor is constructed. First, a line from the height on the y-axis where the center of the conductor is to the point at the x-axis above which the conductor is situated is drawn according to Figure 6.12.

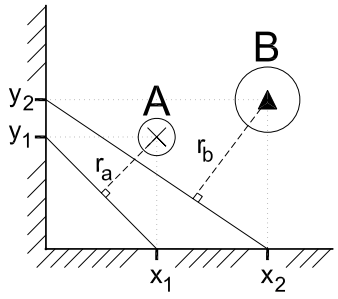

Figure 6.12. Two conductors and their equivalent planes.

Since the part of the ground structure that is nearest to the conductor will influence the parameters most, a line from the center of the conductor, perpendicular to the other line is drawn and will constitute the distance from the conductor to the equivalent plane.

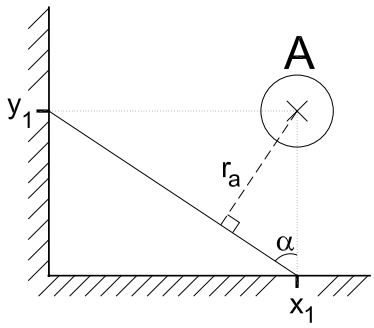

Figure 6.13. Conductor A and the equivalent ground plane.

The distance r_a in Figure 6.13 is determined by finding the angle α as

$$\alpha = \arctan\left(\frac{y_1}{x_1}\right) \tag{6.45}$$

This gives the distance r_a as

$$r_a = y_1 \cdot \sin(\alpha) \tag{6.46}$$

When this distance is determined, the conductor and its equivalent plane can be drawn as Figure 6.14.

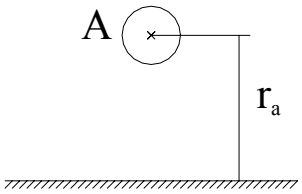

Figure 6.14. Conductor A and the equivalent ground plane.

When the equivalent plane is created, the method of images can be utilized to get the equation for the self inductance and capacitance of the conductor.

Inductance

According the Chapter 6.1, the method of images for a conductor carrying the current I over a ground plane will look like

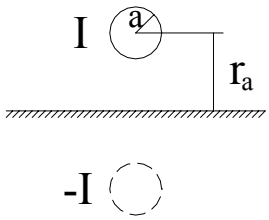

Figure 6.15. A current carrying conductor above a ground plane and the image current.

The self inductance of the conductor is determined by using equation 6.7, which will gain the following equation

$$L = \frac{\mu_0}{2 \cdot \pi}\left(\ln\left(\frac{1}{a}\right) - \ln\left(\frac{1}{2 \cdot r_a}\right)\right) = \frac{\mu_0}{2 \cdot \pi} \ln\left(\frac{2 \cdot r_a}{a}\right) \qquad (6.47)$$

In order to calculate the mutual inductance it is not possible to use the equivalent ground plane, since both conductors shall be taken into account. The approach will instead be to calculate one mutual inductance for the two conductors when only the vertical part of the ground structure is present and one mutual inductance when only the horizontal part of the ground structure is present. These two inductances will then be coupled in parallel.

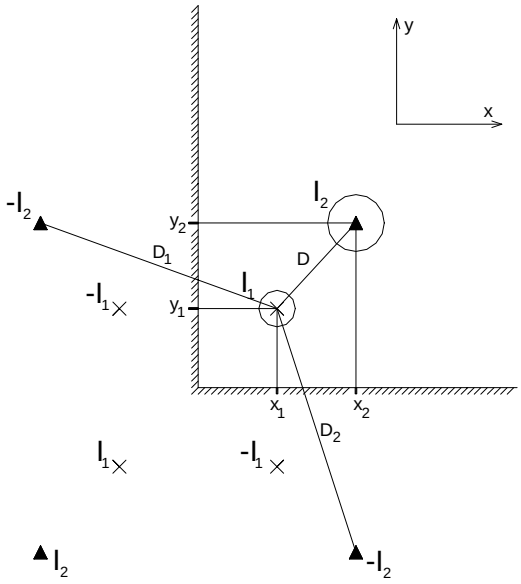

Figure 6.16. The distances D, D_1 and D_2 are employed in the mutual inductance calculations.

The distances in Figure 6.16 are given by using Pythagorean theorem

$$D = \sqrt{(x_1 - x_2)^2 + (y_1 - y_2)^2} \tag{6.48a}$$

$$D_1 = \sqrt{(x_1 + x_2)^2 + (y_1 - y_2)^2} \tag{6.48b}$$

$$D_2 = \sqrt{(x_1 - x_2)^2 + (y_1 + y_2)^2} \tag{6.48c}$$

This will give the expressions for the mutual inductance as

$$M_1 = \frac{\mu_0}{2 \cdot \pi}\left(\ln\left(\frac{1}{D}\right) - \ln\left(\frac{1}{D_1}\right)\right) = \frac{\mu_0}{2 \cdot \pi}\ln\left(\frac{D_1}{D}\right) \tag{6.49a}$$

$$M_2 = \frac{\mu_0}{2 \cdot \pi}\left(\ln\left(\frac{1}{D}\right) - \ln\left(\frac{1}{D_2}\right)\right) = \frac{\mu_0}{2 \cdot \pi}\ln\left(\frac{D_2}{D}\right) \tag{6.49b}$$

$$M = M_1 // M_2 = \left(\frac{1}{\frac{\mu_0}{2 \cdot \pi}\ln\left(\frac{D_1}{D}\right)} + \frac{1}{\frac{\mu_0}{2 \cdot \pi}\ln\left(\frac{D_2}{D}\right)}\right)^{-1} \tag{6.49c}$$

Capacitance

As mentioned above, the insulation of the conductors will not be taken into account. The figure for the electrostatic calculations will then look like

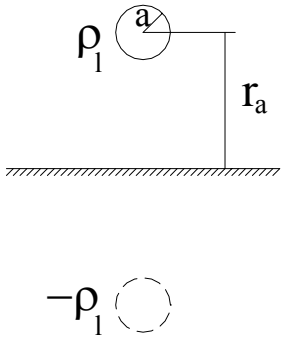

Figure 6.17. A line charge over a ground plane and the image charge.

According to equations 6.18 and 6.19, the self-partial capacitance for the conductor can be described as

$$V = \frac{\rho_l}{2 \cdot \pi \cdot \varepsilon_0}\left(\ln\left(\frac{1}{a}\right) - \ln\left(\frac{1}{2 \cdot r_a}\right)\right) = \frac{\rho_l}{2 \cdot \pi \cdot \varepsilon_0}\ln\left(\frac{2 \cdot r_a}{a}\right) \qquad (6.50a)$$

$$C = \frac{\rho_l}{V} = \frac{2 \cdot \pi \cdot \varepsilon_0}{\ln\left(\frac{2 \cdot r_a}{a}\right)} \qquad (6.50b)$$

The mutual capacitance between the two conductors, C_M, is calculated by assuming that both conductors have the line charge ρ_l but with opposite signs. For this calculation, no ground structure is taken into account since this would yield a far more complicated expression. The image charges are therefore not taken into account.

The mutual capacitance for the two conductors in Figure 6.16 will be found by dividing the line charge with the potential difference between the two cables as equation 6.51 below shows

$$C_M = \frac{\rho_l}{V_1 - V_2} \qquad (6.51a)$$

$$V_1 = \frac{\rho_l}{2 \cdot \pi \cdot \varepsilon_0}\left(\ln\left(\frac{1}{a}\right) - \ln\left(\frac{1}{D}\right)\right) = \frac{\rho_l}{2 \cdot \pi \cdot \varepsilon_0}\ln\frac{D}{a} \qquad (6.51b)$$

$$V_2 = \frac{-\rho_l}{2 \cdot \pi \cdot \varepsilon_0}\left(\ln\left(\frac{1}{b}\right) - \ln\left(\frac{1}{D}\right)\right) = \frac{\rho_l}{2 \cdot \pi \cdot \varepsilon_0}\ln\frac{D}{b} \qquad (6.51c)$$

$$C_M = \frac{\rho_l}{\frac{\rho_l}{2 \cdot \pi \cdot \varepsilon_0}\left(\ln\left(\frac{D}{a}\right) + \ln\left(\frac{D}{b}\right)\right)} = \frac{2 \cdot \pi \cdot \varepsilon_0}{\ln\left(\frac{D^2}{a \cdot b}\right)} \qquad (6.51d)$$

Where a and b are the radii of the two conductors and D the distance between them.

Results

Just as in Chapter 6.2, the parameters for the five cases will be calculated. The values for the radii are the same as in Table 6.2 and the notations will be the same as in Figure 6.11.

Case 1

Case 1 is the case when only one conductor, the thin conductor intended for communication, is present. The coordinates for the conductor is given in Table 6.3. Before the self inductance and capacitance can be calculated, an equivalent plane for the conductor must be constructed.

The coordinates (see Figure 6.13) will give the angle α according to equation 6.52

$$\alpha = \arctan\left(\frac{x_1}{y_1}\right) = \arctan\left(\frac{11.1}{11.1}\right) = 45° \qquad (6.52)$$

Equation 6.53 will then give the distance from the center of the conductor to the ground plane as

$$r_a = y_1 \cdot \sin(\alpha) = 11.1 \cdot \sin(45°) = 7.85\ mm \qquad (6.53)$$

Inserting this values into equation 6.47 and 6.50 will yield the values for the self inductance and capacitance per meter conductor as

$$L = \frac{\mu_0}{2 \cdot \pi} \ln\left(\frac{2 \cdot r_a}{a}\right) = \frac{\mu_0}{2 \cdot \pi} \ln\left(\frac{2 \cdot 7.85}{0.3989}\right) = 0.73\ \mu H / m \qquad (6.54)$$

$$C = \frac{2 \cdot \pi \cdot \varepsilon_0}{\ln\left(\frac{2 \cdot r_a}{a}\right)} = \frac{2 \cdot \pi \cdot \varepsilon_0}{\ln\left(\frac{2 \cdot 7.85}{0.3989}\right)} = 15\ pF / m \qquad (6.55)$$

Case 2

In Case 2, two conductors are present and therefore both the mutual inductance and the mutual capacitance between the conductors must be calculated.

The two equivalent planes for the conductors in Figure 6.11 must be constructed first (see Figure 6.13).

$$\alpha = \arctan\left(\frac{x_1}{y_1}\right) = \arctan\left(\frac{1.35}{1.35}\right) = 45° \tag{6.56}$$

$$r_a = y_1 \cdot \sin(\alpha) = 1.35 \cdot \sin(45°) = 0.955\ mm \tag{6.57}$$

$$\beta = \arctan\left(\frac{x_2}{y_2}\right) = \arctan\left(\frac{4.55}{2.35}\right) = 62.7° \tag{6.58}$$

$$r_b = y_2 \cdot \sin(\beta) = 2.35 \cdot \sin(62.7°) = 2.09\ mm \tag{6.59}$$

When the distances r_a and r_b to the equivalent planes are known for the conductors, the self inductances will be

$$L_a = \frac{\mu_0}{2 \cdot \pi} \ln\left(\frac{2 \cdot r_a}{a}\right) = \frac{\mu_0}{2 \cdot \pi} \ln\left(\frac{2 \cdot 0.955}{0.3989}\right) = 0.31\ \mu H / m \tag{6.60}$$

$$L_b = \frac{\mu_0}{2 \cdot \pi} \ln\left(\frac{2 \cdot r_b}{b}\right) = \frac{\mu_0}{2 \cdot \pi} \ln\left(\frac{2 \cdot 2.09}{1.382}\right) = 0.22\ \mu H / m \tag{6.61}$$

The mutual inductance is given by equation 6.49 and will be

$$D = \sqrt{(x_1 - x_2)^2 + (y_1 - y_2)^2} = \\ = \sqrt{(1.35 - 4.55)^2 + (1.35 - 2.35)^2} = 3.35\ mm \tag{6.62a}$$

$$D_1 = \sqrt{(x_1 + x_2)^2 + (y_1 - y_2)^2} = \\ = \sqrt{(1.35 + 4.55)^2 + (1.35 - 2.35)^2} = 5.98\ mm \tag{6.62b}$$

$$D_2 = \sqrt{(x_1 - x_2)^2 + (y_1 + y_2)^2} = \\ = \sqrt{(1.35 - 4.55)^2 + (1.35 + 2.35)^2} = 4.89\ mm \tag{6.62c}$$

$$M = M_1 // M_2 = \left(\frac{1}{\frac{\mu_0}{2 \cdot \pi} \ln\left(\frac{5.98}{3.35}\right)} + \frac{1}{\frac{\mu_0}{2 \cdot \pi} \ln\left(\frac{4.89}{3.35}\right)} \right)^{-1} = \\ = 0.046\ \mu H / m \tag{6.63}$$

For the self-partial capacitance calculations, the equivalent planes are utilized again.

$$C_1 = \frac{2 \cdot \pi \cdot \varepsilon_0}{\ln\left(\frac{2 \cdot r_a}{a}\right)} = \frac{2 \cdot \pi \cdot \varepsilon_0}{\ln\left(\frac{2 \cdot 0.955}{0.3989}\right)} = 35\ pF/m \tag{6.64a}$$

$$C_2 = \frac{2 \cdot \pi \cdot \varepsilon_0}{\ln\left(\frac{2 \cdot r_b}{b}\right)} = \frac{2 \cdot \pi \cdot \varepsilon_0}{\ln\left(\frac{2 \cdot 2.09}{1.382}\right)} = 50\ pF/m \tag{6.64b}$$

$$C_M = \frac{2 \cdot \pi \cdot \varepsilon_0}{\ln\left(\frac{D^2}{a \cdot b}\right)} = \left[D = 3.35\ mm\right] = \frac{2 \cdot \pi \cdot \varepsilon_0}{\ln\left(\frac{3.35^2}{0.3989 \cdot 1.382}\right)} = 18\ pF/m \tag{6.64c}$$

Case 3

Case 3 is the case where the conductors are located at a distance of 5 mm up and 5 mm away from the ground structure. With the method described in this chapter, the following per meter values for the parameters are given:

$$L_1 = 0.62\ \mu H/m$$
$$L_2 = 0.42\ \mu H/m$$
$$M = 0.15\ \mu H/m$$
$$C_1 = 18\ pF/m$$
$$C_2 = 26\ pF/m$$
$$C_M = 18\ pF/m$$

Case 4

In Case 4 the communication conductor is placed close to the ground and the voltage feed cable is placed 5 mm up and 5 mm away from the frame rail. The coordinates yield the following parameter values per meter

$$L_1 = 0.31\ \mu H/m$$
$$L_2 = 0.40\ \mu H/m$$
$$M = 0.023\ \mu H/m$$
$$C_1 = 35\ pF/m$$
$$C_2 = 28\ pF/m$$
$$C_M = 12\ pF/m$$

Case 5

In Case 5, the thin conductor is located 5 mm up and 5 mm out from the ground structure. The thick conductor is located 6 mm away in the horizontal direction from the thin conductor and 5 mm above the ground structure. According to the method described in this chapter, the per meter parameters in this case will be:

$$L_1 = 0.62\ \mu H/m$$
$$L_2 = 0.45\ \mu H/m$$
$$M = 0.075\ \mu H/m$$
$$C_1 = 18\ pF/m$$
$$C_2 = 25\ pF/m$$
$$C_M = 12\ pF/m$$

Chapter 7

Simulation

By using electromagnetic simulation software it can be easy to test a variety of conductor layouts to find an optimal layout. This chapter describes simulations carried out to determine the values of the parasitic components for the different conductor layouts.

7.1 Simulation software

CableMod from SimLab Software GmbH is the simulation software that is utilized in this thesis. This is mainly a software program for modeling cable harnesses and crosstalk. There are different ways to define the conductor layouts and ground structure (chassis). One way is to import the whole vehicle structure as a ground shape (see Figure 7.1).

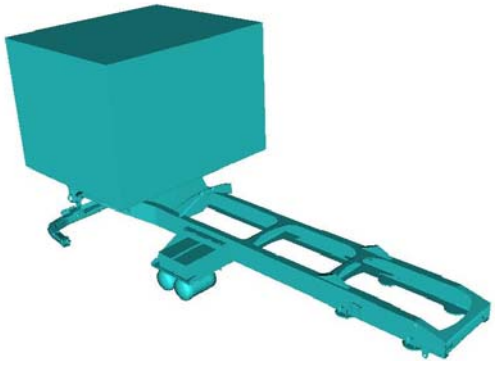

Figure 7.1. A simplified 3D simulation model of a heavy duty vehicle.

When this is done, the cable harnesses could either be imported from a CAD

file or the harness could be defined by inserting knots and connect them via sections in order to create routes for the conductors.

In some cases only the conductor cross-sections, layouts and the presence of metallic structures are important. It is then possible to create a simulation model by only defining a two dimensional cross-section of the setup.

When the ground structure and conductor layouts are defined, also the types of conductors should be defined. There is a library of predefined conductor types, and it is also possible to define new conductors knowing the cross-sectional area and the thickness and type of insulation.

When the physical characteristics are described, the software makes a two dimensional transmission line model of the setup. Since this modeling uses a two dimensional field approach it is necessary that it is possible to create homogeneous and uniform cross-sections along a certain line length of the cable harness. In the case when the two dimensional cross-section is defined from the user, this is never an issue. In more general cases, the software will subdivide the geometry into partly homogenous and uniform cross-sections. The user will select the conductors of interest and then CableMod will extract these conductors and divide them into a set of transmission line systems with variable lengths depending on the frequency and surrounding geometry. The software will also prepare all cross-sections for the field calculations in order to provide connectivity from any conductor terminal on one side of the transmission line system to the other.

The two dimensional transmission line models will contain per unit length parameters as resistance, mutual inductances, mutual capacitances and conductances. These parameters are derived by employing a static two dimensional field calculation which is applied to the cross-sections. The field calculation requires that all cross-sections are further subdivided into smaller segments, called a mesh. The smaller the size of the mesh, the more accurate the field calculations will be, but it will also mean a higher number of unknowns. When all cross-sections are meshed, the model is created. This model is valid up to a specified frequency (this frequency will determine whether the model shall be lumped or distributed depending on whether it is electrically long or short), and the user must also decide whether the model shall include ohmic (the resistance of each conductor) and/or dielectric losses (the conductance of each conductor).

The model can then be used for AC (frequency), transient (time), impedance or scatter analysis in CableMod. It is also possible to create and export either a Spice or Saber model or to view the model as a text file.

7.2 Method

CableMod utilizes two types of electromagnetic simulations methods, boundary element method (BEM) and partial element equivalent circuit (PEEC). The two methods are briefly described in Chapter 4.2.

7.3 Model and settings

For the investigated models in this thesis, five different cross-sectional layouts are created in CableMod. The ground structure is defined as a U-shape with a thickness of 8.3 mm, a width of 301 mm and a height of 93.5 mm. The material of the ground structure is defined as iron.

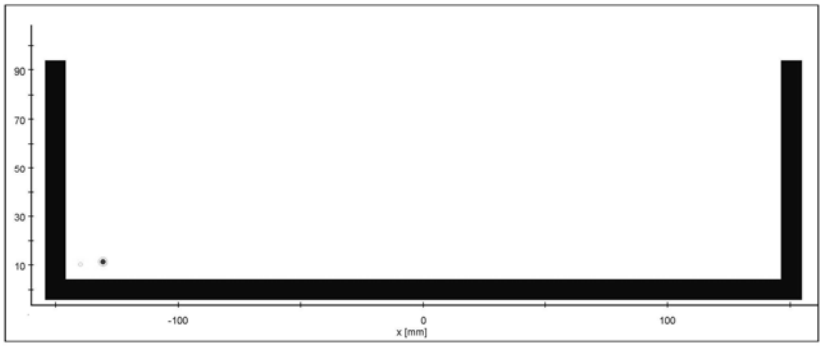

Figure 7.2. The cross-section of the simulation model.

Two types of conductors are defined. One is a thin conductor intended for communication. The copper part of this conductor has a circular cross-sectional area of 0.5 mm^2 and the PVC insulation around this conductor has a thickness of 0.7 mm. The other conductor is thicker and intended for voltage feed. This is also made of copper and has a cross-sectional area of 6 mm^2 and a 0.76 mm thick layer of PVC insulation. The two conductors are routed differently in the five cases under investigation (see Chapter 5.3).

In the two dimensional model setting of CableMod, the models are chosen to be cascaded (lumped) models since the lengths of the conductors are set to 0.1 m and the maximum frequency of interest is set to 30 MHz. The ohmic losses are included in order to provide a value for the resistance of each conductor.

7.4 Simulation results

The five different cases described in Chapter 5.3 are all implemented in CableMod. As mentioned above will the conductor layouts will be defined in the two dimensional "wire-dialogue" in the program.

The values for the resistance, the mutual inductances and the mutual capacitances are extracted from the two dimensional transmission line model view after the model is created.

Case 1

The first case contains only one conductor and the cross-section will look like Figure 7.3.

As can be seen from Figure 7.2 the origin of the ground structure is located in the middle of the structure's horizontal extension and in the middle of the thickness. The conductor under investigation will therefore have coordinates differing from Chapter 6.2 since the origin there was located at the intersection of the two perpendicular thin ground planes.

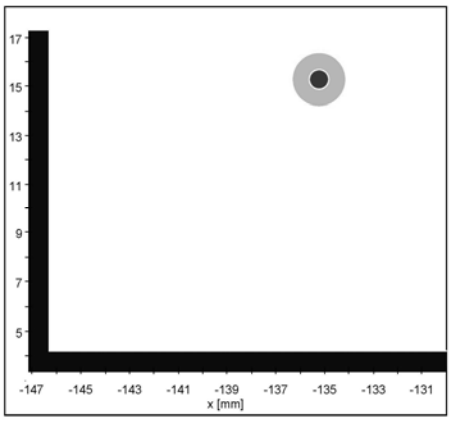

Figure 7.3. Simulation model, Case 1.

The results will be extracted from the two dimensional transmission line view which looks like

```
* Model                              : TLM_31_TLM_31
* Number of lines                    : 1
* Type                               : Lumped/Cascade
Model (slsim P)
.model           TLM_31_TLM_31    P
+ INDINVERT=YES    CAPINVERT=YES    TERMINALS=2
NODES=2          GNDNODES=0
+  EDGES=1          GNDEDGES=0       F(G)=1
+
+ TC1S1            TC1S2
+ NC1S1            NC1S2
+
+     E=(NC1S1,NC1S2)
+     R(1)=0.0038300734
+     D(1)=128594.28
+     L(1,1)=7.4742015e-008
+     C(1,1)=9.530651e-013    C(2,2)=9.530651e-013
+
+ V(1)=1
.include "D:\...\ tlmodel.tlm"
*
* Top Circuit
* Model Name                         : TLM_31
* Simulator                          : slsimpt
* Ohmic Losses                       : Yes
* Dielectric Losses                  : No
* Model Type                         : Cascade Model
* TLM Length [m]                     : 0.1
* Valid up to Frequency [Hz]         : 30000000
* Number of Terminals                : 2
* Number of Cross Sections           : 1
* Number of Cross Instances          : 1
*
.subckt          TLM_31           IN_0q5mm
OUT_0q5mm
*instances of cross sections
* TL Instance                        : TLM_31
* Number of Wires                    : 1
PTLM_31          OUT_0q5mm        IN_0q5mm
TLM_31_TLM_31
.ends
```

$$L = 0.75\ \mu H / m$$

This will give the per meter values for the inductance and capacitance as

$$C = 9.53 \cdot 2 = 19\ pF / m$$

Case 2

In Case 2, both conductors are present. As can be seen in Figure 7.4 they are conductors located close to each other and near the ground structure.

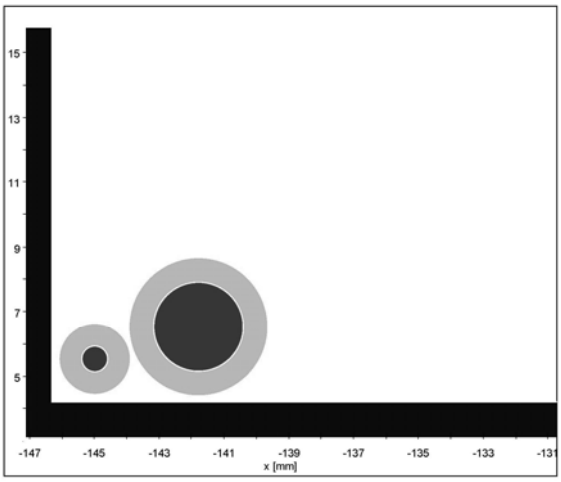

Figure 7.4. Simulation model, Case 2.

Since there are two conductors present, also the mutual inductances and capacitances between the conductors are determined. An extract from the two dimensional transmission line model will then look like

```
+      L(1,1)=2.1176138e-008   L(1,2)=4.2374323e-009
       L(2,1)=4.2374323e-009   L(2,2)=3.1726309e-008
+
```

```
+      C(1,1)=3.69019745e-012  C(2,2)=3.69019745e-012
       C(1,3)=9.6969555e-013   C(2,4)=9.6969555e-013
+      C(3,1)=9.6969555e-013   C(4,2)=9.6969555e-013
       C(3,3)=2.7655214e-012   C(4,4)=2.7655214e-012
```

Where L(1,2) and L(2,1) are the mutual inductance between the conductors and C(1,3), C(2,4), C(3,1) and C(4,2) are the mutual capacitances. This gives the parasitic components per meter as

$$L_1 = 0.32\ \mu H/m$$
$$L_2 = 0.21\ \mu H/m$$
$$M = 0.042\ \mu H/m$$
$$C_1 = 55\ pF/m$$
$$C_2 = 74\ pF/m$$
$$C_M = 19\ pF/m$$

Case 3

In Case 3, both conductors are located at a distance of 5 mm up and 5 mm away from the ground structure (see Figure 7.5).

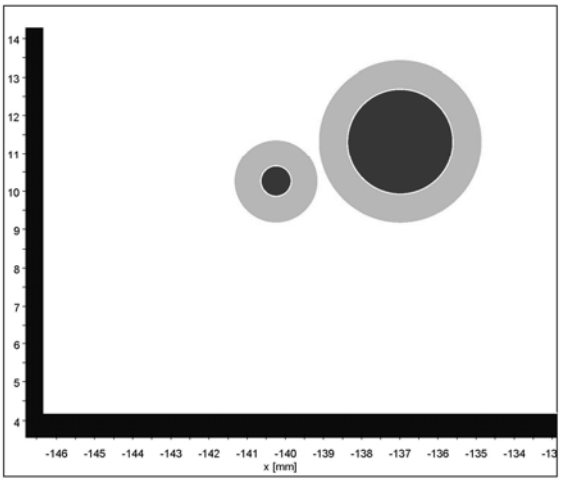

Figure 7.5. Simulation model, Case 3.

The created model has the following parameter values per meter

$$L_1 = 0.61\ \mu H/m$$
$$L_2 = 0.43\ \mu H/m$$
$$M = 0.23\ \mu H/m$$
$$C_1 = 14\ pF/m$$
$$C_2 = 24\ pF/m$$
$$C_M = 27\ pF/m$$

Case 4

In Case 4 is the thin communication conductor placed in the corner of the structure and the voltage feed conductor 5 mm up and 5 mm out.

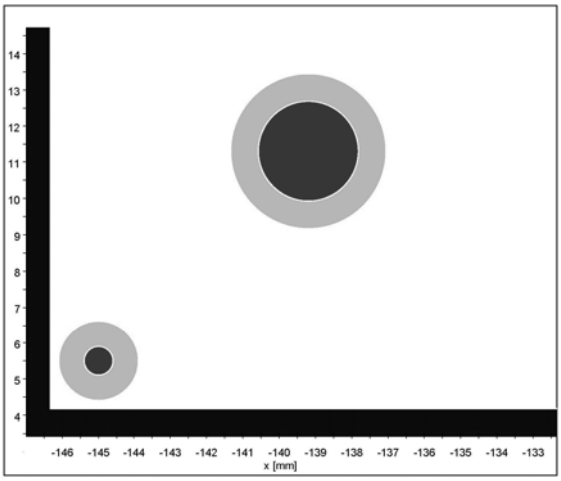

Figure 7.6. Simulation model, Case 4.

This setup yields the following values per meter

$$L_1 = 0.32\ \mu H/m$$
$$L_2 = 0.40\ \mu H/m$$
$$M = 0.014\ \mu H/m$$
$$C_1 = 63\ pF/m$$
$$C_2 = 32\ pF/m$$
$$C_M = 2.2\ pF/m$$

Case 5

Finally, in Case 5, the thin communication conductor is placed 5 mm up and 5 mm out from the ground structure. The voltage feed cable is located 5 mm above the ground plane and 6 mm away from the communication conductor. The setup can be seen in Figure 7.7.

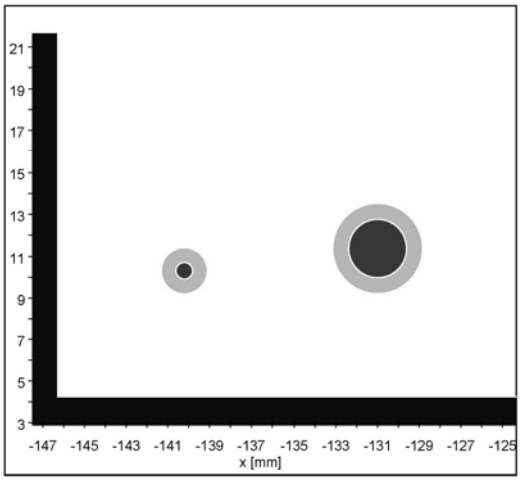

Figure 7.7. Simulation model, Case 5.

The values for the parasitic components per meter conductor in the model are

$$L_1 = 0.63\ \mu H/m$$
$$L_2 = 0.45\ \mu H/m$$
$$M = 0.078\ \mu H/m$$
$$C_1 = 20\ pF/m$$
$$C_2 = 26\ pF/m$$
$$C_M = 4.8\ pF/m$$

Chapter 8

Measurements

In the previous chapters, the values of the parasitic components are estimated analytically and by simulation. As described in Chapter 2, it is useful to have a measurement to compare the computed or simulated results with if possible. The previous developed values will therefore be compared to measured values.

This chapter describes the experimental setup and the methods for measuring the parasitic inductances and capacitances. The measurement results of the components for the different conductor layouts are also presented.

8.1 Experimental setup

Two conductors and a ground structure are used in the measurements,. The aim is to find the parasitic inductances and capacitances between the conductors and the ground structure. A schematic of the setup is shown in Figure 8.1.

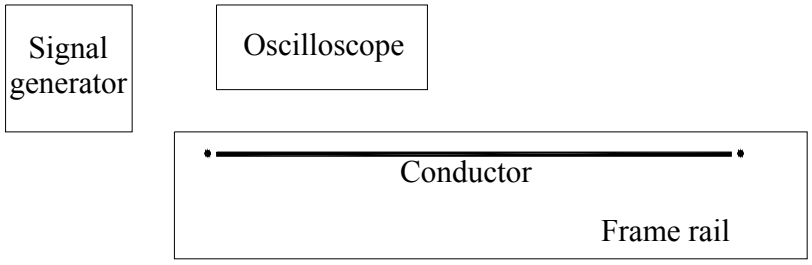

Figure 8.1. Overview of the different parts of the measurement setup.

Ground structure

As described in Chapter 5.2, a part of a frame side rail from a heavy-duty vehicle is used as a ground structure in the investigations. The frame part is 1.6 m long U-channel originating from a 4x2 tractor. A cross-section of the frame is shown in Figure 5.3.

The frame is made of high-strength steel and has a thin (approximately 70 μm) thick layer of coating. There are 128 holes with a diameter of 155 mm drilled in the frame rail. Since the diameter of these holes is smaller than 1/20 of the wavelength of the highest frequency of interest [48], and the holes only constitutes a small part of the total surface, the holes will not have any effect on the results.

In order to facilitate electrical contact with the frame, another two holes are drilled. The coating surrounding these two holes is removed and two terminals are attached for easy mounting of conductors. One of these holes is located 10 cm from the end of the frame, and the other one is located 1 m further away from the end. A top view of the frame rail is shown in Figure 8.2.

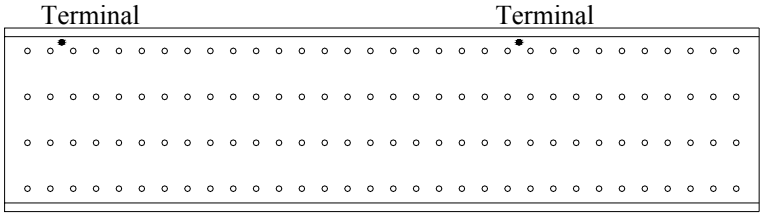

Figure 8.2. The frame rail.

Conductors

As mentioned in Chapter 5.2, two types of conductors are used in the experimental setup. The thin conductor, intended for communication, has a cross-sectional area of 0.5mm^2 and a 0.7 mm thick PVC insulation [17]. The thicker conductor, intended for voltage feed to the load, has a cross-sectional area of 6 mm^2 and a 0.76 mm thick PVC insulation [61]. Each conductor has a length of 1 m.

Signal generator and oscilloscope

The signal generator used in the measurements is an old fashioned vacuum tube amplifier of type Oltronix RC-oscillator RCO-6K. This generator is chosen since it has the ability to generate a pure sine with high amplitude and high current limit. For measurements, an oscilloscope from Tektronix (TDS 640A) is used.

In Figure 8.3 the whole setup is shown.

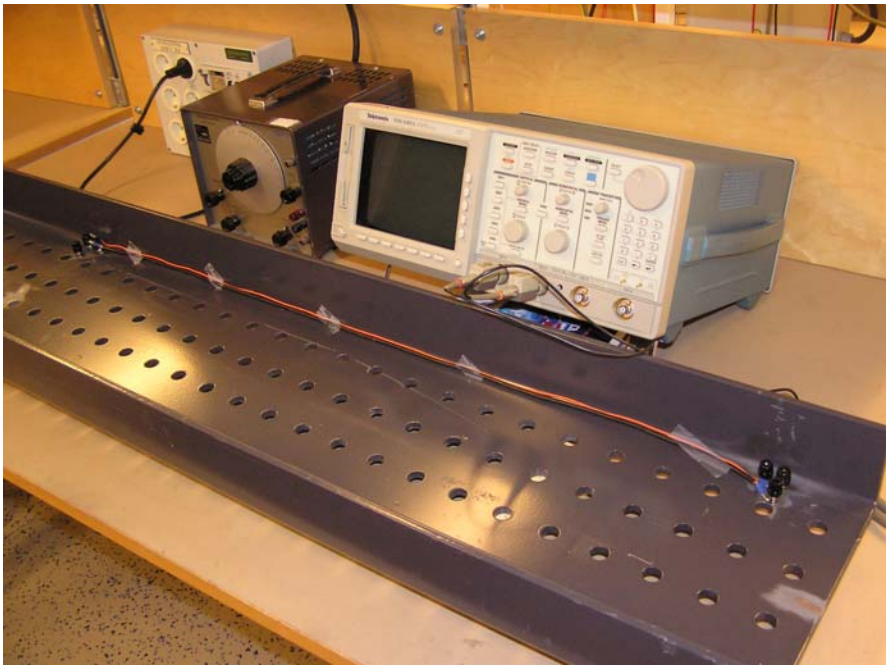

Figure 8.3. The measurement setup.

8.2 Inductance measurements

Two types of inductances are measured; the inductance from each conductor to the frame (ground) and the mutual inductance between the two conductors. Due to the lack of a sinusoidal generator with a very high current limit, the measurements of the self inductance for each conductor are not possible to measure without also getting the inductance of the frame. Since the inductance of the frame is hard to estimate, all inductance values for the

frame and conductors are to be seen only as comparative values. The measurement of the inductance between one conductor and the frame is performed by applying a sinusoidal voltage to the frame via a 0.1 Ω resistance. The conductor under investigation is placed on the frame and connected to the frame in one end and the oscilloscope and generator in the other. The setup is shown in Figure 8.4.

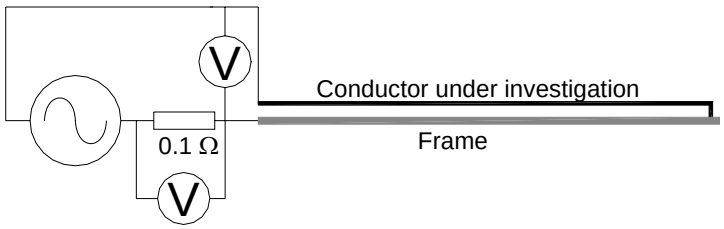

Figure 8.4. Measurement setup for measuring the self inductance of a conductor.

The equivalent circuit for the inductance measurement shown in Figure 8.4 looks like (Figure 8.5)

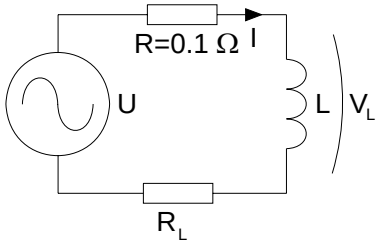

Figure 8.5. Equivalent circuit for measuring the self inductance.

where R_L is the DC resistance of the frame and conductor under investigation.

The value for the inductance of the conductor and the frame will then be given by:

$$\overline{V}_L = j \cdot \omega \cdot L \cdot \bar{I} = j \cdot \omega \cdot L \cdot \frac{\overline{V}_R}{R} \qquad (8.1a)$$

$$L = \mathrm{Im}\left(\frac{\overline{V}_L \cdot R}{j \cdot \omega \cdot \overline{V}_R} \right) \qquad (8.1b)$$

In this setup, the frequency of the sinusoidal is set to be 100 kHz.

The mutual inductance between the two cables is measured in a similar way. Both conductors are connected to the frame in one end. In the other end, one conductor is connected to the signal generator via the 15 Ω resistance and the other is connected to the oscilloscope as seen in Figure 8.6.

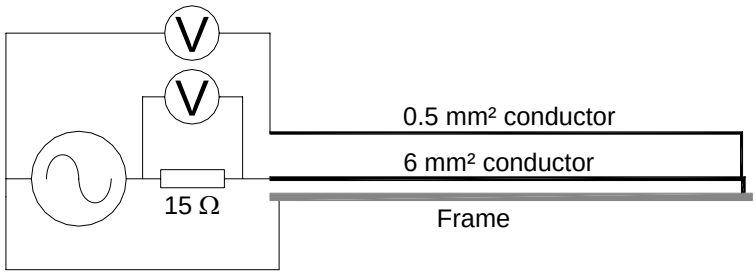

Figure 8.6. Measurement setup for measuring the mutual inductance.

The equivalent circuit for the setup looks like in Figure 8.7 and the expressions for calculating the inductance are given in equation 8.2.

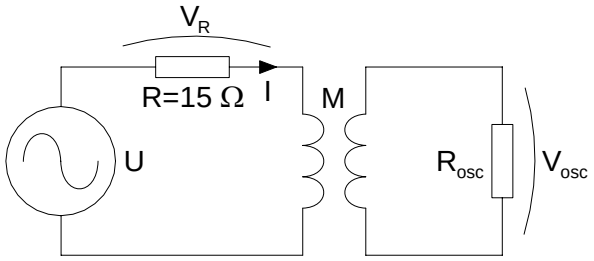

Figure 8.7. Equivalent circuit for measuring the mutual inductance.

Applying Kirchoff's voltage law for the equivalent circuit in Figure 8.7 yields the following expressions:

$$\bar{V} = \bar{V}_R + M \cdot \frac{d\bar{I}}{dt} = R \cdot \bar{I} + j \cdot \omega \cdot M \cdot \bar{I} \qquad (8.2a)$$

$$\bar{V}_{osc} = M \cdot \frac{d\bar{I}}{dt} = j \cdot \omega \cdot M \cdot \bar{I} \qquad (8.2b)$$

$$M = \mathrm{Im}\left(\frac{\bar{V}_{osc} \cdot R}{j \cdot \omega \cdot \bar{V}_R} \right) \qquad (8.2c)$$

In the setup, the resistance, R, is chosen to 15 Ω and the frequency set to 200 kHz. The two voltages V_{osc} and V_R are measured and will together with equation 8.2 give the inductance.

8.3 Capacitance measurement

In the experimental setup, the capacitance from each conductor to the frame (ground) and the capacitance between the two conductors are measured. The measurement of the capacitance between a conductor and the frame is carried out as shown in Figure 8.8. The conductor under investigation is placed on the frame, and at each end of the conductor, a resistance is connected. A closed loop for the current in the conductor is created by connecting the two resistances with each other via a conductor situated away from the frame and the voltage over one of the resistances is measured.

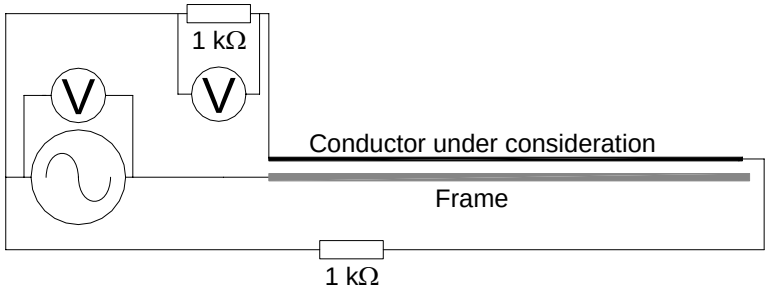

Figure 8.8. Measurement of the self-partial capacitance.

The voltage connected to the frame is coupled to the conductor via the capacitance between the frame and conductor as shown in the equivalent circuit in Figure 8.9.

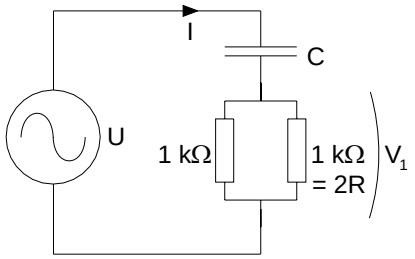

Figure 8.9. Equivalent circuit for measurement of the self-partial capacitance.

An investigation of the equivalent circuit in Figure 8.9 will give equation 8.3. Since the resistances are connected in parallel, the resulting resistance in the equivalent circuit has only half the value of the physical resistances.

$$\bar{V} = \frac{1}{j \cdot \omega \cdot C} \bar{I} + \bar{V}_1 \tag{8.3a}$$

$$\bar{I} = \frac{\bar{V}_1}{R} \tag{8.3b}$$

$$C = \mathrm{Im}\left(\frac{1}{\omega \cdot R \left(\frac{\bar{V}}{\bar{V}_1} - 1 \right)} \right) \tag{8.3c}$$

Since the resistance R, is known and the voltages V and V_1 are measured, equation 8.3 gives the capacitance between the conductor and the frame. The frequency of the sinusoidal voltage is in these setups set to be 10 kHz.

In the setup where the capacitance between two conductors is measured, the two conductors are placed next to each other on the frame. One conductor is connected to two resistances as in the previous setup and the other conductor is connected to the signal generator in one end and remains unconnected in the other. The setup looks like Figure 8.10.

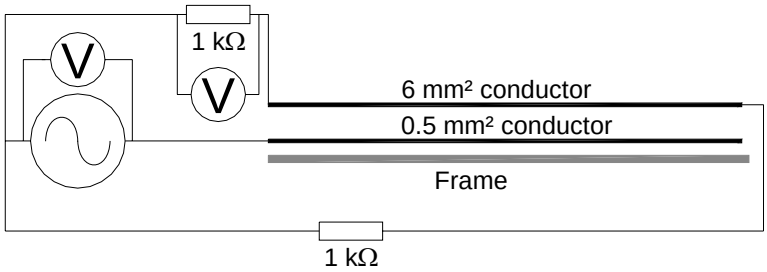

Figure 8.10. Measurement of the mutual capacitance between two conductors.

There is no difference on the equivalent circuit for this setup compared to the previous one. The equivalent circuit can therefore be seen in Figure 8.9 and the value for the capacitance between the two conductors is calculated by using equation 6.51.

8.4 Measurement uncertainties

It is only in theory that a measured value is exact and correct. In the real world, a measured value is defective and not as accurate as wanted. The measurements that are made in this thesis are only carried out once why no standard deviations or mean values are calculated. However, it is possible to estimate the uncertainties of the measurement results by looking at the specified uncertainties of the different components of the setup. These uncertainties and the results from them will be described in this chapter.

Oscilloscope and probes

As mentioned in Chapter 8.1 the oscilloscope that is used during the measurements is of type Tektronix TDS 640A [70]. According to the datasheet from the oscilloscope, the vertical accuracy is 1.5%, which implies that the voltage levels could either be 1.5% higher or lower than the levels shown on the oscilloscope.

The probes that are used together with the oscilloscope are of type Tektronix P6139A [71]. These are 10X probes which means that there will be a voltage division between the oscilloscope and the probe. The input resistance of a probe can together with the oscilloscope vary between 9.95 MΩ and 10.05 MΩ. The input capacitance is specified in the datasheets as 8 pF ± 0.8 pF.

Inductance measurements

The inductance measurements, as well as the capacitance measurements are performed as indirect measurements since the currents in the setups are measured as a voltage over a resistance. In the setup for measuring both the self and mutual capacitances this resistance had a value of 0.1 Ω with an accuracy of 5%. The resistance is called R_m in Figure 8.11.

In Figure 8.11 the whole measurement setup is shown. The two voltages that are measured, V_1 and V_2, are depending on the probes (one of the probes is encircled by the dashed rectangle to the left in the figure).

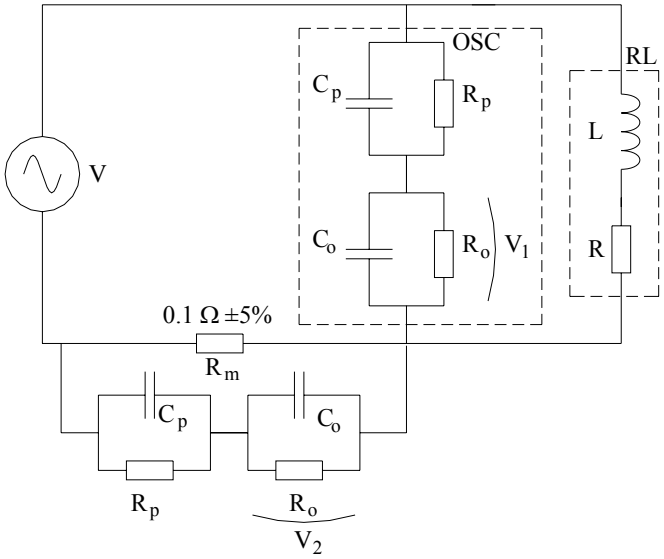

Figure 8.11. Measurement setup including oscilloscope and probes.

An equivalent circuit for the measurement is shown in Figure 8.12.

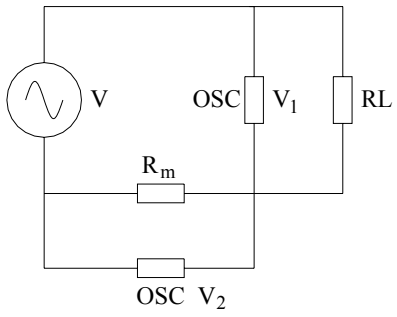

Figure 8.12. Equivalent circuit for the measurement setup.

For the circuit, the inductance value is calculated by taking the quotient of the two voltages, V_q, and then finding the total impedance RL consisting of the inductance in series with the resistance of both the ground structure and the conductor. The inductance will then be the imaginary part of the impedance as:

$$V_1 = V \cdot \frac{R_o // C_o}{R_o // C_o + R_p // C_p} \cdot \frac{OSC // RL}{OSC // RL + OSC // R_m} \tag{8.4a}$$

$$V_2 = V \cdot \frac{R_o // C_o}{R_o // C_o + R_p // C_p} \cdot \frac{OSC // R_m}{OSC // RL + OSC // R_m} \tag{8.4b}$$

$$V_q = \frac{V_1}{V_2} = \frac{OSC // RL}{OSC // R_m} = \frac{\dfrac{OSC \cdot RL}{OSC + RL}}{\dfrac{OSC \cdot R_m}{OSC + R_m}} = \frac{RL \cdot (OSC + R_m)}{R_m \cdot (OSC + RL)} \tag{8.4c}$$

$$L = \frac{\mathrm{Im}\left(\dfrac{V_q \cdot R_m \cdot OSC}{OSC + R_m (1 - V_q)} \right)}{2 \cdot \pi \cdot f} \tag{8.4d}$$

In the case where the mutual inductance is measured, a 15 Ω resistance is used. This resistance has an accuracy of 10%.

Capacitance Measurements

The capacitance measurements are as mentioned above also indirect

measurements where two voltages are measured and employed for calculation of the sought parameter. In the measurements, two resistors of 1 kΩ each are used (denoted R in Figure 8.13). These resistances each have an accuracy of 5%.

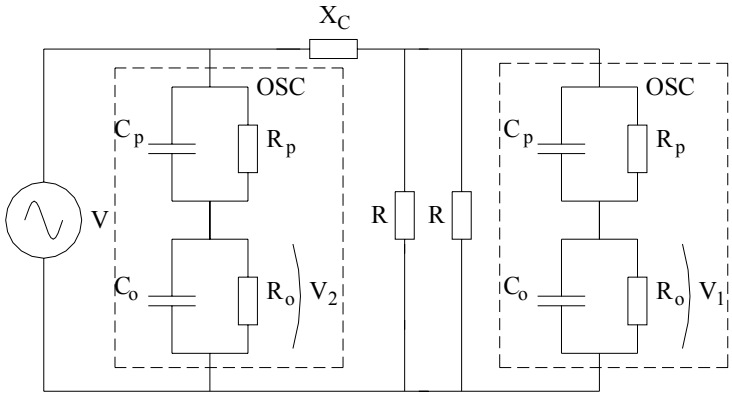

Figure 8.13. Measurement setup for capacitance measurements including oscilloscope and probes.

A simplified equivalent circuit for the setup is shown in Figure 8.14.

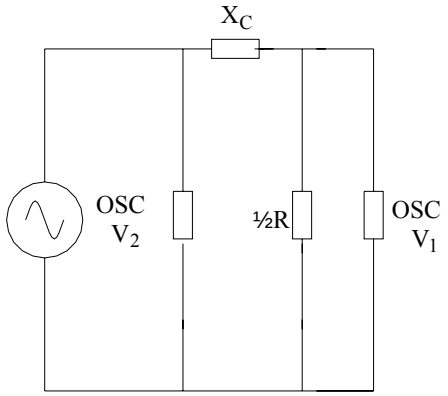

Figure 8.14. Equivalent circuit for measurement of capacitances.

In the case of the capacitances the two voltages are also measured and an unknown impedance is calculated. The reactance is then found as the

imaginary part of this reactance.

$$V_1 = V \cdot \frac{R_o // C_o}{R_o // C_o + R_p // C_p} \cdot \frac{(OSC // 1/2 \cdot R)}{(OSC // 1/2 \cdot R) + X_C} \tag{8.5a}$$

$$V_2 = V \cdot \frac{R_o // C_o}{R_o // C_o + R_p // C_p} \tag{8.5b}$$

$$\frac{V_1}{V_2} = V_q = \frac{(OSC // 1/2 \cdot R)}{(OSC // 1/2 \cdot R) + X_C} \tag{8.5c}$$

$$X_C = (OSC // 1/2 \cdot R)\left(\frac{1}{V_q} - 1\right) = \frac{OSC \cdot 1/2R}{OSC + 1/2R}\left(\frac{1}{V_q} - 1\right) \tag{8.5d}$$

$$C = \frac{1}{2 \cdot \pi \cdot f \cdot \mathrm{Im}(X_C)} \tag{8.5e}$$

Uncertainty estimations

In order to estimate the uncertainties in the measurements, equations 8.4 and 8.5 are implemented into Matlab and the different combinations of resistance values and voltage values are all tested in order to get a maximum and a minimum value for the parameter. These values are presented in next chapter for the parameters of each case.

8.5 Measurement results

The aim of the experiments is to find how the parameters depend on the geometrical properties of the conductor layout. Five different layouts are therefore utilized and they are described more in detail in Chapter 5.3.

Case 1, Single conductor

In Case 1, only the communication conductor is present. The conductor is placed at a distance of 10 mm out from the frame and 10 mm up.

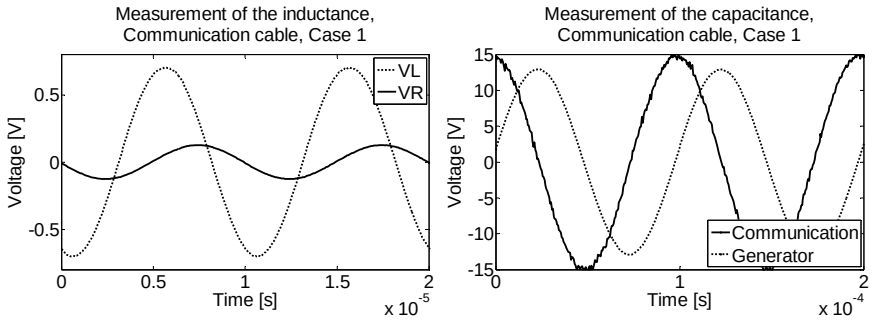

Figure 8.15. Left: The results from the measurement of the inductance. The dotted line is the voltage over the inductance and the black line the voltage over the resistance in the setup. Right: The voltage from the generator (dotted) and the voltage over the resistance (x1000, black) in the measurement setup for the capacitance measurement.

The results are presented in Figure 8.16. By using equations 8.4 and 8.5, the following values will be obtained.

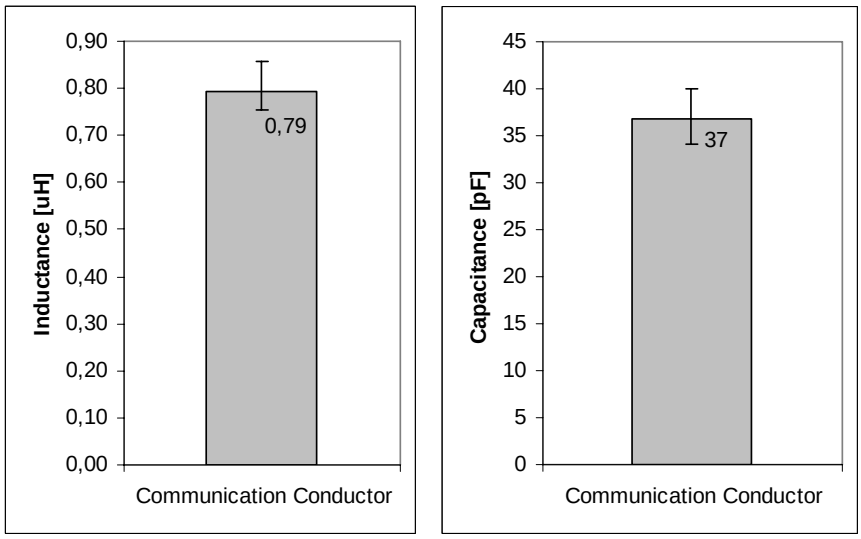

Figure 8.16. Left: The result from the measurement of the inductance with the margins of error indicated. Right: The results from the capacitance measurement.

Case 2, Two conductors together, close to ground

In Case 2, both conductors are present and routed next to each other close to the corner of the frame. The results from the inductance measurements are shown in Figure 8.17.

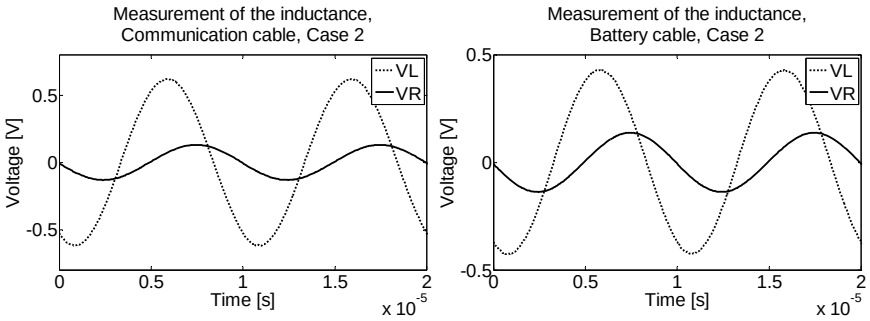

Figure 8.17. The results from the measurement of the self inductances of the communication conductor (left) and the battery conductor (right). The dotted line is the voltage over the inductance and the black line the voltage over the resistance in the setup.

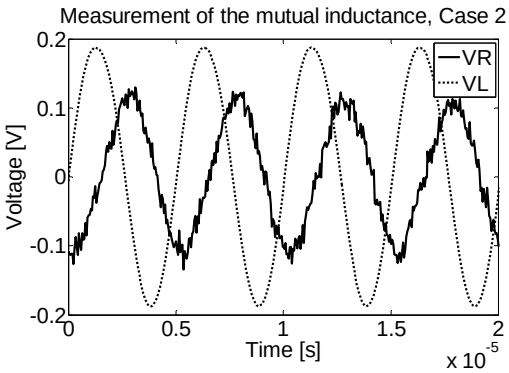

Figure 8.18. The result from the measurement of the mutual inductance between the conductors. The dotted line is the voltage over the inductance and the black line the voltage over the resistance in the setup.

This will yield the following self inductances and mutual inductance.

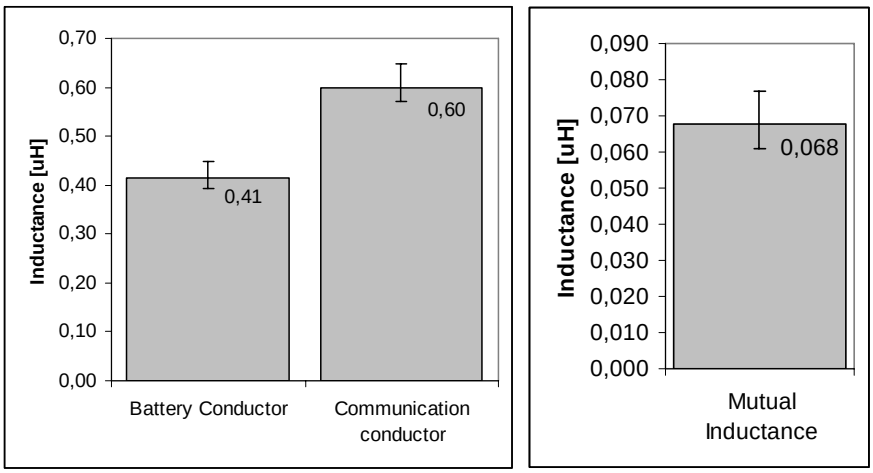

Figure 8.19. The results from the measurement of the self and mutual inductances with the margins of error indicated.

The capacitance measurements are shown in Figure 8.20 and 8.21, and the results are given below in Figure 8.22.

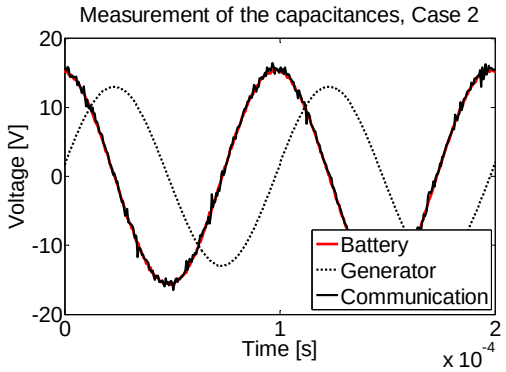

Figure 8.20. The result from the measurement of the self-partial capacitances. The dotted line is the voltage from the generator and the black (communication conductor, x500) and red (battery conductor, x500) lines are the voltages over the resistances in the setup.

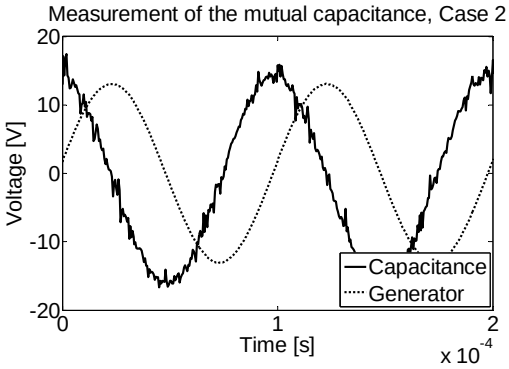

Figure 8.21. The result from the measurement of the mutual capacitance. The dotted line is the voltage from the generator and the black line is the voltage over the resistance (x1000) in the setup.

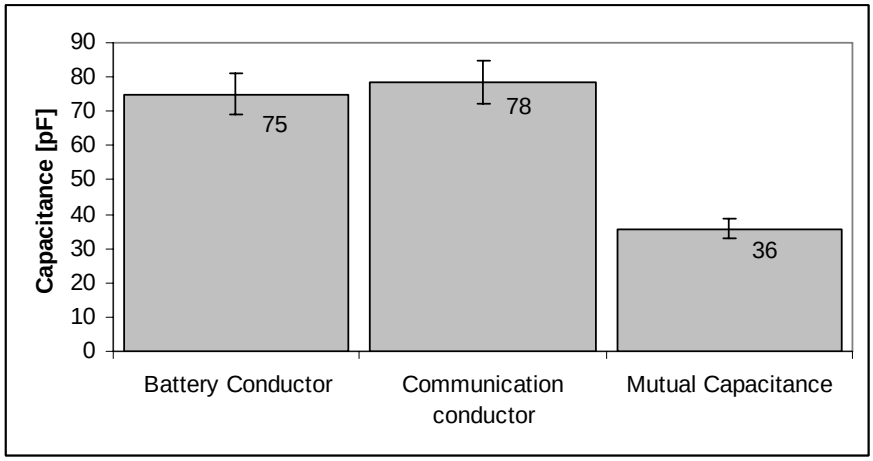

Figure 8.22. The results from the measurement of the self and mutual capacitances of Case 2 with the margins of error indicated.

Case 3, Two conductors together, away from ground

In Case 3 both conductors are lifted 5 mm up from the frame. The thin communication conductor is placed 5 mm out from the vertical side of the frame. Figure 8.23 and 8.24 show the results from the inductance measurements.

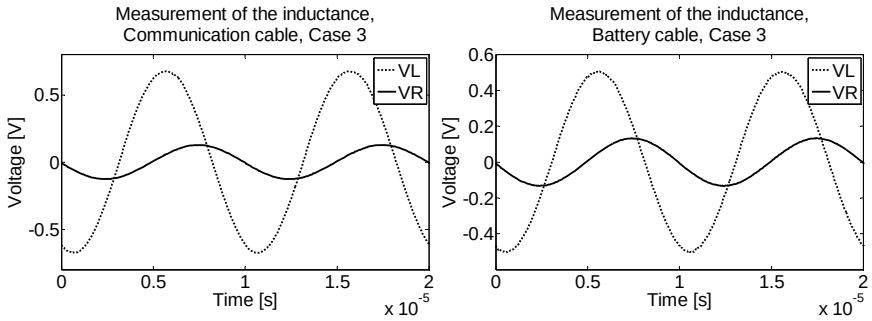

Figure 8.23. The results from the measurement of the self inductances in Case 3 of the communication conductor (left) and the battery conductor (right). The dotted line is the voltage over the inductance and the black line the voltage over the resistance in the setup.

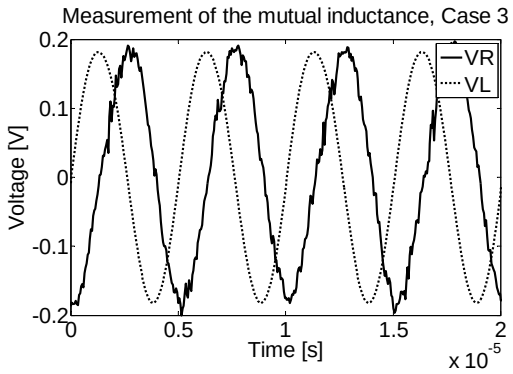

Figure 8.24. The results from the measurement of the mutual inductances in Case 3. The dotted line is the voltage over the inductance and the black line the voltage over the resistance in the setup.

An analysis of the results will yield the following inductance values (Figure 8.25).

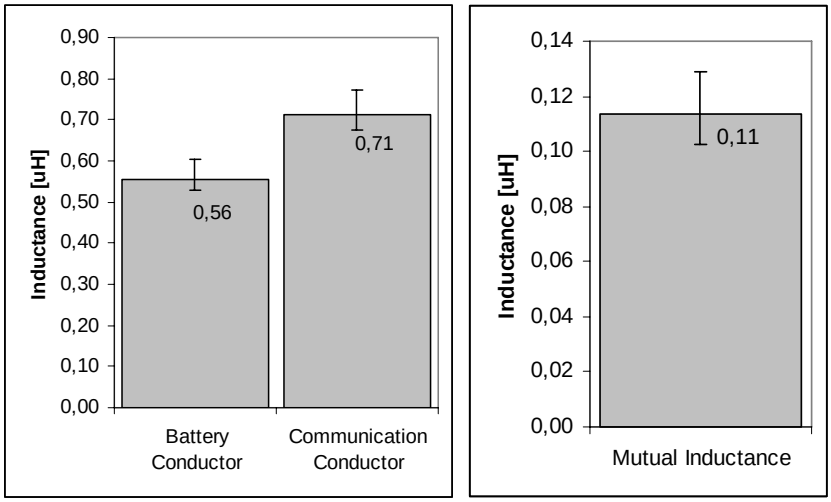

Figure 8.25. Results from the measurement of the self and mutual inductances of Case 3 with the margins of error indicated.

The capacitance measurements are shown in Figure 8.26 and 8.27 from which the following capacitance values are received.

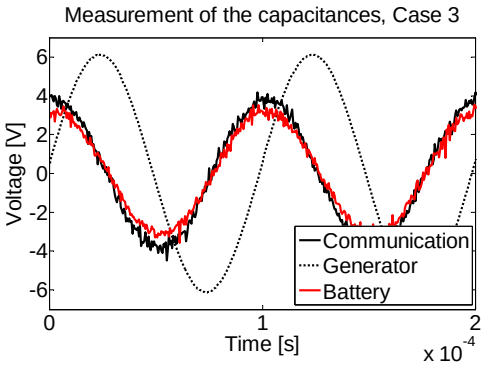

Figure 8.26. The result from the measurement of the self-partial capacitances. The dotted line is the voltage from the generator and the black (communication conductor, x500) and red (battery conductor, x500) lines are the voltages over the resistances in the setup.

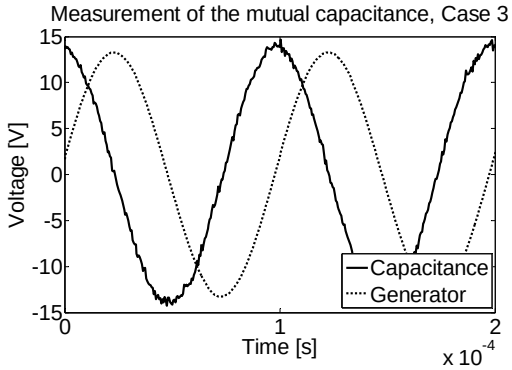

Figure 8.27. The result from the measurement of the mutual capacitance. The dotted line is the voltage from the generator and the black line is the voltage over the resistance (x1000) in the setup.

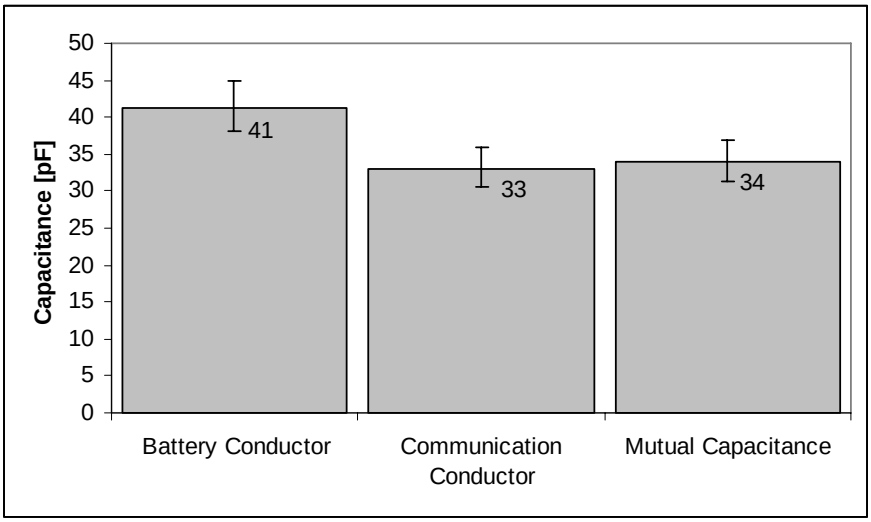

Figure 8.28. Results from the measurement of the self and mutual capacitances of Case 3 with the margins of error indicated.

Case 4, Two conductors apart, one close to ground

The thin conductor for communication will be placed in the corner of the frame in Case 4, whereas the thick conductor for voltage feed is located 5 mm up and 5 mm out from the frame.

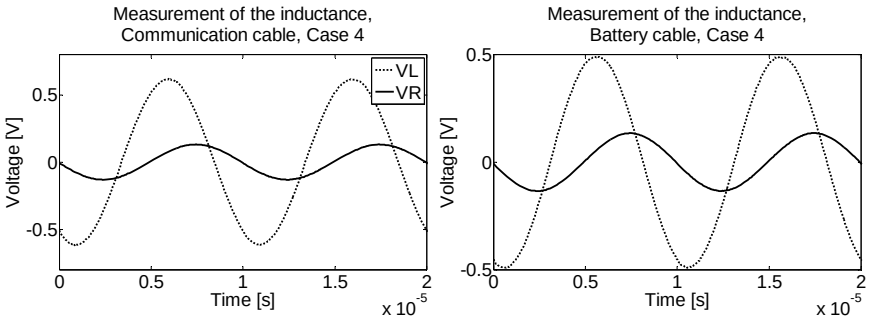

Figure 8.29. The results from the measurement of the self inductances in Case 4 of the communication conductor (left) and the battery conductor (right). The dotted line is the voltage over the inductance and the black line the voltage over the resistance in the setup.

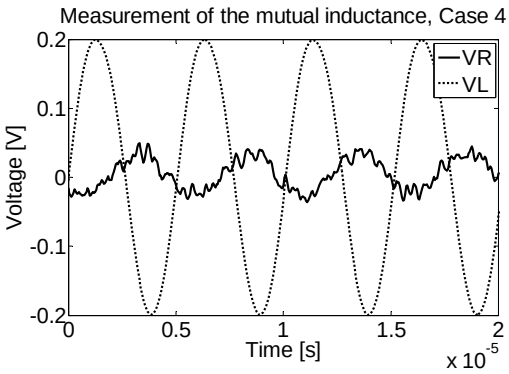

Figure 8.30. The results from the measurement of the mutual inductances in Case 4. The dotted line is the voltage over the inductance and the black line the voltage over the resistance in the setup.

The measurement results for the inductances in Figure 8.29 and 8.30 will give the following inductance values (Figure 8.31).

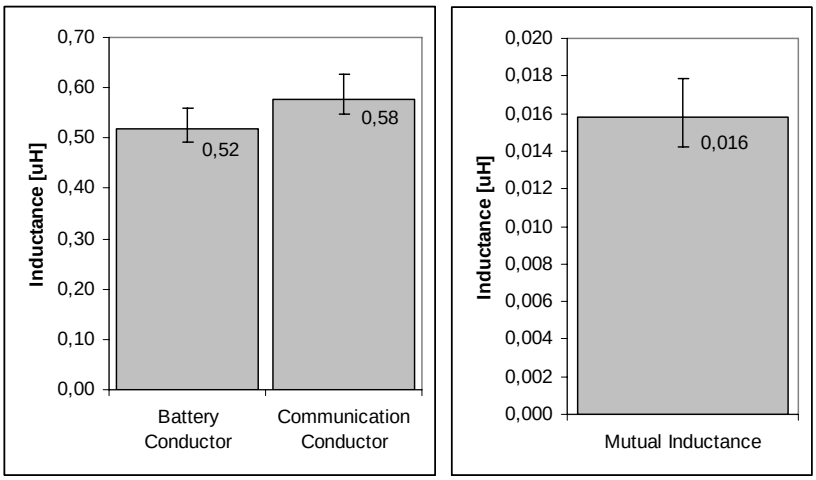

Figure 8.31. Results from the measurement of the self and mutual inductances of Case 4 with the margins of error indicated.

In Figure 8.32 are the results from the capacitive measurements.

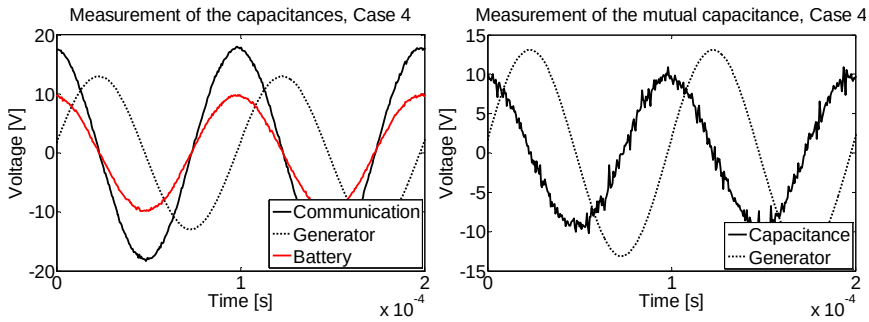

Figure 8.32. Left: The result from the measurement of the self-partial capacitances. The dotted line is the voltage from the generator and the black (communication conductor, x500) and red (battery conductor, x500) lines are the voltages over the resistances in the setup. Right: The result from the measurement of the mutual capacitance. The dotted line is the voltage from the generator and the black line is the voltage over the resistance (x1000) in the setup.

The graphs in Figure 8.32 will gain capacitance values as

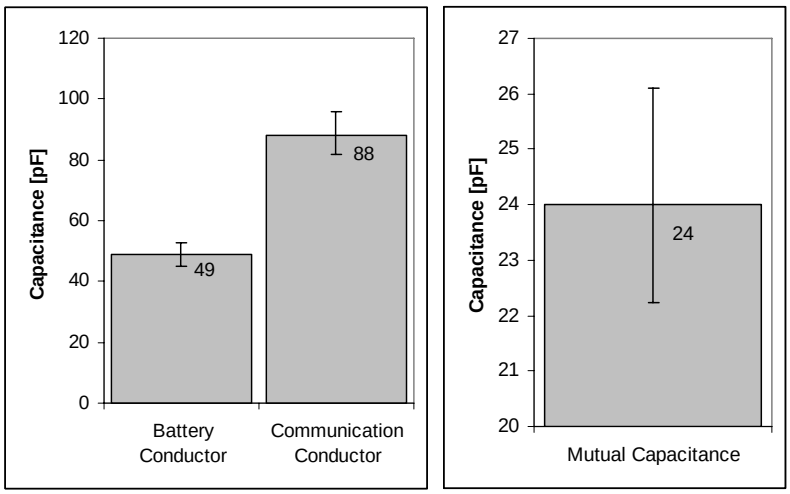

Figure 8.33. Results from the measurement of the self and mutual capacitances with the margins of error indicated.

Case 5, Two conductors apart, away from ground

In the last case is the thin communication conductor placed 5 mm up and 5 mm out from the frame. The battery conductor is located 6 mm away from the communication conductor, and 5 mm up. The inductance measurement results are shown in Figure 8.34.

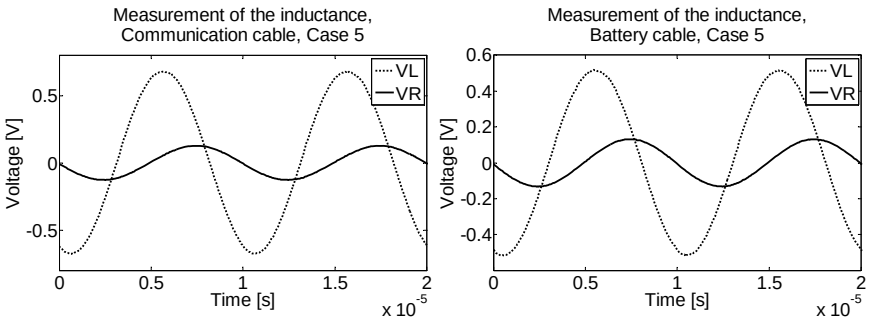

Figure 8.34. The results from the measurement of the self inductances in Case 5 of the communication conductor (left) and the battery conductor (right). The dotted line is the voltage over the inductance and the black line the voltage over the resistance in the setup.

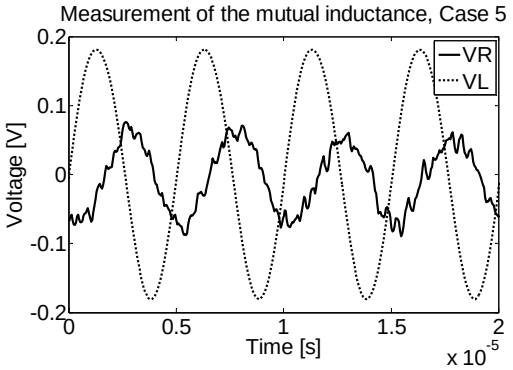

Figure 8.35. The results from the measurement of the mutual inductances in Case 5. The dotted line is the voltage over the inductance and the black line the voltage over the resistance in the setup.

The inductance values gained from these measurements are

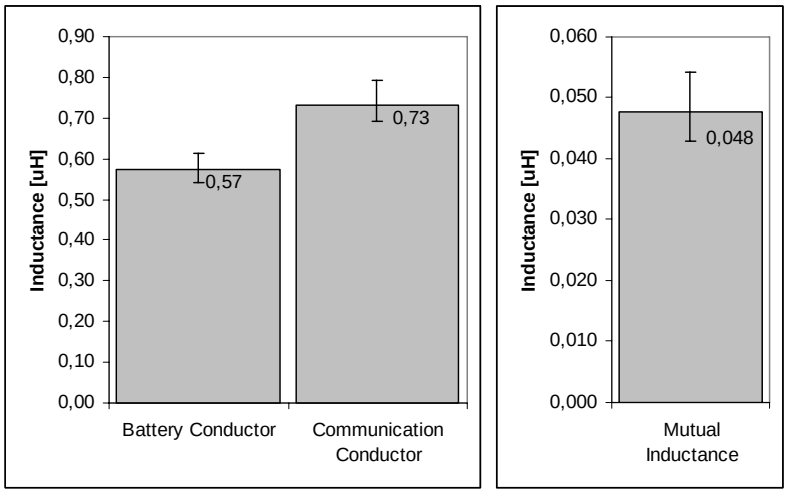

Figure 8.36. Results from the measurement of the self and mutual inductances of Case 5 with the margins of error indicated.

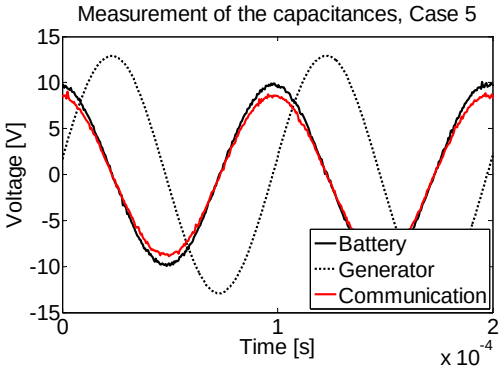

Figure 8.37. The result from the measurement of the self-partial capacitances. The dotted line is the voltage from the generator and the black (battery conductor, x500) and red (communication conductor, x500) lines are the voltages over the resistances in the setup.

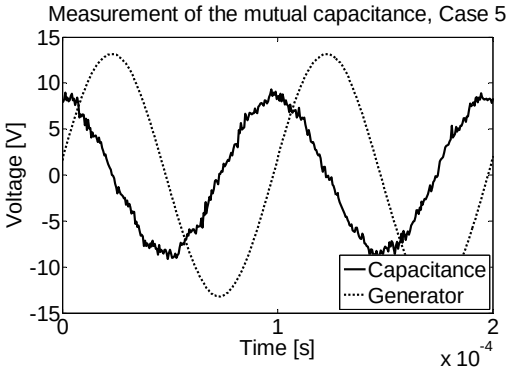

Figure 8.38. The result from the measurement of the mutual capacitance. The dotted line is the voltage from the generator and the black line is the voltage over the resistance (x1000) in the setup.

The capacitances values obtained from the measurements in Figure 8.37 and 8.38 will be

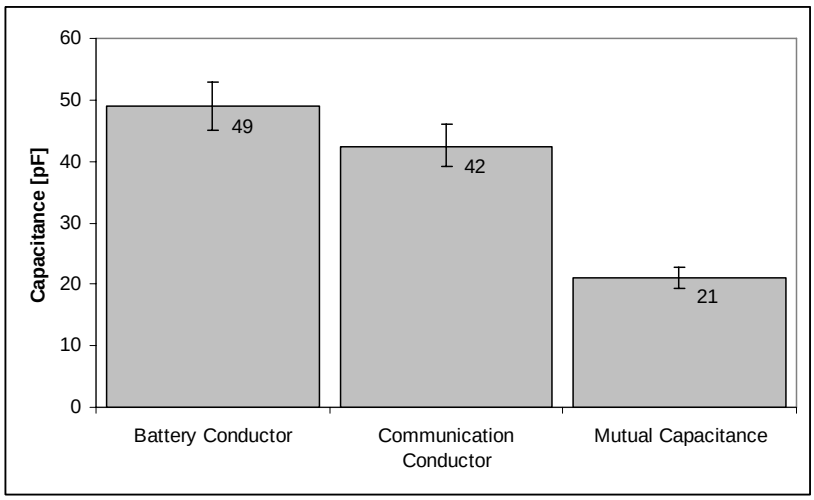

Figure 8.39. Results from the measurement of the self and mutual capacitances with the margins of error indicated.

Chapter 9

Analysis of the results

In the previous chapters, different ways of determining the parasitic components for two conductors in different conductor layouts are presented with results. In this chapter, all results will be summarized and the circuit models for the different setups will be presented and analyzed. Finally, some general guidelines will be presented for design of an electromagnetically compatible system.

9.1 Case 1

In Case 1 only the thin communication conductor is present according to Figure 9.1.

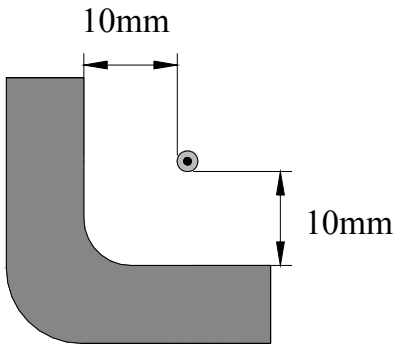

Figure 9.1. Cross-section of the conductor layout in Case 1.

The calculated, simulated and measured values for the parasitic components are shown in Figure 9.2.

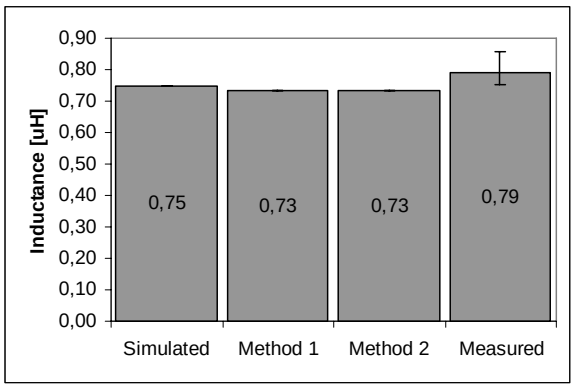

Figure 9.2. Summary of the results for the inductance in Case 1.

As can be seen, the values for the self inductance of the conductor agree fairly well. The uncertainties of the measured value indicate that the self inductance could be as low as 0.75 µH, which agrees even better with the simulated and calculated values.

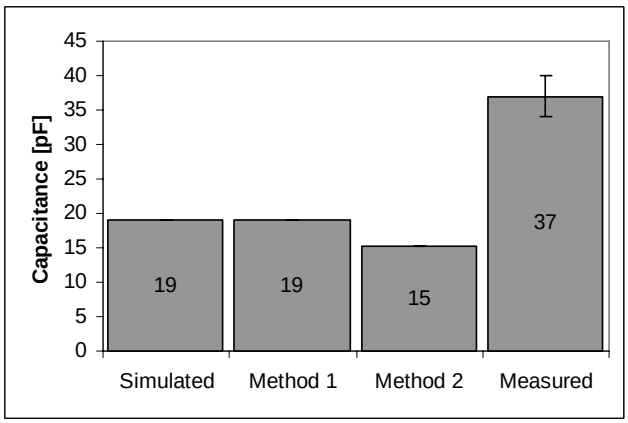

Figure 9.3. Summary of the results for the capacitance in Case 1.

The values for the self-partial capacitance for the accurate analytical calculations and the simulations agree well. Since the distance between the conductor and the ground structure is rather large, the assumption that the line charge is located at the centre of the conductor does not affect the value of the capacitance. In the case where Method 2, the approximate method

with the equivalent planes, is used, the value of the self-partial capacitance is lower. This is due to the fact that the equivalent plane will be located at a distance of about 7 mm from the line charge and thereby only give one "contribution" to the self-partial capacitance, whereas the accurate method will have three contributions although not all with the same sign (one from the vertical part of the ground structure, one from the horizontal part and one from the positive line charge located diagonally to the conductor). The measured value of the self-partial capacitance deviates from the simulated and calculated values and the reasons for this will be discussed in Section 9.3.

9.2 Case 2

In Case 2, both conductors are present and routed close to each other in the corner of the ground structure, as in Figure 9.4.

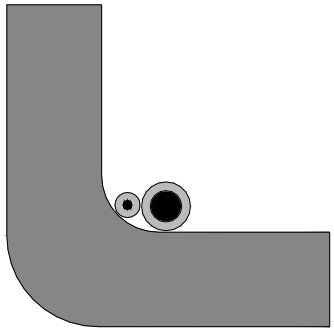

Figure 9.4. The conductor layout in Case 2.

Compared to Case 1, the inductance is expected to decrease and the capacitance to increase due to the reduction in distance between the conductor and the ground structure.

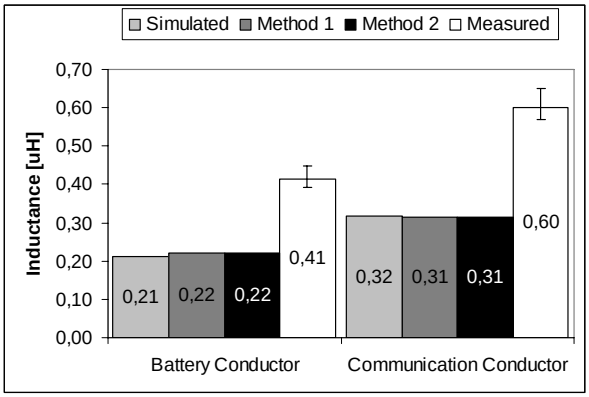

Figure 9.5. Summary of the results for the inductances in Case 2.

As can be seen in the diagram of Figure 9.5, the self inductance does decrease as expected. The inductance of the battery conductor is lower than the inductance for the communication conductor. This is due to the increase in the radius of the conductor. The magnetic flux density B outside a conductor is defined as

$$B = \frac{\mu_0 \cdot I}{2 \cdot \pi \cdot r} \qquad (9.1)$$

where I is the current of the conductor, and r the radius of the conductor. From this equation, it is possible to see that when the radius of the conductor is increased, the flux density will decrease. Since the inductance is proportional to the flux density, also the inductance will decrease.

For both the communication conductor and the battery conductor there is a rather large difference between the measured values for the self inductances and the calculated/simulated. This is due to the approximation that is made in both the simulations and the calculations that the conductivity of the ground structure is very high wherefore the method of images can be employed. This is however not true as can be seen from the measurements. The ground structure was modelled to have a conductivity of 10 MS/m, but the material of which it is made has actually a conductivity of only 3 MS/m [63]. The skin depth is depending on the conductivity according to equation 6.1, and a lower conductivity will give a larger skin depth. The phenomena can be seen in Figure 9.6 where Case 2 is simulated in a FEM

analyser and the current density, J, and vector potential, A, are studied for different values of the conductivity, σ.

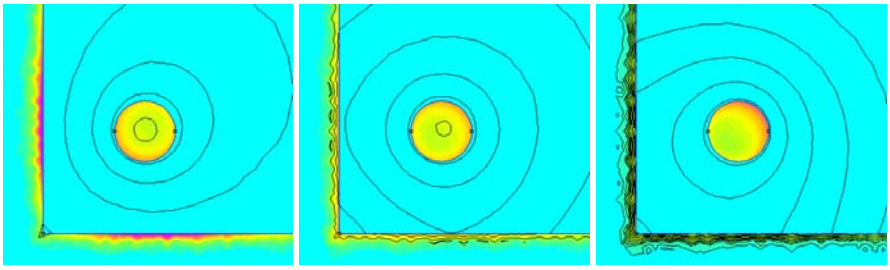

Figure 9.6. A FEM simulation of a current carrying conductor and a ground structure. The vector potential A and the current density, J are plotted. The three ground structures have different conductivities; Left: σ = 100 MS/m, Middle: σ = 10 MS/m and Right: σ = 3 MS/m. Frequency = 100 kHz.

For the three different conductivities of the ground structure in Figure 9.6, the self inductance of the communication conductor will be 0.27 μH (σ = 100 MS/m), 0.45 μH (σ = 10 MS/m), and 0.66 μH (σ = 3 MS/m). In the case where the conductivity is high, the skin depth will be almost negligible and the value of the self inductance will be close to the simulated and analytically calculated values. In the case where the true value for the conductivity is used, the measured value for the self inductance will be close to the value from the FEM simulation. This implies that for an accurate analysis of the setup, the conductivity of the ground plane must be taken into account. This will however not affect the crosstalk to any larger extent if the crosstalk is considered to be weak and coupled via the mutual inductance and capacitance.

Since the two conductors are routed close to each other in this setup, the mutual inductance will not be very high, but also in this case the conductivity of the frame does affect the measurement results. Not as much as in the case of the self inductance since the mutual inductance is depending on the flux between the two conductors, but it will increase the mutual inductance compared to the simulated and analytically calculated values.

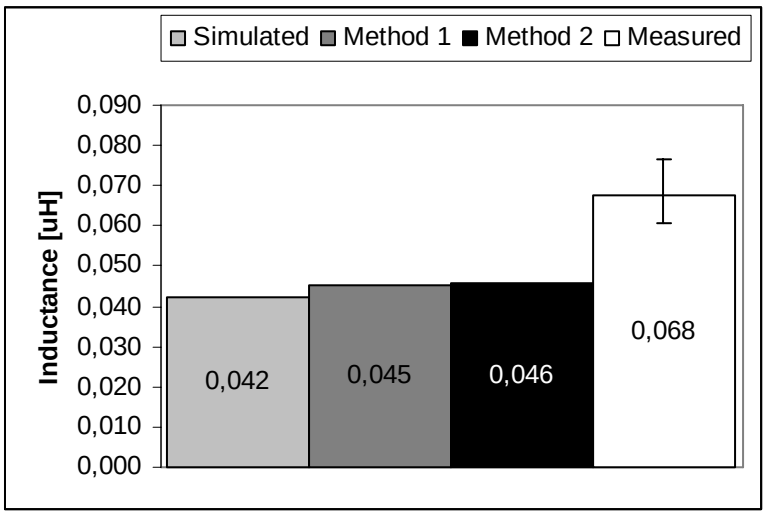

Figure 9.7. Summary of the results for the mutual inductance in Case 2.

The measurement of the mutual inductance is larger than the simulated and calculated values since the conductors are clamped together in reality.

The capacitance of the thin communication conductor is expected to increase in this case compared to Case 1. The results in Figure 9.8 confirm this theory. Since both conductors are clamped to the ground structure, the effect from the assumption in the calculations, that the line charge is located in the middle of the conductor, will be significant here. This is clearly seen from the differences between the simulated and calculated self-partial capacitance for the battery conductor. The effect is less obvious for the communication conductor since a displacement of the line charge from the centre of the conductor will not imply any larger difference in the distance between the line charge and ground structure.

The measured value for the self-partial capacitances agree well with the simulated values in the case where the battery conductor is investigated. The measured capacitance value for the communication conductor deviates a bit since it is closer to the ground structure in reality than in the simulation and calculations.

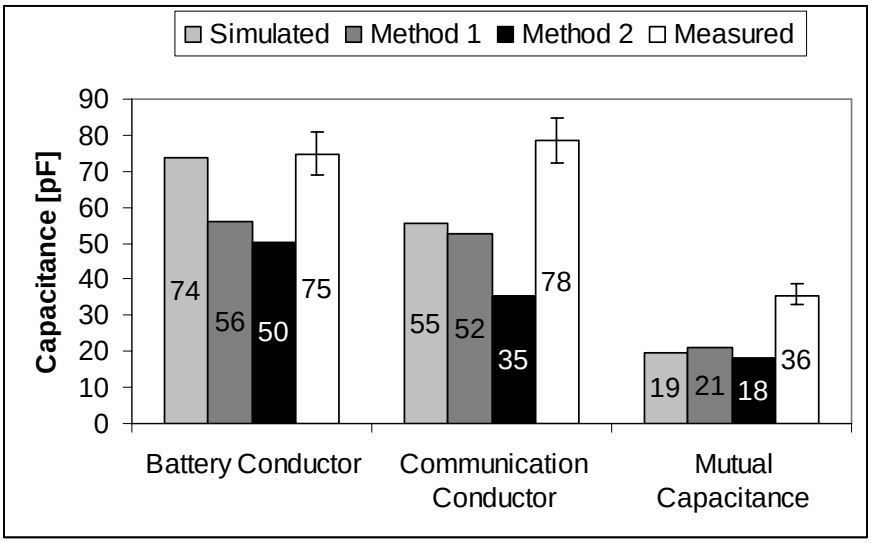

Figure 9.8. Summary of the results for the capacitances in Case 2.

9.3 Case 3

In Case 3 both conductors are elevated 5 mm above ground and routed next to each other. This is the most realistic case since the conductors due to mounting reasons seldom are routed as close to the frame as in Case 2.

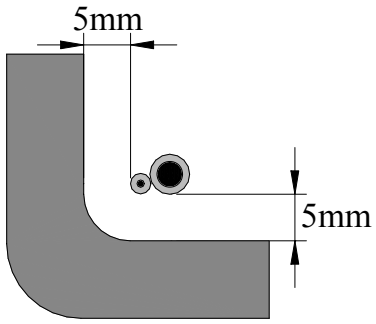

Figure 9.9. Conductor layout, Case 3.

When the conductors are located at a larger distance from the ground

structure, their self inductances are expected to increase at the same time as their self-partial capacitances decrease.

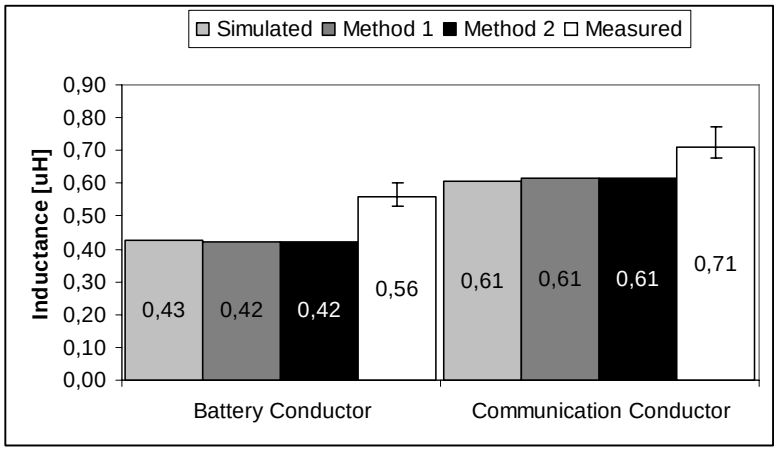

Figure 9.10. Summary of the results for the inductances in Case 3.

As seen in Figure 9.10 the self inductances do increase. The difference between the measured values and the simulated/calculated values are smaller in this case since the distance to the ground structure is larger and hence the skin depth does not have as much effect as in Case 2.

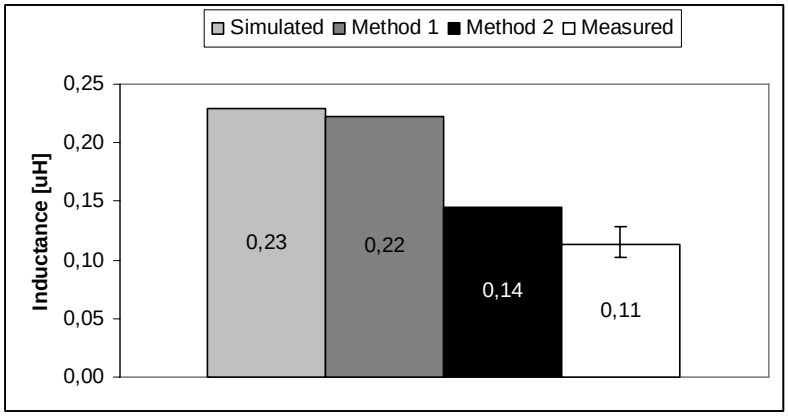

Figure 9.11. Summary of the results for the mutual inductance in Case 3.

The measurement of the mutual inductance will give a smaller value than the simulated and calculated values. This is most likely because the conductors are closer to each other in the measurements than in the simulations and calculations.

The measured values for the self-partial capacitances deviate a lot from the simulated and calculated values. This tendency is shown already in Case 1 and it is obvious here again (see Figure 9.12).

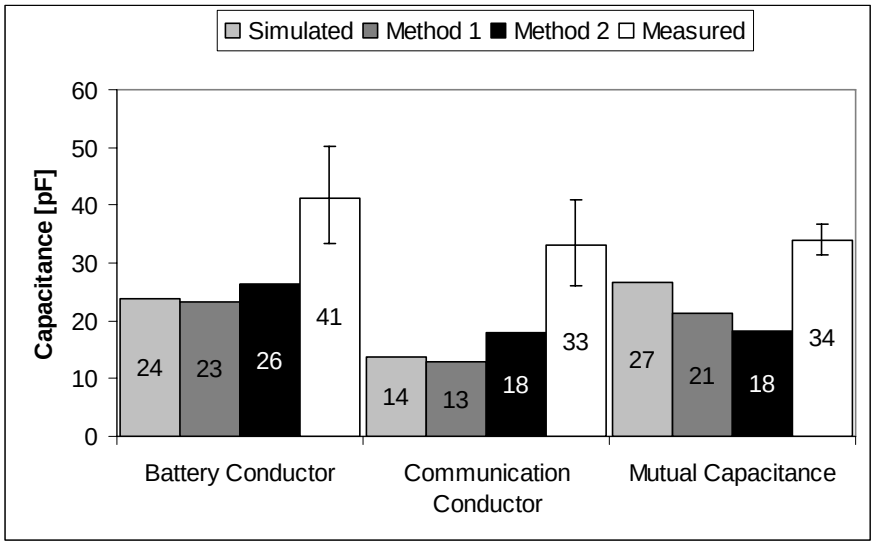

Figure 9.12. Summary of the results for the capacitances in Case 3.

Since there is a better agreement in Case 2 between theoretical and measured values for the self-partial capacitances, a measurement error is probably introduced when the cables are raised from the ground structure. In order to raise the conductors, 5 mm thick books are employed. Paper has a relative permittivity of about 5 [35], which means that the presence of the paper instead of air will enable that more charges can be stored and hence the capacitance increased. In order to see if this assumption is correct, an electrostatic FEM model is built.

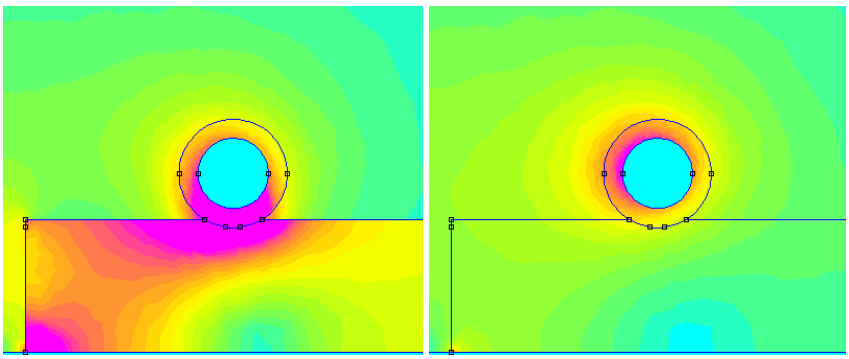

Figure 9.13. FEM model of a conductor on a rectangular area that is made of paper (left) and air (right). The flux density, D, is shown.

The FEM model contains only the battery conductor located 5 mm above the ground structure and about 7 mm out from the vertical part of the ground structure. In the FEM model, a rectangular area between the ground structure and the conductor is defined. This rectangle is defined as paper with a relative permittivity of 5 in one case and as air in the other case. The energy stored in all areas except the conductor and its insulation is integrated, and the stored energy will yield the capacitance by using the following formula:

$$W = \frac{1}{2} C \cdot V^2 \quad \Rightarrow \quad C = \frac{2 \cdot W}{V^2} \tag{9.2}$$

Where W is the energy and V the voltage of the conductor. This will give a capacitance value for the battery conductor in Figure 9.13 of 36 pF for the case where the rectangle is defined as paper and 22 pF in the case where it is defined as air. Since the simulated and analytically calculated values are 23-24 pF and the measured value is 41 pF, the presence of the paper in the measurements is most likely the reason for the deviation in value. Since there are no papers available as spacers in the real setup, the simulated and calculated values will in this case be the most realistic values.

9.4 Case 4

In Case 4 the communication conductor is located in the corner of the ground structure and the battery conductor raised diagonally above.

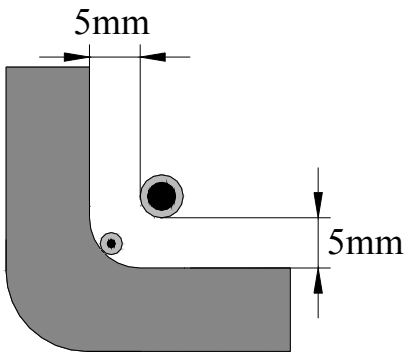

Figure 9.14. Cross-sectional view of the conductor layout in Case 4.

For this case the inductance value for the communication conductor is expected to be the same as in Case 2, and the self inductance value for the battery conductor is expected to be somewhat smaller than in Case 3, since the conductor is a bit closer to the frame. Although the communication conductor is in the same position as in Case 2, the value for the self-partial capacitance is expected to change since the physical surrounding of the conductor has changed (the battery conductor is moved away from the communication conductor). The self-partial capacitance for the battery conductor is also expected to change compared to Case 3, partly due to the distance to the communication conductor, but also due to it being located closer to the ground structure.

The determination of the inductance shows that the measured value deviates most for the communication conductor since this one is located closest to the ground structure and thereby most affected by the skin depth. The values gained from the simulation and the analytical calculations (both Method 1 and 2) agree well with each other.

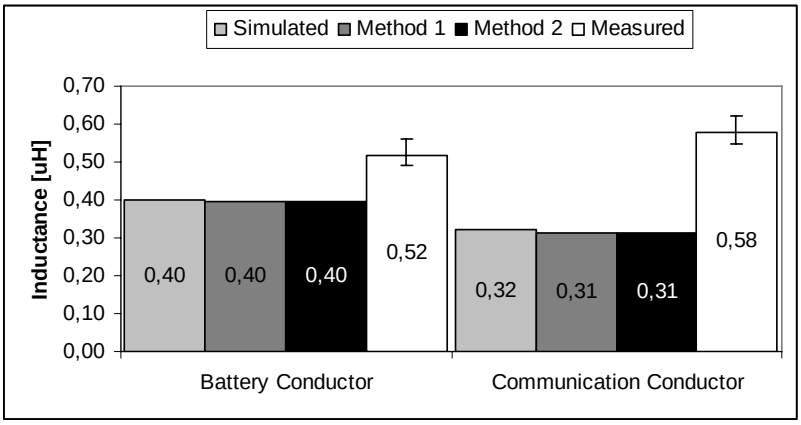

Figure 9.15. Summary of the results for the inductances in Case 4.

The values for the mutual inductance agree well for all methods for determination except for Method 2. This is due to the fact that the diagonal currents in Figure 6.9 are not taken into account in the analysis.

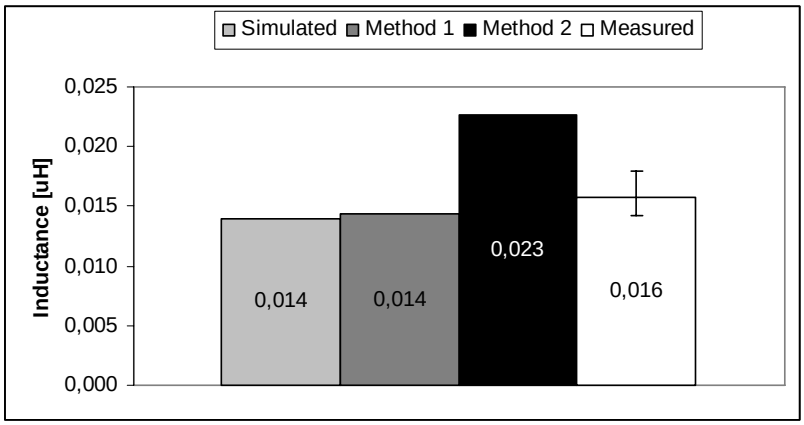

Figure 9.16. Summary of the results for the mutual inductance in Case 4.

The differences in self-partial capacitance between the measured and simulated/calculated values originates from the location of the line charge and the stack of paper situated next to the conductor. Method 2 for the self-partial capacitance of the communication conductor deviates from the other

simulated and calculated values since it does not take the surrounding environment into account. In the case of the battery conductor the paper underneath the conductor is the main reason for the deviation in the measured value compared to the other values.

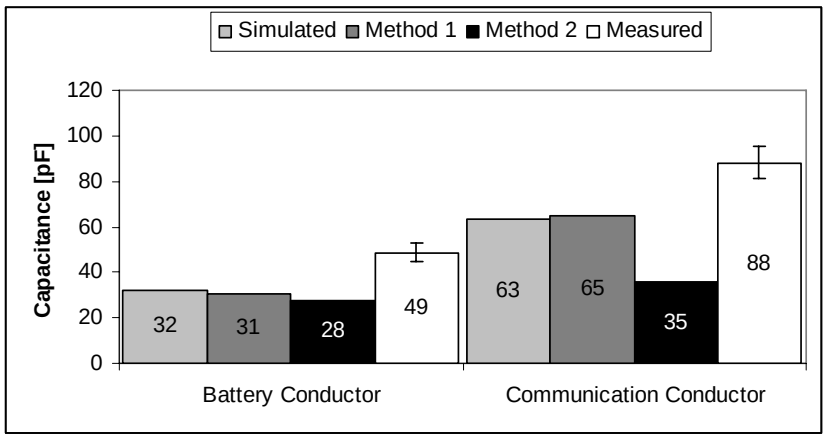

Figure 9.17. Summary of the results for the capacitances in Case 4.

In the fourth case the mutual capacitance between the conductors is so low that it is hard to measure with the used equipment.

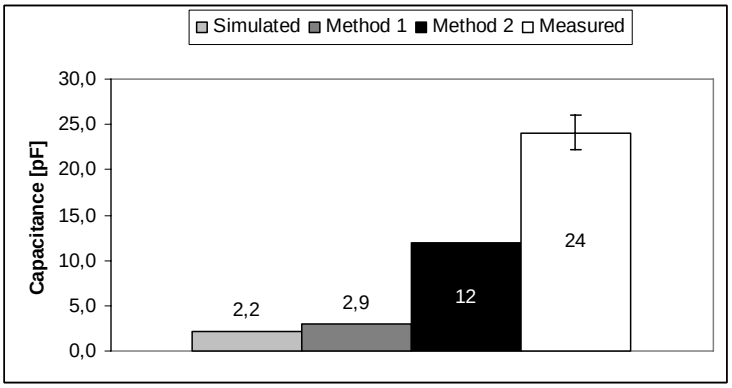

Figure 9.18. Summary of the results for the mutual capacitance in Case 4.

9.5 Case 5

In the last case, both conductors are elevated 5 mm from the ground structure and separated 6 mm.

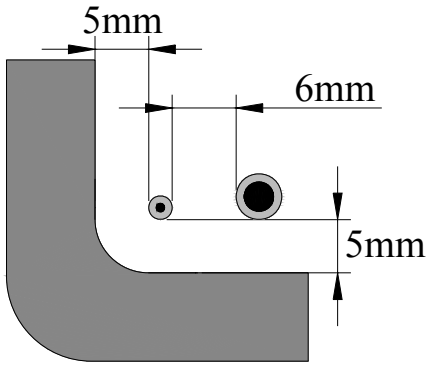

Figure 9.19. Conductor layout, Case 5.

In this case the mutual inductance is expected to be rather low due to the distance between the conductors and the distance to the ground structure. Also the mutual capacitance is expected to be low.

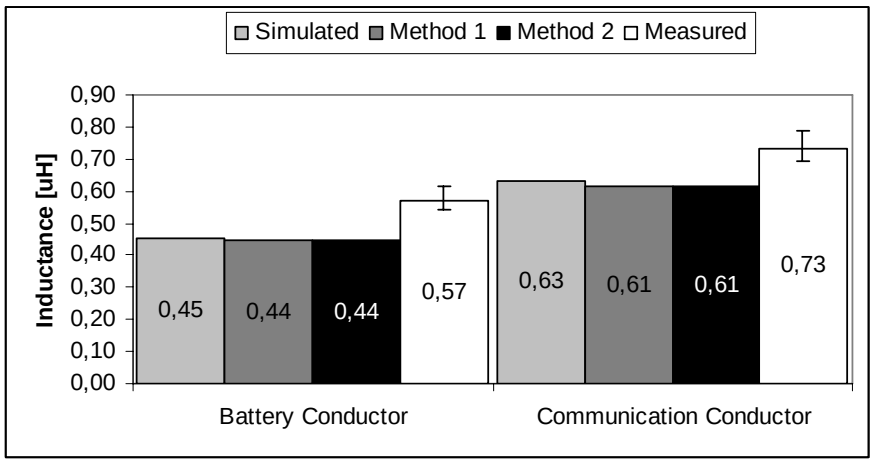

Figure 9.20. Summary of the results for the inductances in Case 5.

Since both conductors are raised above the ground structure the skin depth in the ground structure does not affect the measurement results to any larger extent and thus the values from the simulations and calculations agree well with the measurements.

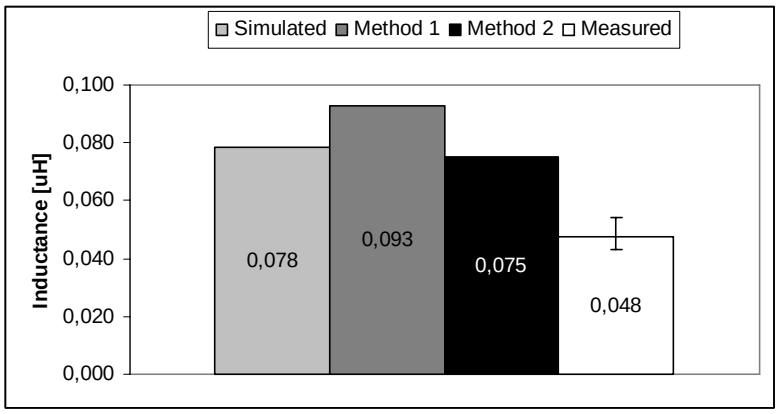

Figure 9.21. Summary of the results for the mutual inductance in Case 5.

As in Case 2, the conductors are closer in reality than in the theoretical models, why the measured value of the mutual inductance deviates from the simulated and calculated.

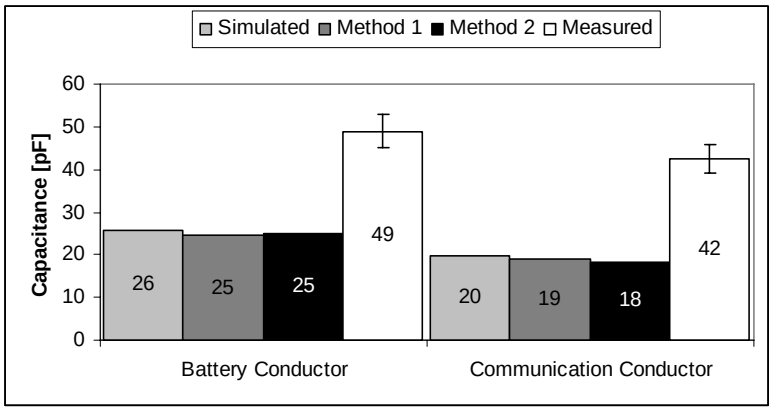

Figure 9.22. Summary of the results for the self-partial capacitances in Case 5.

In the measurements of the self-partial capacitances, the books that are used to raise the conductors affect the results to a large extent, which can be seen in Figure 9.22.

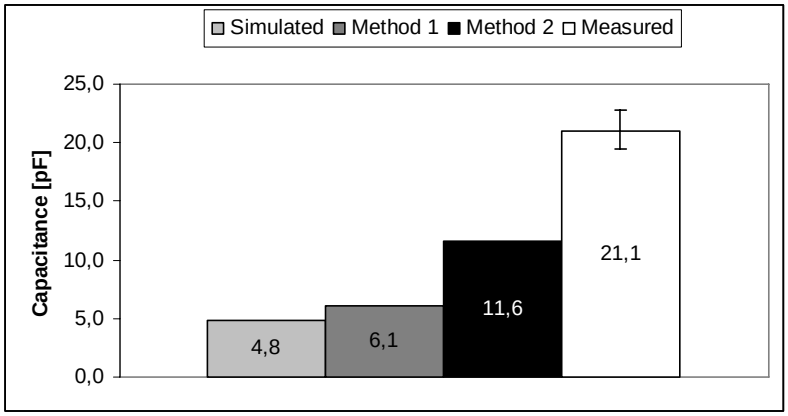

Figure 9.23. Summary of the results for the mutual capacitance in Case 5.

As in the previous case the mutual capacitance is low and the paper books present, why the measured value deviates from the theoretical values.

9.6 Influences on the parameters

In the earlier sections of this chapter, it has been shown how both the conductor layout and the surroundings affect the parasitic components. It is therefore interesting to investigate some basic physical properties of the electrical system and how these affect the parameters.

Conductor insulations

In the investigations of this thesis, conductors that are isolated with polyvinyl chloride (PVC) are employed. This is the most common insulation material for conductors, but there are also others like polyethylene (PE) or polytetrafluoroethylene (PTFE). Both of these have lower relative permittivity than PVC (see Table 6.1). The different insulations are dielectric materials and do only affect the capacitances of the setup.

A lower value on the permittivity implies that a higher electric field is needed to store a certain amount of charges. This can be seen in Figure 9.24.

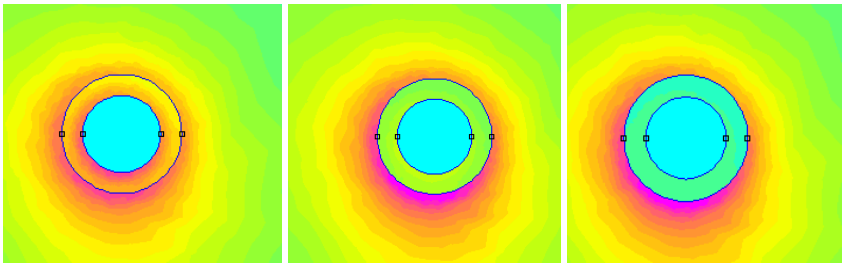

Figure 9.24. The flux density plots for three conductors with different insulation materials. The material around the conductor to the left has a relative permittivity of 1.5, the material in the middle: 3.8 (as PVC) and the material to the right 10.

This implies that a conductor will have a higher self-partial capacitance for a higher value of the permittivity of the insulator. This is illustrated in Figure 9.25 for a single conductor over a ground plane.

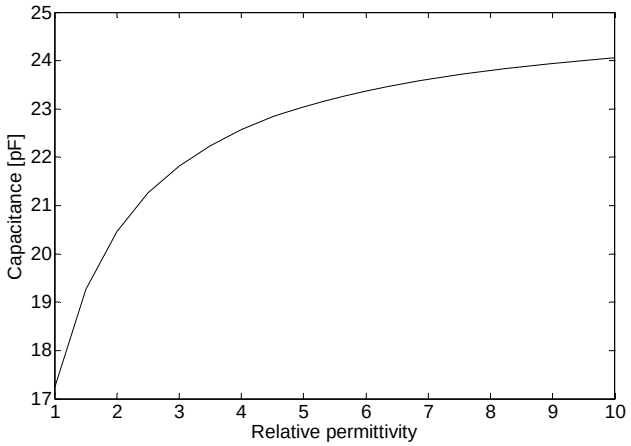

Figure 9.25. The capacitance for a thin communication conductor 5 mm above a ground plane as a function of the relative permittivity of the insulation material.

Also the mutual inductance between two conductors will increase when a material with a high permittivity is employed as insulation.

Conductor types

When it comes to the dimension of the conductor the cross-sectional area is usually a parameter which the designer of the system can not affect. It is however still useful to know what the different conductor sizes imply for the circuit.

If the skin effect in the conductors is neglected (this is often possible to do for long, thin conductors) the resistance of the conductor will increase with a decreased cross-sectional area since there is less copper to carry the current (see equation 6.3).

Regarding the inductance, this will decrease when the cross-sectional area increases according to Figure 9.26.

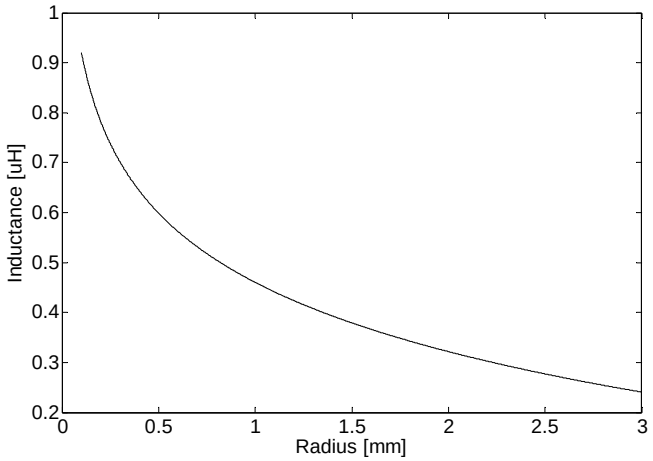

Figure 9.26. The self inductance of a conductor as a function of the radius of the conductor.

The decrease in inductance emanates from the fact that the flux density B is inversely proportional to the radius of the conductor according to equation 9.1. In order to find the inductance of a conductor, the flux density is integrated which will give the flux, proportional to the inductances according to equation 6.5.

When a conductor has a large cross-sectional area, it will also have a large self-

partial capacitance, see Figure 9.27.

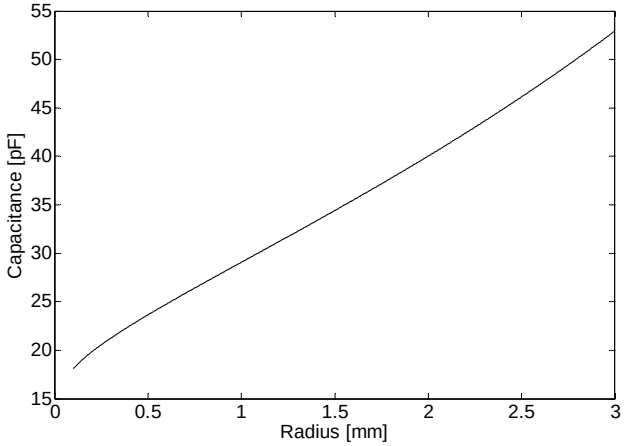

Figure 9.27. The self-partial capacitance of a conductor as a function of the radius of the conductor.

The reason for the increase in self-partial capacitance is that the electrically stored energy is dependent on both the capacitance and the voltage according to

$$W_e = \frac{1}{2} C \cdot V^2 \qquad (9.3)$$

The voltage V is proportional to the electric field, which in turn is reversely proportional to the radius of the conductor. This implies that the capacitance will increase if the voltage decreases in order for the electrical energy to stay constant.

Distances

In previous sections of this chapter it is demonstrated that the layout of the conductors influences the parasitic components of the conductor. In the case of the self inductance, it is only the conductor and the ground structure that interacts, but in the case of the self-partial capacitance also the presence of the other conductor is of importance. The results from the cases in this thesis and the underlying physics can be summarized as follows.

The self inductance of a conductor is only depending on the surrounding

ground structure and not any other conductors. When the conductor is close to ground, the magnetic field surrounding the conductor will create an image current in the ground structure. This image current will have opposite sign (as shown in Chapter 6.1) and hence decrease the magnetic flux and thereby also the inductance. This implies that when the conductor is moved further away from the ground plane, the distance between the current in the conductor and the image current will increase and the image current will not cancel the magnetic flux very effectively. The self inductance of the conductor will thereby increase as can be seen in Figure 9.28(d).

The mutual inductance between two conductors is affected by both the distance between the conductors and the vicinity to the ground structure. When the conductors are routed close to each other, the magnetic field from one conductor that affects the other conductor will be higher in the vicinity of the conductor. When the conductors are raised above the ground structure, the mutual inductance will also increase since the mirror current that will exist in the ground plane will be located further away from the conductor and thus not cancel the magnetic field from the conductor to any larger extent. These effects can be seen in Figure 9.28(b) and (d).

Already in the basic formula for a plate capacitor (see equation 2.3) it can be seen that the capacitance is inversely proportional to the distance between the two plates. The self-partial capacitance for a conductor is defined as the capacitance between the conductor and infinity (ground). This implies that the closer the conductor is to ground, the higher the capacitance (see Figure 9.28(c)). The capacitance is however more complex and also nearby conductors will affect the self-partial capacitance. As can be seen in Figure 9.28(a) and (c) the self-partial capacitance of one conductor increases when the other conductor is moved further away from the conductor.

Also in the case of the mutual capacitance the distance is of importance. The distance to the ground structure plays a minor role whereas the distance between the conductors is more important (see Figure 9.28(a)). When the conductors are placed close to each other the mutual capacitance will increase as in the case of the mutual inductance.

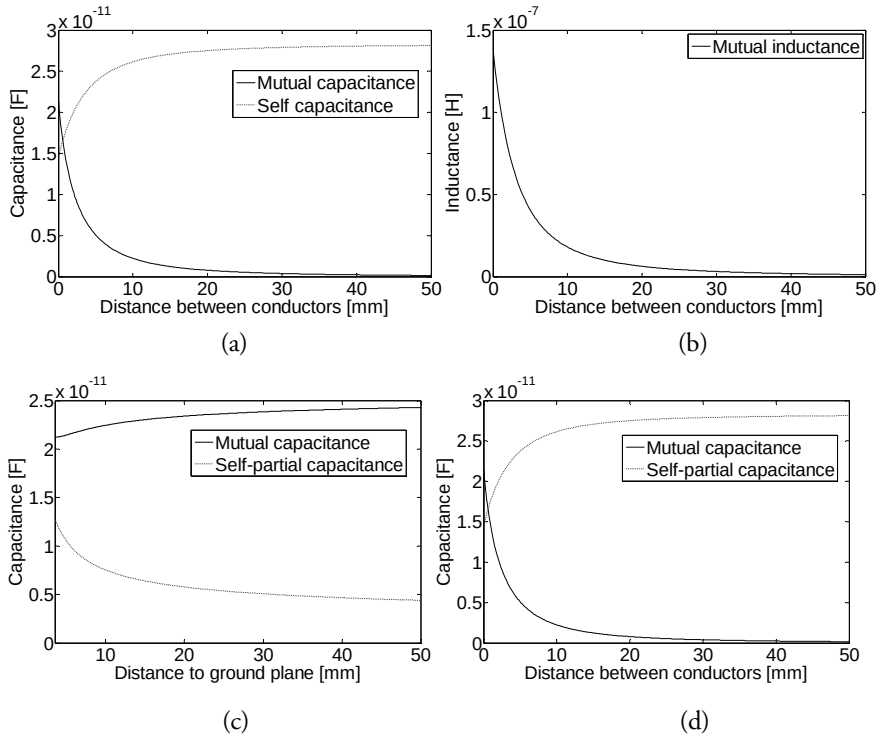

Figure 9.28. (a) The mutual capacitance between two conductors and the self-partial capacitance of one conductor as a function of the distance between them. (b) The mutual inductance between two conductors as a function of the distance between them. (c) The mutual capacitance between two conductors and the self-partial capacitance of one conductor as a function of the distance to the ground plane (the distance between the conductors remains unchanged). (d) The mutual inductance between two conductors and the self inductance of one conductor as a function of the distance to the ground plane (the distance between the conductors remains unchanged).

9.7 Circuit models

When the parasitic components of a circuit are known, they can be used in a circuit simulation. There are different circuit simulation software programs on the market, and most electrical engineers have at some point got in contact with this type of software why it is a good tool to use when analyzing

crosstalk.

In this thesis, free software from Linear Technology called LTSpice/Switchercad III [40] is employed. The simulation model contains the two conductors with their parasitic components. Four simulation models are built for each case, one for each parameter setup for the parasitic components.

In the simulation model the communication conductor is terminated with a voltage source that has a sampled CAN bus signal as output. This signal looks like Figure 9.29 and is sampled directly from the CAN High conductor in the brake system of the Volvo FH12 heavy truck.

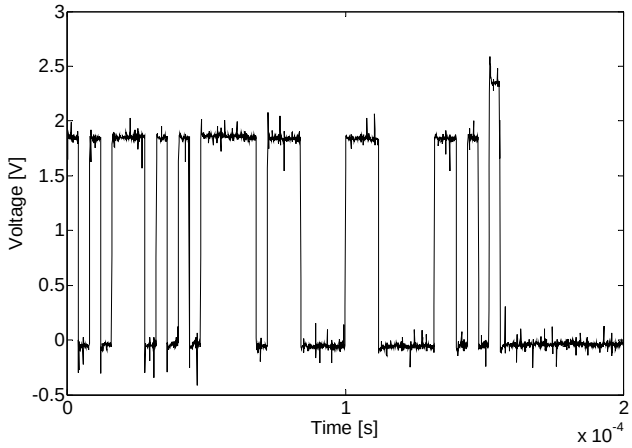

Figure 9.29. CAN High signal sampled from the Volvo FH12.

The other end of the communication conductor is terminated in a simple model of a CAN transceiver, consisting of a 10 pF capacitance in parallel with 25 kΩ.

The battery conductor has a model of a 24 V battery in one end [5] that includes a 24 V DC voltage source with a series resistance of 0.5 Ω and 0.16 F in parallel. The other end of the battery conductor is connected to a simple model of a 1-quadrant step down converter (see Appendix B).

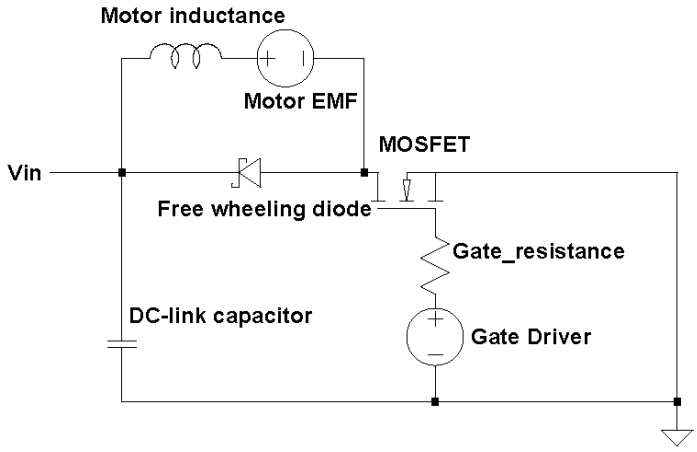

Figure 9.30. Power electronic converter and motor model.

The converter contains a small DC-link capacitor of 1 nF, a schottky diode of type MBRB2545Ct from International Rectifier for freewheeling, and a MOSFET for automotive applications of type IRF1405 from International Rectifier. The gate driver for the MOSFET is built by an ideal voltage source and a gate resistance of 4.4 Ω.

A picture of the complete simulation model is shown in Figure 9.31.

Two measurement points are inserted; Vdc, which is the DC-link voltage and Vcan, which is the voltage at the input of the CAN transceiver.

The simulation software is written as a SPICE (Simulation Program with Integrated Circuit Emphasis) software. It can be used for both transient (time) and frequency analysis. The transient simulation can be used for investigation of the voltage level at the input of the CAN transceiver in order to see if the voltage levels will be so high that they can interfere with the CAN signal or possibly break the transceiver. The frequency analysis can be used to plot transfer functions.

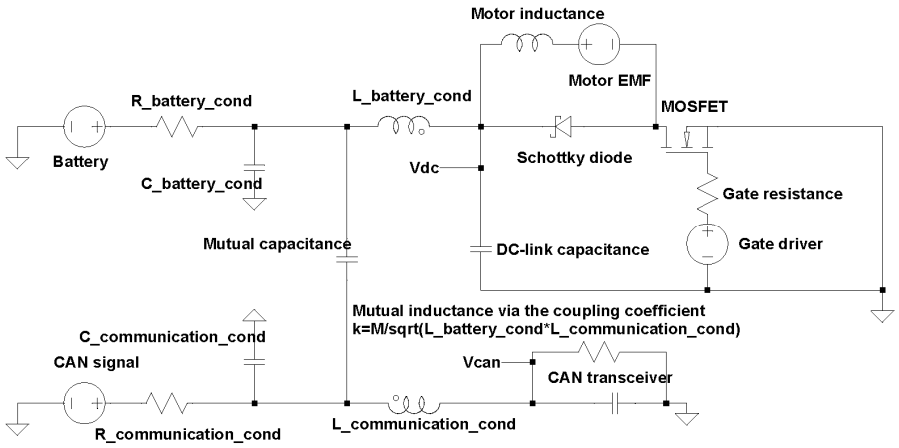

Figure 9.31. Complete simulation model for battery, battery conductor, power electronic converter and motor (upper part) and communication conductor and CAN transceiver.

In this thesis, the circuit models are used in order to compare and calibrate the different parameter setups from the simulations, calculations and measurements.

Comparison between the parameter values

In Chapters 6.2, 6.3, 7.4 and 8.5 parameter values for the different setups are presented. These parameter values are estimated by using analytical calculations, simulations and measurements. One of the goals for this thesis is to see if the analytically calculated values are good enough for prediction of crosstalk between two wires. This is done by comparing crosstalk at the CAN transceiver input in the LTSpice simulation circuit in Figure 9.31.

In the simulation model the CAN transceiver is the most vulnerable part and thus the voltage at the input of the transceiver is most interesting to study.

In Case 2, where the conductors are located close to each other in the corner of the ground structure, both the mutual inductance and capacitance are higher than the values from simulation and calculation. The resulting voltage at the input of the CAN transceiver can be seen in Figure 9.32.

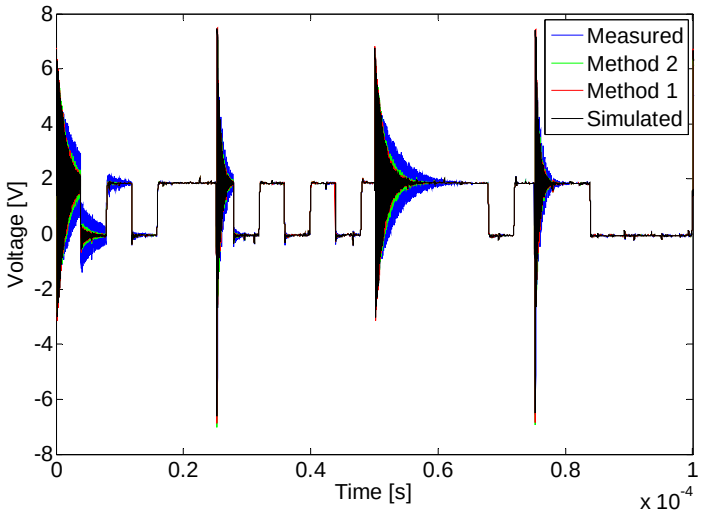

Figure 9.32. Voltage at the CAN transceiver, Case 2.

In the simulation model, a CAN signal is put on the CAN conductor the first 160 µs and after that, no signal is present on the conductor but the disturbances from the switching of the motor.

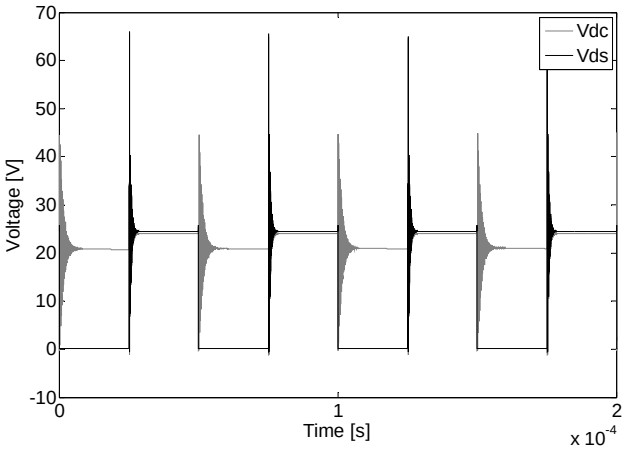

Figure 9.33. DC-link voltage (grey) and drain source voltage over the MOSFET in Case 2.

The DC-link voltage and the drain-source voltage looks like Figure 9.33.

As can be seen on the DC-link voltage, there are very high oscillations in the system. If only the battery conductor is present in the simulation model, these oscillations will remain as they result from the parasitic components of the conductor together with the power electronic control of the inductive load and the battery. An AC analysis of the circuit will give a node voltage at the DC-link for the frequency span that looks like Figure 9.34. The resonance frequencies in this figure agree with the different oscillating frequencies that are seen in Figure 9.34.

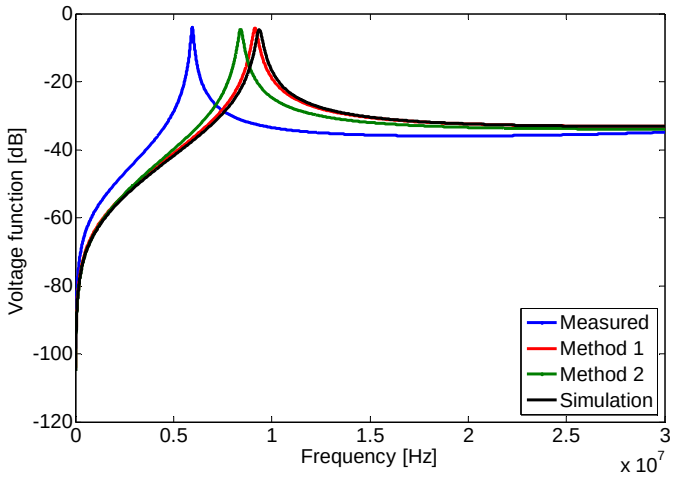

Figure 9.34. The voltage at the DC-link as a function of the frequency.

However, as seen in Figure 9.34, the results for the different parameter setups are very similar. This implies that in the case where the conductors are close to each other and to the ground the analytically calculated values are accurate enough to foresee the behaviour of the circuit.

In Case 3 where both conductors are moved away from the ground structure but still located next to each other, the results from the different parameter setups differ more in the circuit simulations as can be seen in Figure 9.35.

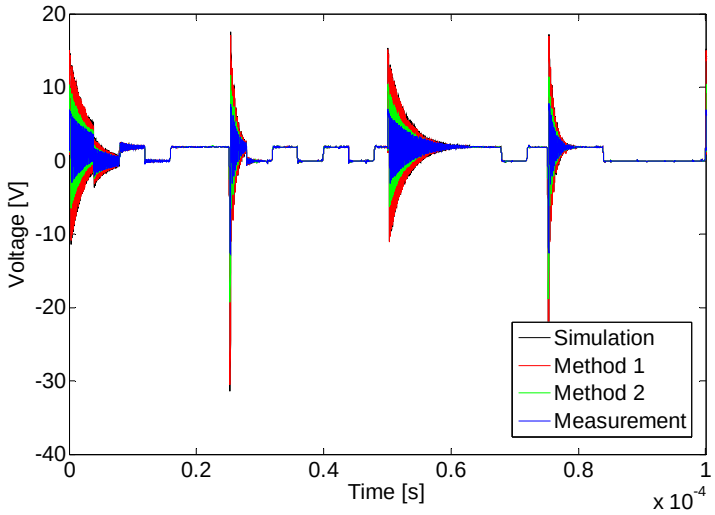

Figure 9.35. Voltage at the CAN transceiver, Case 3.

There are higher disturbances in Case 3 than in Case 2, which can be seen when the two figures are compared. The disturbances at the input of the CAN transceiver are lowest for the circuit model using parameter values gained from the measurements. When the different DC-link voltages are studied, it is also possible to see that the disturbances in the model with the measured values are lowest, which implies that the level of disturbances not only are connected to the mutual inductance and capacitance of the circuit but also to the other parasitic components like self inductance and capacitance. In this case, both the measurement and Method 2 give smaller disturbances than Method 1, which is most likely due to the fact that the measurement and Method 2 give a lower value for the mutual inductance, since the disturbances at the DC-link voltage are of the same magnitudes as in Method 1.

In Case 4, where the communication conductor is located in the corner of the ground structure and the battery conductor is raised and moved away from the ground structure, the circuit simulation results are almost the same in all cases except for Method 2. The disturbances when the parameters calculated with Method 2 are employed are higher since the coupling factor, k (see equation 3.1) is higher for Method 2 (0.064) compared with the other parameter setups (0.027-0.041).

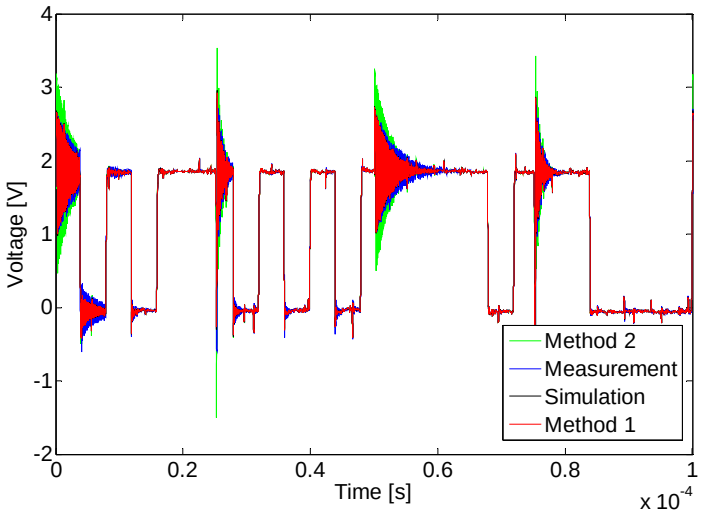

Figure 9.36. Voltage at the CAN transceiver, Case 4.

For the last case, Case 5, where the conductors are located at a distance away from the ground structure and separated, the results from the circuit simulation deviate between the different parameter setups. The circuit where the parameters from Method 1 are employed has the highest disturbances although the disturbances at the DC-link voltage are almost the same as for the circuit with the parameters gained from simulation. This is due to the high coupling factor between the two inductances in the circuit with parameters calculated by using Method 1, and vice versa for the coupling factor in the case of the parameters from simulation.

The coupling factor for the measured parameters is rather low, but the disturbances are in this case coupled via the mutual capacitance.

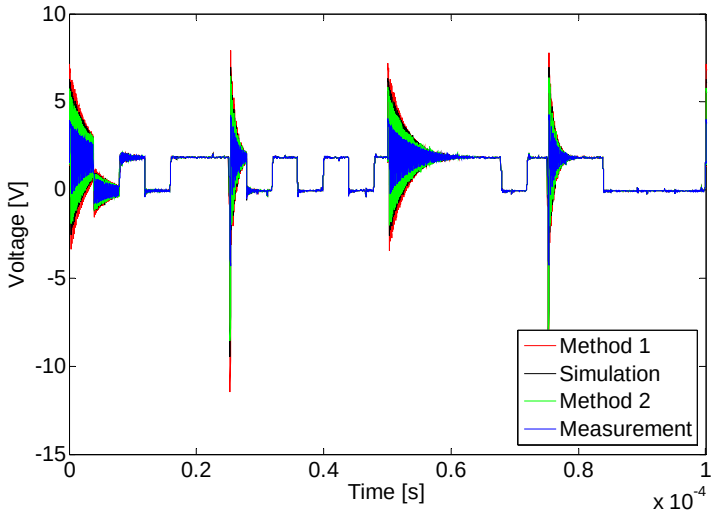

Figure 9.37. Voltage at the CAN transceiver, Case 5.

An over all view of the four cases with two conductors and the different parameter setups gives at hand that the parameter values gained from both analytical calculation methods will give satisfactory results for estimating worst case crosstalk. The disturbances at the DC-link are almost the same for all parameters except for the parameters gained from the measurement that are higher.

Comparison between different parameter setups

The methods for estimating the parasitic components of a system that are presented and used in this thesis all aim to give an understanding of how the conductor layout affects the crosstalk.

The results for the cases when the parameters estimated using Method 1 are employed are shown in Figure 9.38.

It is possible to see that the conductor layout in Case 4 has the lowest disturbances. In this case the communication conductor is located in the corner of the ground structure and the battery conductor is located 5 mm up and out from the corner of the ground structure. In Case 4 both the mutual inductance and capacitance of the conductors are rather low, and the ground structure will work as a shield for the communication conductor.

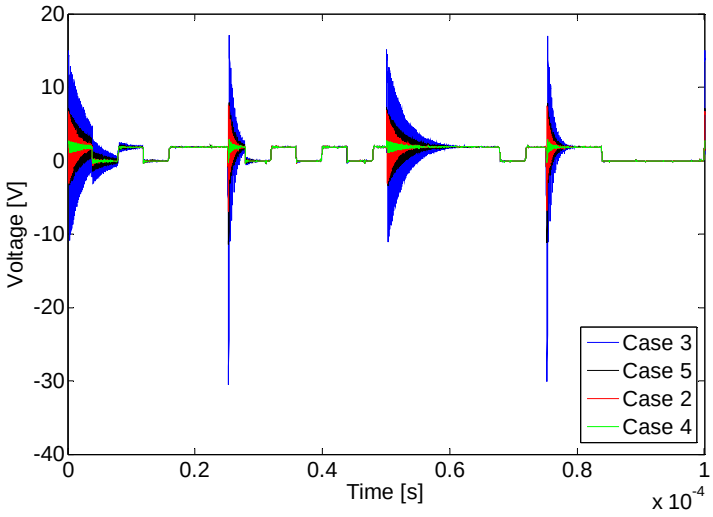

Figure 9.38. Voltage at the CAN transceiver when accurate analytical calculations are employed (Method 1).

Case 3 where both conductors together are moved away from the ground structure will have the highest disturbances due to the high values for both the mutual inductance and capacitance.

Although Method 2 is an approximate method, it will still point out the conductor layout in Case 4 as the most robust one against crosstalk. It will also be possible to se that Case 3 is the layout with the highest disturbances. Case 2 and 5 are almost the same as for Method 1. Case 2 has the highest amplitude in the beginning but the disturbances are dampened faster than in the layout of Case 5.

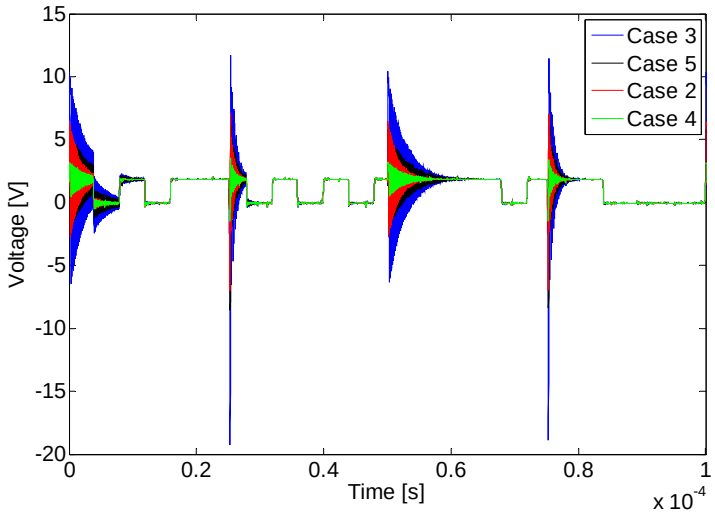

Figure 9.39. Voltage at the CAN transceiver when approximate analytical calculations are employed (Method 2).

The results from the circuit models when the parameter values from the simulations are used look about the same as seen in Figures 9.38 and 9.39.

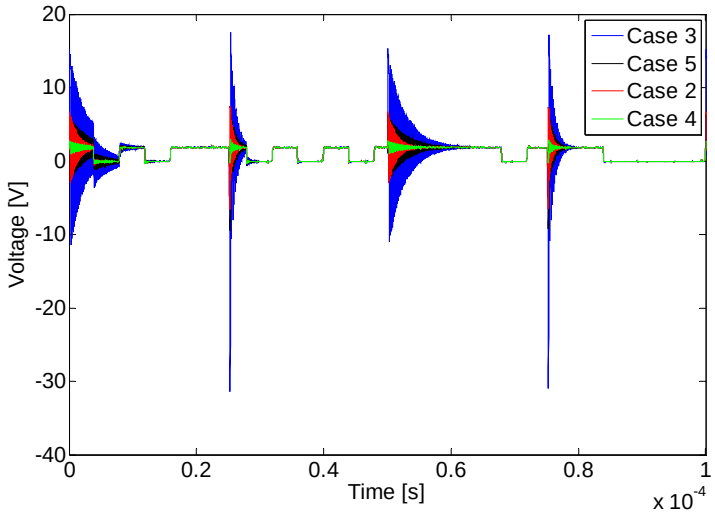

Figure 9.40. Voltage at the CAN transceiver when the values from the simulation software are employed.

The results from the circuit simulation when parameter values from the measurements are employed differ a bit from the other circuit simulation results. This emanates from the fact that the parameters deviates from the theoretical values due to differences between the measurement setup and the theoretical models. Although the results deviate from the other results, the same conclusions can be drawn from the circuit simulations regarding Case 3 and 4. When it comes to Case 2 and 5, the capacitances are highly affected by the presence of the books used to raise the conductors.

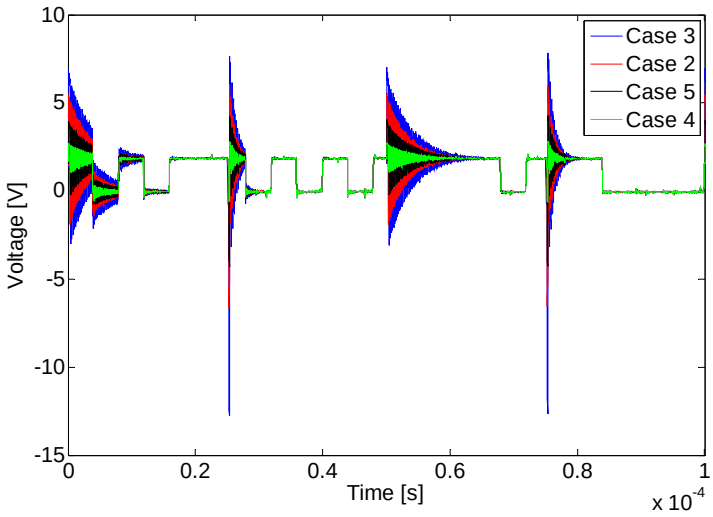

Figure 9.41. Voltage at the CAN transceiver when the parameter values from the measurements are employed.

In this section, the parameter values for the different layouts and from the different methods to estimate them are employed in circuit simulation models. It is possible to see that all parameter setups will give a good apprehension of which conductor layouts that most likely will suffer from crosstalk. It has been shown that also an approximate method for estimating the parameters can be useful for comparison between different conductor layouts.

9.8 Guidelines

There is no single solution that will solve all problems with crosstalk. However, there are some guidelines that could be good to keep in mind when

a system is designed, and this thesis would not be complete without mentioning them. Many of the general advices that exist for building an electromagnetic compatible system are not applicable in the automotive industry due to cost, weight and spacing, but they are still mentioned in this section.

An important thing to remember is that all metallic conductors are in fact functioning as radio antennas. This implies that non-metallic communications paths such as for example fiber-optics would be a better choice for communication. But fibre-optic conductors are sensitive to vibrations, hard to mount (due to their sensitivity) and connect why they are better suited for use in non-automotive applications.

A good way to limit disturbances is to use a conductor for ground return and to route this as close to the lead in conductor as possible. This has been shown in Chapter 2.3, and will decrease the common mode currents in the system. In the automotive industry it is common to use the chassis as ground return instead of a conductor. This can create problems, not only due to common mode currents, but also due to the common ground impedance that different loads will share and that is described in Chapter 3.2.

An even better solution for the lead in and current return conductor are if they are twisted to form a twisted pair. This will further increase the robustness of the system since such a twisted conductor pair will ensure a homogeneous distribution of the capacitances and reduce the magnetic loop to almost zero.

Some disturbances and crosstalk can be avoided by separating communication conductors from conductors with high switching currents. This will decrease both the mutual inductance and capacitance according to Chapter 9.6. The technical report IEC 61000-5-2 [32] recommends that all conductors are classified after their frequency and current content and routed so that the conductors that are in the vicinity of each other contains about the same frequency and current content.

Many systems that work as disturbance sources are pulse width modulated. Some benefits can be gained by restricting the frequency spectrum through limiting the rise and fall times. This method is studied in [41] and shows that this could be effective in the higher frequency ranges. The limitation can be done rather easily but will increase the switching losses of the system.

Shielding of the conductors is an effective way to decrease disturbances and crosstalk, but it is important to ground the shield properly and to ensure that the "pigtail" (the parts at the ends of the conductor that are not shielded) are as short as possible. It is also important to make sure that the shield remains grounded during the life time of the product. This demand together with increased cost and more complex assembly often makes shielding a poor alternative for the automotive industry.

Even if all of these guidelines are followed, there might still be problems in a system that may have to be solved by use of filters at the output and/or input of the different systems.

Chapter 10

Conclusions

The aim of this thesis is to investigate different ways to predict the parasitic components of a two conductor system where the conductors are located near a ground structure that expands in three directions. An approximate method for analytical calculation of the components is also proposed in order to find a way to easily estimate the parasitic components.

10.1 Summary of results

Four different ways for determining the self and mutual inductances and capacitances of a system with two conductors and a ground structure are investigated in this thesis.

First, the parameters are estimated by using ordinary analytical calculations. The ground structure is assumed to have a very high conductance wherefore the method of images is employed and each conductor is mirrored in both the horizontal and vertical part of the ground structure.

The second method for analytical calculations is a method proposed by the author. For the estimation of the self inductances and capacitances of each conductor an equivalent ground plane is constructed. The parameters are then estimated by only looking at a ground plane and one conductor at a time. The mutual inductance is calculated by a parallel coupling of the mutual inductance between the two wires when only the horizontal part of the ground structure is present and when only the vertical part is present. The mutual capacitance is calculated between the two conductors without taking the ground structure into account.

The parameters are also estimated by using an electromagnetic simulation software called “CableMod”, by SimLab. This software utilizes the boundary

element method on a two dimensional model of the cross section of the setup. In the software, a two dimensional transmission line model is built and from this it is possible to extract the values of the parasitic components.

Finally, a real setup is used for measurements of the different components. A ground structure, equal to the one used in the previous investigations, is used together with two conductors.

The results from the different estimations are evaluated for five different conductor layouts. First, the values of the parameters are compared. It can be seen that the conductance of the real ground structure is not as high as expected which affects the inductance values, and that the physical distance bodies of paper used to raise the conductors from the ground structure affects the capacitance values. The values yielded from the approximate calculations deviates from the more accurately estimated values as expected.

In order to see how good the different parameter setups are for predicting crosstalk, circuit models are constructed in a SPICE simulation software. The circuit simulations show that although the different parameter setups vary when it comes to exact levels of crosstalk, they agree on which conductor layout that is most robust against crosstalk. It is also possible to see that even if the approximate calculation method is rather rough, it will provide results that are good enough for both understanding of the phenomena and comparison between different conductor layouts.

10.2 Future work

One thought behind this thesis is to facilitate for the engineers in the automotive industry to decide how a system should be realized in order to minimize crosstalk by routing the conductors properly. The thesis has only brought up the case where two conductors are present and neither of them is shielded nor twisted. In future automotive applications it might be that shielded cables have to be used which implies that an approximate method where shielded, twisted and multi conductor systems are present should be constructed and investigated. All of these cases are possible to simulate with the correct type of software today, but in order to save time and money and to get a feeling for what is happening in the system for different layouts, approximate methods are useful. Approximate methods for twisted pair and shielded conductors should therefore also be developed.

10.3 Reflections

In this section, some of my thoughts and experiences will be described.

During the last years, I have had the opportunity to talk to and work together with skilled engineers in the Swedish automotive industry. The different challenges that they meet at a daily basis have inspired me and given me valuable input for my research.

It is obvious that if some time can be saved in a project, this means a lot to the industry. Being able to predict and/or build a simulation model of the system is a great help for the designers since it will facilitate easy and quick alternations of the system in the simulation model to see the responses. It will also build up knowledge for an inexperienced EMC engineer, since EMC is not something that can be easily learned from a book. When it comes to the simulation software programs there are some problems. To start with there are, as mentioned earlier in the thesis, numerous software programs on the market that are applicable for different problems. These might be expensive and some of these software programs are not very intuitively to use for beginners.

This thesis shows that an approximate calculation of the values of the parasitic components is almost as good as values from an electromagnetic simulation software program. An approximate calculation will, even though it is rough, give the user a better apprehension about which parameters that affects the parasitic components of the setup. This is important knowledge and can tell about the "roots of causes" of a problem. It will also be easier for the EMC engineers to talk to engineers from other engineering sciences about how the system will respond to different changes in the design.

It is therefore my personal recommendation that not only electromagnetical simulation software programs should be used at an early stage of a product development, but also approximate calculations based on the physics of the system in order to decide whether a solution or design is feasible or not.

References

[1] M. Alaküla, “Power Electronic Control”, Lund University, Industrial Electrical Engineering and Automation, August 2002.

[2] S. Alexandersson, “EMC and Functional Safety for the Automotive Industry”, NORPIE 2006 Nordic Workshop on Power and Industrial Electronics, Lund, Sweden, June 12-14, 2006, CD-ROM pages 6.

[3] K. Armstrong, “Review of EMC design rules, a brief tour of some of the majorissues”, IEE Seminar on The ‘Hows’ and ‘Whys’ of EMC Design (Ref. No. 1999/001), 1999 pp. 1/1 - 112

[4] K. Armstrong, “Why EMC Immunity Testing is Inadequate for Functional Safety”, International Symposium on Electromagnetic Compatibility, 2004. EMC 2004. Volume 1, 9-13 Aug. 2004 pp 145 – 149.

[5] R. Aronsson, ETC Battery and FuelCells Sweden AB, mail correspondence 080326

[6] K. Attback, “Att tanka bilen med bränsle – ett elektrostatiskt fenomen”, E^3 2007 EMC, ESD, Elsäkerhets mässa, Konferenskompendium, 17-18 Apr. 2007, pp 86-88.

[7] Bondeson, T. Rylander, P. Ingelström, “Computational Electromagnetics”, School of Electrical and Computer Engineering, Sweden 2002.

[8] P.O. Brandt, Volvo 3P, mail correspondence, 080407

[9] BMW E38, “Bus System Troubleshooting”, www.e38.org/bussystem.pdf, 080426

[10] F. Canavero, J-. C. Kedzia, P. Ravier and B. Scholl, “Automotive EMC: Numerical simulation for early EMC design of cars”, 4th European Conference on Electromagnetic Compatibility 2000, Tutorials, 11–15 September 2000, pp. 32–39.

[11] P. Carlsson, S. Johansson, “Modern Elektronisk Mätteknik”, Liber AB, Stockholm, 1997

[12] CENELEC, ”European Standard EN55025 January 2003 Radio disturbance characteristics for the protection of receivers used on board vehicles, boats and on devices Limits and methods of measurement (CISPR 25:2002)”, CENELEC European Committee for Electrotechnical Standardization, Ref. No. EN 55025:2003 E

[13] P.A. Chatterton, M.A. Houlden, “EMC Electromagnetic Theory to Practical Design”, John Wiley and Sons, West Sussex, England, 1992

[14] S. Chen et al, ”Towards EMI Prediction of a PM Motor Drive for Automotive Applications”, Applied Power Electronics Conference and Exposition, 2003. APEC '03. Eighteenth Annual IEEE Volume 1, 9-13 Feb. 2003 pp. 14 – 22.

[15] D. K. Cheng, “Field and Wave Electromagnetics”, Second Edition, Addison-Wesley Publishing Company Inc., United States of America, 1992.

[16] J.C. Clements, et al, “Computation of the Capacitance Matrix for Systems of Dielectric-Coated Cylindrical Conductors”, IEEE Transactions on Electromagnetic Compatibility, Nov. 1975, Vol. EMC-17, Issue 4, pp. 238-248.

[17] Concord Cables, Product information, www.concordiacables.com/products.htm, 080417

[18] COSIME, “Final Report, Growth Project GRD1-2000-00305”, 2003

[19] J.D. Curtis, I. Straus, “Follow these 18 rules for better EMC design”, Professional Program Proceedings Electro 98., 9-11 Jun 1998 pp. 83 - 95

[20] J. Ekman et al, “Impact of partial element accuracy on PEEC model stability”, IEEE Transactions on Electromagnetic Compatibility, Volume 48, Issue 1, Feb. 2006 pp. 19 - 32

[21] S. Frei, R.G. Jobava, D. Topchishvili, “Complex Approaches for the Calculation of EMC Problems of large Systems“, 2004 International Symposium on Electromagnetic Compatibility. EMC 2004. Volume 3, 9-13 Aug. 2004 pp. 826 – 831.

[22] Försvarsmakten, “Handbok för programvara i säkerhetskritiska tillämpningar”, Publikation M7762-000531, 2002, Försvarsmakten

[23] GEMCAR, “GEMCAR Guidelines”, 2003

[24] D. J. Groot Boerie, “EMC and Functional Safety, Impact of IEC61000-1-2”, 2002 IEEE International EMC Symposium on Electromagnetic Compatibility. EMC 2002. Volume 1, Issue , 19-23 Aug. 2002 pp. 353 - 358

[25] M. Gustafsson, “Elektromagnetiska beräkningar”, Lecture notes, Lunds Tekniska Högskola, 2002

[26] E. Hallén, “Elektricitetslära”, Almqvist & Wiksell, Uppsala, Sweden, 1953

[27] R. F. Harrington, “Matrix Methods for Field Problems”, Proceedings of the IEEE, Volume 55, Issue 2, Feb. 1967 pp. 136 – 149.

[28] T. Heikkilä, ” Time Domain Methods for Measuring Crosstalk for PCB Quality Verification”, Application note, Tektronix Inc.

[29] IEC, “International Electrotechnical Commission CISPR 16-1 Second edition 1999-10 Specification for radio disturbance and immunity measuring apparatus and methods – Part 1: Radio disturbance and immunity measuring apparatus”, IEC International Electrotechnical Commission, Reference number CISPR 16-1:1999

[30] IEC, “International Electrotechnical Commission CISPR 16-4-2 First edition 2003-11 Specification for radio disturbance and immunity measuring apparatus and methods – Part 4-2: Uncertainties, statistics and limit modeling – Uncertainties in EMC modelling”, IEC International Electrotechnical Commission, Reference number CISPR 16-4-2:2003

[31] IEC, “IEC TS 61000 Part 1-2: General . Methodology for the achievement of the functional safety of electrical and electronic equipment with regard to electromagnetic phenomena”, IEC International Electrotechnical Commission, reference number CEI/IEC/TS 61000-1-2:2001

[32] IEC, “IEC 61000-5-2 Technical Report Type 3, Electromagnetic compatibility (EMC) - Part 5: Installation and mitigation guidelines - Section 2: Earthing and cabling”, IEC International Electrotechnical Commission, reference number CEI/IEC 61000-5-2:1997

[33] IEC, “IEC 61508 Part 4: Definitions and abbreviations” IEC International Electrotechnical Commission

[34] IEE; “IEE Guidance Document on EMC and Functional Safety”, www.iee.org/policy/areas/electro/ 080417

[35] E. Ingelstam, et al, ”TEFYMA Handbok för grundläggande tenisk fysik, fysik och matematik”, 3:e upplagan, Sjöbergs Bokförlag AB, Helsingborg, 1995.

[36] V. Jithesh, D.C. Pande, “A review on computational EMI modelling techniques”, 8th International Conference on Electromagnetic Interference and Compatibility, 2003. INCEMIC 2003., 18-19 Dec. 2003 pp. 159 - 166

[37] P. Karlsson, “Kraftelektronik”, Lund University, Industrial Electrical Engineering and Automation, Oct. 1998

[38] W.-J. Liao, B.a. Baertlein, W. Gilmore, “The role of automotive EMC”, IEEE International Symposium on Electromagnetic Compatibility, Aug. 2-6, 1999, vol. 2 pp. 745-750.

[39] LIN, Local Interconnect Network, “Technical Overview”, www.lin-subbus.org/, 080426

[40] LTSpice, www.linear.com/designtools/software/, 080417

[41] S. Marksell, “EMC Aspects of PWM Controlled Loads in Vehicles”, Licentiate Thesis, Media Tryck, Lund University, Sweden, 2004

[42] MatWeb Material Property Data http://www.matweb.com/, 080114

[43] E.K. Miller, “A selective survey of computational electromagnetics”, IEEE Transactions on Antennas and Propagation, Volume 36, Issue 9, Sep 1988 pp.1281 – 1305.

[44] E.K. Miller, “Computational electromagnetics from a user's perspective”, IEEE International Symposium on Antennas and Propagation 1990, 1990 7-11 May, pp. 1493-1496.

[45] E.K. Miller, “Electromagnetics without equations – Why isn’t studying EM more popular?”, IEEE Potentials, Volume 20, Issue 2, Apr/May 2001 pp.16 – 20.

[46] R. Neumayer, A. Stelzer, F. Haslinger, J. Held, F. Schinco, R. Wiegel, “Continuous Simulation of System-Level Automotive EMC Problems”, 2003 IEEE International Symposium on Electromagnetic Compatibility, Volume 1, 18-22 Aug. 2003 pp. 409 – 413.

[47] M. O’Hara, J. Colebrooke, “Automotive EMC test harnesses: standard lengths and their effect on conducted emissions”, 2003 IEEE International Symposium on Electromagnetic Compatibility, 2003. EMC ‘03. Volume 1, 16-16 May 2003 pp. 233 - 236

[48] H.W. Ott, “Noise Reduction Techniques in Electronic Systems”, Second edition, Wiley-Interscience, John Wiley and Sons, Inc., New York, United States of America, 1988.

[49] Papadopoulus Y., Grante C; “Techniques and Tools for Automated Safety Analysis & Decision Support for Redundancy Allocation in Automotive Systems”, 27th Annual International Computer Software and Applications Conference, 3-6 Nov. 2003 pp. 105 – 110.

[50] C.R. Paul, “A Brief History of Work in Transmission Lines for EMC Applications”, IEEE Transactions on Electromagnetic Compatibility, Volume 49, Issue 2, May 2007pp.237 – 252.

[51] C.R. Paul, “A simple SPICE model for coupled transmission lines”, IEEE 1988 International Symposium on Electromagnetic Compatibility, 1988. Symposium Record. 2-4 Aug 1988 pp. 327 - 333

[52] C.R. Paul, “Computation of Crosstalk in a Multiconductor Transmission Line”, IEEE Transactions on Electromagnetic Compatibility, Nov. 1981, Vol. EMC-23, Issue 4, pp. 352-358.

[53] C.R. Paul, A.E. Feather, “Computation of the Transmission Line Inductance and Capacitance Matrices from the Generalized Capacitance Matrix”, IEEE Transactions on Electromagnetic Compatibility, Vol. EMC-18, Issue 4, pp. 175-183

[54] C.R. Paul, “Derivation of common impedance coupling from the transmission-line equations”, IEEE Transactions on Electromagnetic Compatibility, Volume 34, Issue 3, Aug 1992 pp. 315 – 319.

[55] C.R. Paul, “Estimation of Crosstalk in Three-Conductor Transmission Lines”, IEEE Transactions on Electromagnetic Compatibility, Nov. 1984, Vol. EMC-26, Issue 4, pp. 182-192.

[56] C.R. Paul, “On the Superposition of Inductive and Capacitive Coupling in Crosstalk-Prediction Models”, IEEE Transactions on Electromagnetic Compatibility, Aug. 1982, Vol. EMC-24, Issue 3, pp. 335-343

[57] C.R. Paul, “Solution of the Transmission-Line Equations for Three-Conductor Lines in Homogeneous Media”, IEEE Transactions on Electromagnetic Compatibility, Volume 20, Issue 1, Feb 1978 pp. 216 – 222.

[58] C.R. Paul, “Solution of the transmission-line equations under the weak-coupling assumption”, IEEE Transactions on Electromagnetic Compatibility, Volume 44, Issue 3, Aug 2002 pp. 413 - 423

[59] C.R. Paul, “The concept of dominant effect in EMC”, IEEE Transactions on Electromagnetic Compatibility, Volume 34, Issue 3, Aug 1992 pp. 363 – 367.

[60] Pirelli Tyre, www.pirelli.se/web/technology/about-tyres/tyre-function/section/default.page, 080417

[61] Pro Power Tri Rated 6.0 datasheet, www.farnell.com/datasheets/83800.pdf, 080417

[62] S. Ranganathan, D.G. Beetner, R. Wiese, T.H. Hubing, ”An Expert System Architecture to Detect System-Level Automotive EMC Problems”, IEEE International Symposium on Electromagnetic Compatibility, 2002. EMC 2002. Volume 2, 19-23 Aug. 2002 pp. 976 – 981.

[63] M. Ringholm, SSAB Svenskt Stål AB, telephone conversation, 080409

[64] A.E. Ruehli, “Equivalent Circuit Models for Three-Dimensional Multiconductor Systems”, IEEE Transactions on Microwave Theory and Techniques, Volume 22, Issue 3, Mar 1974, pp. 216 - 221

[65] A.E. Ruehli, A.C. Cangellaris, “Progress in the methodologies for the electrical modeling ofinterconnects and electronic packages”, Proceedings of the IEEE, Volume 89, Issue 5, May 2001 pp. 740 - 771

[66] Y. Shaofeng et al, ”Analysis of cable parameters on the real chassis by measurement”, 17th International Zurich Symposium on Electromagnetic Compatibility, 2006, EMC-Zurich 2006, 27 Feb.-3 March 2006, pp. 73 – 76.

[67] El-Sherif, “Elektrisk influens på fordon under kraftledning”, Kungliga Tekniska Högskolan, XR-EE-ETK 2006:012

[68] W.T. Smith et al. “Crosstalk modeling for automotive harnesses”, IEEE International Symposium on Electromagnetic Compatibility, 1994. Symposium Record, 22-26 Aug 1994 pp. 447 – 452.

[69] S. Sundberg, J. Ekman, “PEEC modeling of antenna characteristics”, 2006 IEEE International Symposium on Electromagnetic Compatibility. EMC 2006. Volume 3, 14-18 Aug. 2006 pp. 580 - 585

[70] Tektronix, “Digital Real-Time™ Oscilloscopes TDS 684B • TDS 680B • TDS 644B • TDS 620B • TDS 640A”, Tektronix, USA, 1998.

[71] Tektronix, “P6139A 10X Passive Probes Instruction”, Ref. Number 063-0870-05, Tektronix, USA.

[72] F. M. Tesche, M. V. Ianoz and T. Karlsson, “EMC Analysis Methods and Computational Methods“, Wiley-Interscience, John Wiley and Sons, Inc., New York, United States of America, 1997.

[73] L. Tihanyi, “Electromagnetic Compatibility in Power Electronics”, Butterworth-Heinemann, Oxford, United Kingdom, 1995

[74] M. Tröscher, “Linkage of PCB and Cable Harness Simulations for Automotive EMC Analyses”, Automotive EMC 2005 The road to compliance, May 11, 2005.

[75] M.E. Verbeek, “Partial element equivalent circuit (PEEC) models for on-chip passives and interconnects”, International Journal of Numerical Modelling: Electronic Networks, Devices and Fields, Volume 17, Number 1, 2004, pp. 61-84.

[76] Volvo Trucks, www.volvo.com/trucks/global/en-gb/newsmedia/image_gallery/ 080417

[77] D.D. Ward, “MISRA Software Engineering Activities” www.jasa.or.jp/et/ET2005/conference/05PDF/C-9.pdf, 060130

[78] Warwick Control Technologies, “LIN Frequently Asked Questions”, www.warwickcontrol.com/support/faqlin.php, 080426

[79] D. Weston, “Electromagnetic Compatibilities, Principles and Applications”, Second edition, Marcel Dekker, Inc., USA

[80] J. Winberg, Michelin Nordic AB, mail correspondence, 080222

[81] L. Yaowu, “Simplifying PEEC model to transmission line model”, IEEE International Symposium on Antennas and Propagation 2004. Volume 3, Issue , 20-25 June 2004 pp. 2259 – 2262.

Appendix A

Nomenclature

Abbreviations

AC	Alternating Current
CAN	Controller Area Network
CISPR	International Special Committee on Radio Interference
CM	Common Mode
DC	Direct Current
DM	Differential Mode
ECU	Electrical Control Unit
EMC	Electromagnetic Compatibility
EMF	Electro Motive Force
EMI	Electromagnetic Interference
ESD	Electrostatic Discharge
EU	European Union
EUT	Equipment Under Test

FMEA	Fault Mode and Effects Analysis
FTA	Fault Tree Analysis
IEC	International Electrotechnical Comission
IEEE	Institute of Electrical and Electronics Engineers
ISO	International Organization for Standardization
LIN	Local Interconnect Network
LISN	Line Impedance Stabilization Network
MOSFET	Metal-Oxide-Semiconductor Field Effect Transistor
PCB	Printed Circuit Board
PE	Power Electronics
PVC	Polyvinyl Chloride
PWM	Pulse Width Modulation

Symbols

A	Magnetic Vector Potential
B	Magnetic Flux Density
C	Capacitance
D	Displacement field
E	Electric Field
f	Frequency
G	Conductance
H	Magnetic Field

I	Current
k	Coupling coefficient
L	Inductance
M	Mutual Inductance
R	Resistance
R_g	Gate resistance
V	Voltage
Z	Impedance

Greek Symbols

ε	Dielectric constant, Permittivity
θ	Angle between magnetic field and loop antenna
μ	Permeability
ρ	Line charge
σ	Conductivity
Φ	Magnetic Flux
ω	Angular frequency

Appendix B

Pulse Width Modulation

Pulse width modulation (PWM) is a common way of controlling electrical loads on demand. It is cost effective but is often a source of electromagnetic interferences. In this Appendix, the theory and realisation of a pulse width modulated system are described.

The converter

A power electronic energy converter in an electrical control system operates as a power amplifier. The energy conversion of a process can be influenced by controlling the voltage fed to the load. In a low power system it is possible to control the voltage continuously, but in many cases the output power has to be controlled by modulation in order to reduce the power losses in the converter itself. Voltage modulation means that the instantaneous value of the output voltage alternates between well-defined levels, and is thus not controllable to an arbitrary value in every time instant. The goal when using carrier wave modulation is to obtain linearity between the reference of the output voltage and the average of the output voltage measured over a finite time period.

There are several different ways to modulate the output voltage. This thesis will focus on a type of modulation where a carrier wave is used, but there are also modulation methods that involve a direct control of secondary quantity such as current or torque.

A power electronic converter involves the use of power electronic components, arranged to operate as switches, i.e. as elements that either conduct with ideally with no voltage drop across them or block with ideally

no current – like a mechanical switch. When studied closely it is found that the circuit on each side of the switch element has different electrical properties. One side is always capacitive and one side is inductive. This is the same as to say that a power electronic switch element cannot/should not be used to connect two capacitors of different charge since the initial current through the switch would be infinite, or the switch element cannot/should not be used to break up an inductive circuit since the induced voltage would force the current to continue through the semiconductor chip, in both cases the switch element would be destroyed. The capacitive side of the circuit has a continuous voltage and the inductive side has a continuous current through the switch transition. Correspondingly, the capacitive side has a discontinuous current and the inductive side a discontinuous voltage.

Carrier wave modulation

The principle for modulation can be derived from Figure B.1. A two-position switch that controls the potential v_c is shown in the circuit in Figure B.1. When this switch switches periodically, the output voltage alternates between the potentials v_a and v_b with the same frequency.

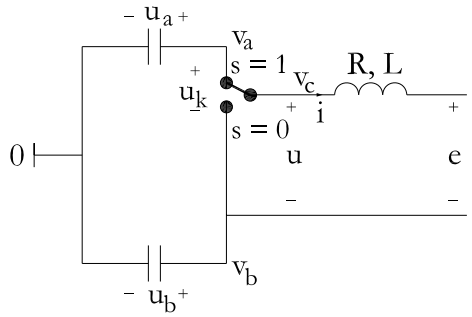

Figure B.1. A power electronic switch, controlling the potential v_c. When the switch is in its upper position, v_c equals v_a and when it is in its lower position, v_c equals v_b.

In this circuit the capacitive side is represented by the capacitive potentials v_a and v_b and the inductive side by an inductive current i flowing through a load consisting of a resistance (R), an inductance (L) and a counter electromagnetic force (e) in series. The output voltage will then be a function of the switch position according to

$$u = s \cdot (v_a - v_b) = s \cdot u_k \qquad \text{(B.1)}$$

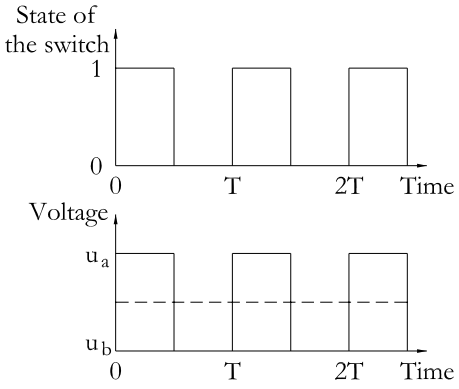

Figure B.2. Upper diagram, state of the switch as a function of time. Lower diagram, output voltage as a function of time, the dashed line is the average output voltage.

For the following discussion, a circuit according to Figure B.3 is assumed. This is a 2-quadrant DC converter that is suitable to explain carrier wave modulation method used in this thesis. The same method, with small additional assumptions, can be used for more complex converters, see [1].

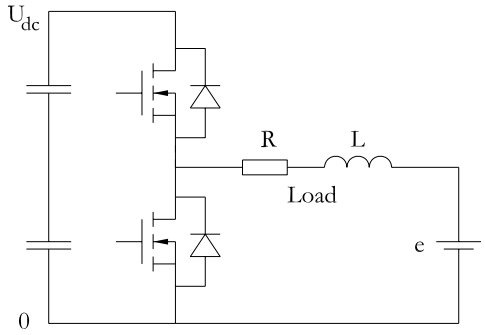

Figure B.3. A 2-quadrant DC converter with an RLE load.

Modulation of power electronic switches is about the selection of time instants to "flip the switch" in order to obtain a desired average output voltage within a certain time interval. In this thesis, the output voltage is created by using carrier wave modulation. The carrier wave itself is derived from a study of the average voltage in one half switch period.

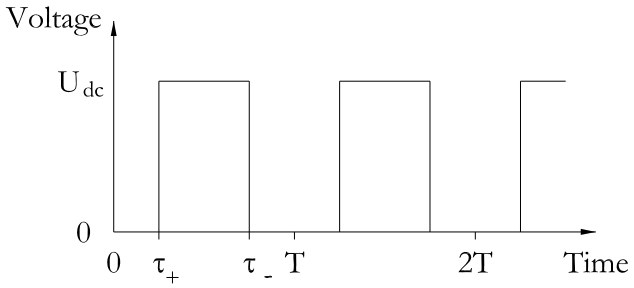

Figure B.4. Output voltage pulses symmetrically positioned in one switch period.

Assume that the output voltage pulses are positioned in the middle of the switch interval, see Figure B.4. The average voltage $\overline{u}$ during the first and second half of the switch interval can then be described according to:

$$\begin{cases} \overline{u}(0 < \tau_+ < T/2) = U_{dc} \cdot \left(1 - \dfrac{\tau_+}{T/2}\right) & \text{(B.2a)} \\ \overline{u}(T/2 < \tau_- < T) = U_{dc} \cdot \dfrac{\tau_-}{T/2} & \text{(B.2b)} \end{cases}$$

where T is the switch period at the assumed switching frequency $f_{sw}=1/T$. Modulation is now about selecting the time instants τ_+ and τ_- to obtain an average value of the voltage that is equal to the voltage reference within the particular half pulse. This is done by using a modulator.

The modulating wave and the modulator

The modulating wave, u_m, used in carrier wave modulation is selected to be equal to the predicted average voltage for each half period, according to:

$$u_m = \overline{u} \qquad \text{(B.3)}$$

The modulator is represented by a comparison between the desired output voltage and the carrier wave, where the switch changes state when the comparison changes sign. This can either be done in an analogue manner with a triangular wave generator and comparators or digital by using a timer circuit or an up/down counter with a digital comparator.

With a carrier wave according to equation B.2, the output voltage is linearized with respect to variations in the supply voltage. Figure B.5 illustrates a few modulation periods with varying voltage reference and supply voltage.

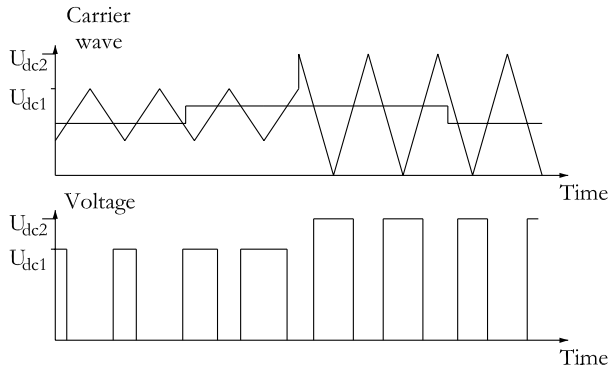

Figure B.5. Upper: Carrier wave and reference, lower: output voltage, note that the pulse width decreases when the supply voltage increases.

If the supply voltage is lowered, the pulse width is increased in order to maintain the desired average output voltage.

Current sampling

When a generic RLE circuit is driven by the output voltage of the converter according to Figure B.6, the current will cross its average value at the time instants when the carrier wave turns.

The current will have one out of two derivatives according to:

$$\frac{di}{dt} = \begin{cases} \dfrac{U_{dc} - e - R \cdot i}{L} \\ \dfrac{-e - R \cdot i}{L} \end{cases} \qquad \text{(B.4)}$$

From Figure B.6 it is indicated that the current ripple will pass through its average value twice every switching period. Assuming that the electric time constant L/R>>T, this occurs at time instants that coincide with the turning of the carrier wave. Thus, in applications where current feedback is needed, there are excellent opportunities to sample the current at these time instants.

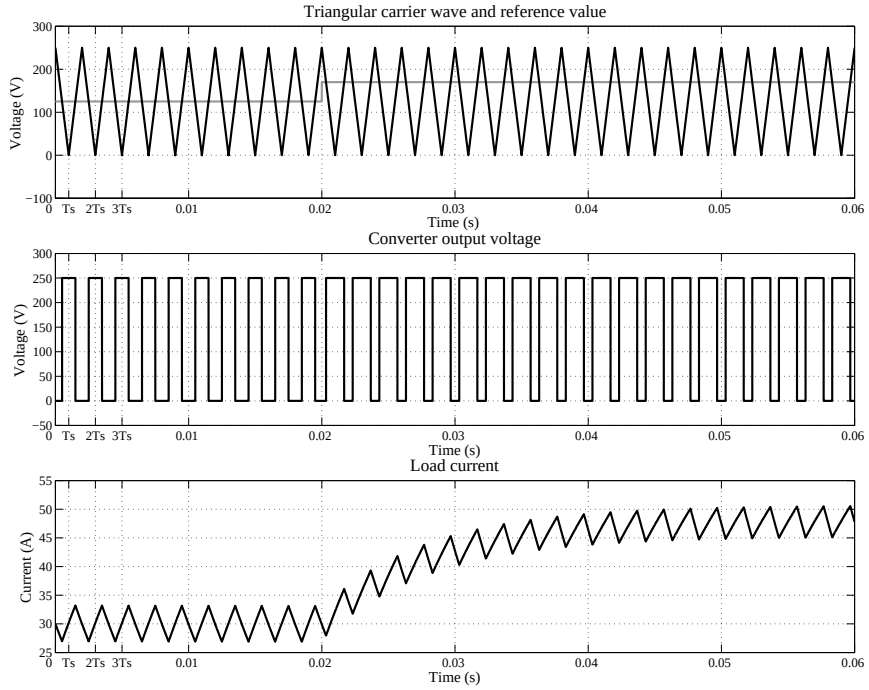

Figure B.6. 2-quadrant converter supplying a resistive-inductive load with a back emf.

Modulation frequency

In some applications, it might be of interest to have a carrier wave frequency much faster than the sampling frequency. When this is implemented, it is important to make sure that the sampling instants still coincides with the

turning of the carrier wave. This implies that the carrier wave has to consist of an integer number of half periods between two sampling instants.

The frequency of the carrier wave is equal to the switching frequency of the converter. This frequency is depending on the application. A high switching frequency implies a faster and more accurate control of the controlled quantities, and in many applications, a switching frequency higher than 20 kHz is used since the human ear does not perceive frequencies higher than this. The problem with a high switching frequency is that the switching losses are proportional to the switching frequency, i.e. selecting switching frequency for an application is a trade off between high frequency in order to spare the human ear and to get an accurate control of the system and switching losses.

This method to create variable output voltage by controlling the pulses voltage pulses is called Pulse Width Modulation (PWM).

Types of converters

There are different types of converters depending on which direction the energy flow should have. Three types are available, 1-quadrant, 2-quadrant and 4-quadrant converters. The quadrants are defined in Figure B.7 where u and i are the converter output voltage and current. A 1-quadrant converter can for example work in an area where the voltage and the current are positive. A 2-quadrant converter could operate with strictly positive voltage but a bi-directional output current, or the opposite combination. This means that the energy flow can have different directions in a 2-quadrant converter. In Figure B.7 it is possible to see the difference between the different types.

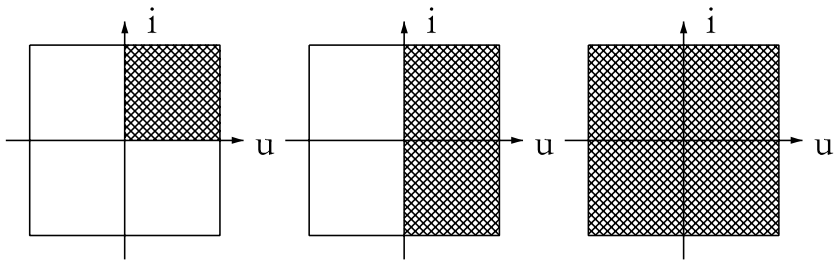

Figure B.7. From left: the working area of a 1-quadrant converter, a 2-quadrant converter and a 4-quadrant converter.

A 4-quadrant converter, or full-bridge converter, is built with two phase legs,

each consisting of two semiconductor switches and their anti-parallel diodes Figure B.8. The semiconductors in a converter are often IGBTs (Insulated Gate Bipolar Transistors) or MOSFETs (Metal-Oxide-Semiconductor Field Effect Transistor). The main focus of this thesis will be on the MOSFETs, since this is the component that has been used in the laboratory setup. The purpose of the anti parallel diodes is to provide an alternative path for the current in some switch states.

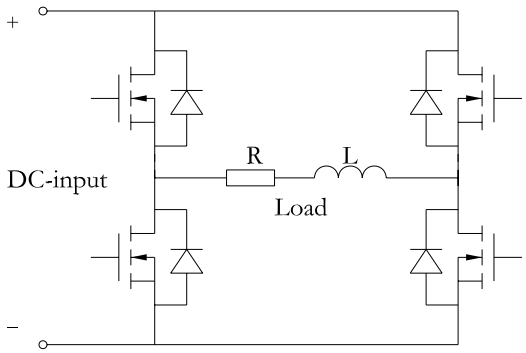

Figure B.8. An H-bridge

The two switches in one of the phase legs in a full-bridge converter are switched such that when one is conducting the other is turned off to avoid short-circuiting the DC-input. In most cases both switches are also never in their off state simultaneously, except for a short time interval called blanking time, which also has the purpose to avoid short-circuiting.

For a full bridge converter it is possible to have any combination of polarities for the voltage and the current. This implies that the converter could be used in only one of the four quadrants if wanted. In this thesis, a full bridge converter has been used as a 1-quadrant step down converter. A step down converter converts energy from a higher voltage to a lower.

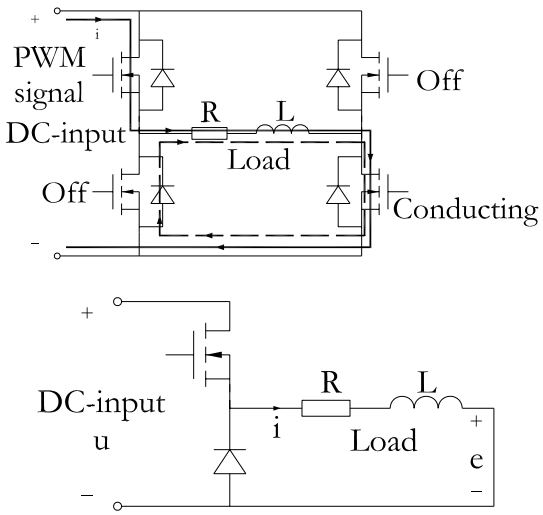

Figure B.9. A 4-quadrant converter (left) used as a 1-quadrant step down converter (right).

Figure B.9 shows a picture of a how the 4-quadrant converter is used as a step down converter. When the semiconductor switch is conducting, the current flows from the dc-input voltage through the MOSFET and to the load. Since the load is inductive the current will increase. When the switch is turned off the inductance will continue to lead the current through the freewheeling diode. Due to the inductive nature of the load, the current will slowly rise during the time period when the MOSFET is conducting and slowly fall when it is freewheeling through the diode.

Appendix C

Matlab codes

In this chapter are the Matlab codes for Method 1 and 2 presented. Each code can be implemented in Matlab as an .m-file, but there is no graphical user interface included wherefore data for each conductor must be inserted into the file for each layout under investigation.

Method 1, accurate method

```
% ***************************************
% *  Calculation of conductor parameters  *
% *           Accurate method             *
% ***************************************
clc
% Origo of the coordinate system is located in the corner of
%the ground structure

a1_x= ;   %Coordinates for conductor A
a1_y= ;

b1_x= ;   %Coordinates for conductor B
b1_y= ;

%Data for conductor A
r_a=0.398942;   %Radius of copper conductor
a_i=0.7;        %Thickness of insulation
i_eps_a=3.8;    %Relative permittivity of insulation

%Data for conductor B
r_b=1.3819766;
b_i=0.76;
i_eps_b=3.8;
```

```
eps=1e-9/(36*pi);   %Permittivity

% Inductance calculations
Inductance_a_uH=2*1e-7*
  log((4*a1_y*a1_x)/(r_a*(sqrt(((2*a1_x)^2)+((2*a1_y)^2)))))

Inductance_b_uH=2*1e-7*
  log((4*b1_y*b1_x)/(r_b*(sqrt(((2*b1_x)^2)+((2*b1_y)^2)))))

Mutual_inductance_uH=2*1e-7*
  (log(sqrt((((b1_y+a1_y)^2)+((b1_x-a1_x)^2))*
  (((b1_y-a1_y)^2)+((b1_x+a1_x)^2)))/
  (sqrt((((b1_x-a1_x)^2)+((b1_y-a1_y)^2))*
  (((a1_y+b1_y)^2)+((a1_x+b1_x)^2))))))

%Capacitance calculations
%Coefficient matrix
k1=((1/i_eps_a)*(log(1/r_a)))+((i_eps_a-1)/i_eps_a)*
  (log(1/(r_a+a_i)))+log((4*a1_y*a1_x)/
  (sqrt(((2*a1_x)^2)+((2*a1_y)^2))));

k2=log(sqrt((((b1_y+a1_y)^2)+((b1_x-a1_x)^2))*
  (((b1_y-a1_y)^2)+((b1_x+a1_x)^2)))/
  (sqrt((((b1_x-a1_x)^2)+((b1_y-a1_y)^2))*
  (((a1_y+b1_y)^2)+((a1_x+b1_x)^2)))));

k3=((1/i_eps_b)*(log(1/r_b)))+((i_eps_b-1)/i_eps_b)*
  (log(1/(r_b+b_i)))+log((4*b1_y*b1_x)/
  (sqrt(((2*b1_x)^2)+((2*b1_y)^2))));

k=[k1 k2; k2 k3];
k=k*(1/(2*pi*eps));

C=inv(k);
Capacitance_a=(C(1,1)+C(1,2))
Capacitance_b=(C(2,1)+C(2,2))
Mutual_capacitance=-1*C(1,2)
```

Method 2, approximate method

```
% ***************************************
% *  Calculation of conductor parameters  *
% *         Approximate method            *
% ***************************************

clc
% Origo of the coordinate system is located in the corner of
% the ground structure

a1_x=  ;   %Coordinates for conductor A
a1_y=  ;

b1_x=  ;   %Coordinates for conductor B
b1_y=  ;

%Data for conductor A
r_a=0.398942;   %Radius of copper conductor
%Data for conductor B
r_b=1.3819766;

eps0=(1e-9)/(36*pi);    %Permittivity of vacuum

%Equivalent plane conductor A
alfa=atan(a1_x/a1_y);   %Angle
a_r=a1_y*sin(alfa);     %Distance to equivalent plane

%Equivalent plane conductor B
beta=atan(b1_x/b1_y);
b_r=b1_y*sin(beta);

%Inductance calculations
Inductance_a=2*(1e-7)*log(2*a_r/r_a)
Inductance_b=2*(1e-7)*log(2*b_r/r_b)

%Distances for the mutual inductance calculation
D=sqrt(((b1_x-a1_x)^2)+((b1_y-a1_y)^2));
D1=sqrt(((b1_x+a1_x)^2)+((b1_y-a1_y)^2));
D2=sqrt(((b1_x-a1_x)^2)+((b1_y+a1_y)^2));
M1=2*(1e-7)*log(D1/D);
M2=2*(1e-7)*log(D2/D);
Mutual_inductance=1/((1/M1)+(1/M2))

%Capacitance calculations
Capacitance_a=2*pi*eps0/log(2*a_r/r_a)
Capacitance_b=2*pi*eps0/log(2*b_r/r_b)
Mutual_capacitance=eps0*2*pi/log((D^2)/(r_a*r_b))
```

Appendix D

Automotive Network Protocols

There are a number of different network protocols within a vehicle. The Controller Area Network (CAN) is probably the most well known protocol, LIN (Local Interconnect Network) is one of the slowest on board network and FlexRay is the future network standard within the vehicles. These three protocols will be briefly described in this Appendix.

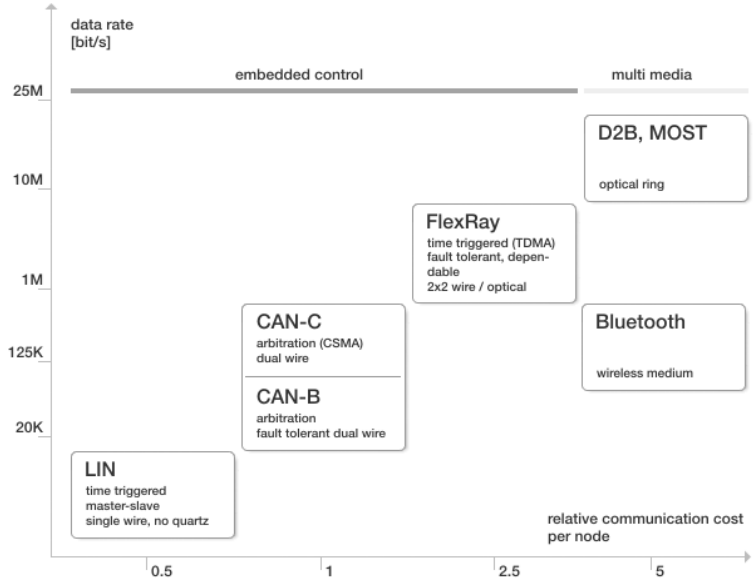

Figure D.1. A comparison between different automotive network protocols [39].

The three protocols can all be present at the same time in a vehicle since they complement each other according to Figure D.1. CAN was introduced in 1988 and was complemented by LIN about 10 years later for loads that did not require high data transmission rates. The increased complexity of the electrical system of the vehicle in combination with a number of electrical loads that are more safety critical has driven the development of FlexRay that today (2008) has started to be used in series production.

Local Interconnect Network (LIN)

The Local Interconnect Network, LIN, is a low cost serial network for distributed electronic systems in vehicles [78]. It complements the faster network protocols like CAN for smart sensors and actuators that do not require the bandwidth or versatility of CAN.

LIN has a single wire 12 V bus with speeds of up to 20 kbit/s. It has one master and several (typically not more than 12 though) slave nodes. More slave nodes can be attached to the network without requiring any hard- or software changes.

Controller Area Network (CAN)

The Controller Area Network (CAN) was developed for the automotive industry in order to combat the increasing size of the cable harnesses in the late 1980's [9]. It is a serial bus for real time control and it operates with a maximum speed of 1 Mbit/s.

The CAN bus consists of two twisted copper wires. On each of the wires is an opposing signal with the exact same information (CAN High and CAN low) in order to make the system more insensitive to disturbances. In CAN all messages are transmitted to all receivers where each receiver has to decide whether to respond to or discard the message. One of the problems with the CAN protocol is that although the messages has a priority number no one can guarantee a maximum transmission time for a message since it might collide several times with other messages of the same priority or higher. This is one of the reasons for developing FlexRay.

FlexRay

In the year 2000 the FlexRay consortium was founded. The aim was to enable new automotive systems and to complement both CAN and LIN. FlexRay communication uses a high data rate (10 Mbit/s for single channel

and 20 Mbit/s for dual channel) compared to the previous network protocols. It is a fault-tolerant and redundant system.

Unlike LIN and CAN, that are two event driven protocols, FlexRay is both time and event triggered. Each electrical control unit (ECU) in the system has a time slot in the static segment of a cycle when it might send messages on the bus, and in each cycle there is also a dynamic segment where the ECUs are allowed to write in case of an event.

Since the time slots in FlexRay guarantees that no messages will be delayed or collide, it is necessary for safety critical electrical loads in the vehicle like x-by-wire.